Purdue University
Purdue e-Pubs

Open Access Dissertations | Theses and Dissertations

Fall 2014

Analysis of the interaction of two parallel surface cracks

Jeeyeon Hahn
Purdue University

Follow this and additional works at: https://docs.lib.purdue.edu/open_access_dissertations

 Part of the Aerospace Engineering Commons

Recommended Citation
Hahn, Jeeyeon, "Analysis of the interaction of two parallel surface cracks" (2014). *Open Access Dissertations*. 279.
https://docs.lib.purdue.edu/open_access_dissertations/279

This document has been made available through Purdue e-Pubs, a service of the Purdue University Libraries. Please contact epubs@purdue.edu for additional information.

Graduate School Form 30
(Updated 11/20/2014)

PURDUE UNIVERSITY
GRADUATE SCHOOL
Thesis/Dissertation Acceptance

This is to certify that the thesis/dissertation prepared

By Jeeyeon Hahn

Entitled
ANALYSIS OF THE INTERACTION OF TWO PARALLEL SURFACE CRACKS

For the degree of Doctor of Philosophy

Is approved by the final examining committee:

Alten F. Grandt, Jr.

Chin-Teh Sun

Weinong Chen

Vikas Tomar

To the best of my knowledge and as understood by the student in the Thesis/Dissertation Agreement, Publication Delay, and Certification/Disclaimer (Graduate School Form 32), this thesis/dissertation adheres to the provisions of Purdue University's "Policy on Integrity in Research" and the use of copyrighted material.

Alten F. Grandt, Jr.

Approved by Major Professor(s): _____

_____

Approved by: Weinong Chen 10/31/2014

Head of the Department Graduate Program Date

ANALYSIS OF THE INTERACTION OF TWO PARALLEL SURFACE CRACKS

A Dissertation

Submitted to the Faculty

of

Purdue University

by

Jeeyeon Hahn

In Partial Fulfillment of the

Requirements for the Degree

of

Doctor of Philosophy

December 2014

Purdue University

West Lafayette, Indiana

To my husband ILCHUNG PARK

ACKNOWLEDGEMENTS

I would like to thank Dr. Alten F. Grandt, Jr. for his help and advice throughout this research. Dr. Grandt's guidance and support were invaluable, and I will forever be grateful.

My eternal thanks are given to my husband, Ilchung Park. Your endless love, friendship and support have enabled me to achieve thing I never thought I could. Finally, I would also like to thank my parents Eung Seop and Chung Soon for their love and devotion.

TABLE OF CONTENTS

Page

LIST OF TABLES

Table Page

LIST OF FIGURES

Figure Page

Figure Page

Figure Page

Figure Page

LIST OF ABBREVIATIONS

FEM	Finite Element Method
LEFM	Linear Elastic Fracture Mechanics
SIF	Stress Intensity Factor

ABSTRACT

Hahn, Jeeyeon. Ph.D., Purdue University, December 2014. Anaysis of the Interaction of Two Parallel Surface Cracks. Major Professor: Dr. Alten F. Grandt, Jr.

The objective of this research is to analyze and predict the interaction of surface cracks that occur in parallel planes. Multiple cracks may form in aging aircraft that forms at stress concentrations such as fastener holes and notched components by stress corrosion and fatigue cracking. The lifetime of the structures are significantly affected by the interaction between these cracks. Depending on relative positions and orientations of neighboring cracks, local stress fields and crack driving forces can be affected by the presence of adjacent cracks. Even small subcritical cracks may rapidly grow to a size that will cause failure in service due to interaction and coalescence with other cracks.

The interaction behavior and crack propagation direction of two parallel surface cracks is studied using three-dimensional finite element analysis (FEA). FEA models with wide range of crack configurations in a finite plate under tension are evaluated to investigate the correlation between the crack shapes and the separation distance between two cracks. The relative distance (vertical and horizontal) between two cracks and size and shape of these cracks are varied to create different stress interaction fields. Stress intensity factors (SIF) along the crack fronts are obtained from FEA, and then,

cracking behaviors of the cracks are predicted by considering the influence of the interaction on the SIF and the coalescence of two cracks. The results obtained are then compared with existing experimental and analytical data for validation. All of the data analyses are presented in tabular forms and figures.

CHAPTER 1. INTRODUCTION

1.1 Motivation

Cracks and other forms of defects in engineering structures may be introduced due to porosity, inclusions, forging or casting defects, or improper thermal and mechanical treatment of the material during manufacturing and processing [6]. Eventually, these small subcritical cracks will grow to a size that will cause failure in service.

Cracks are often originate at stress concentrations such as fastener holes and notched components. Also, multiple cracks, which are likely initiated due to stress corrosion and fatigue cracking, have been observed in aging aircraft and mechanical components such as multi-site damage and pressure vessel fatigue [6]. At the tip of these cracks, stress exceeds the material strength and this stress concentration leads to catastrophic failure of the components. In addition, when multi-site damage is present in a component, the interaction and coalescence of the cracks causes a sudden increase in crack size and accelerates the growth of the crack which reduces the time to failure [2, 5, 7, 11, 12, 13, 17].

When assessing the structural integrity of engineering structures, propagation of fatigue cracks are predicted to evaluate the safety and lifetime of the structure. Most

common approach applied for this evaluation is by using the relationship between Stress Intensity Factor (SIF) and growth rate of fatigue crack to predict the crack growth. Therefore, growth behavior of the interacting cracks can be predicted by considering the effect of the interactions and coalescence of those cracks. The studies on the interaction effect between cracks are mostly dealt with coplanar cracks. Since there are relatively few studies on non-planar parallel crack interactions, there is a need to study the crack growth behavior or fatigue life of parallel cracked structures.

1.2 Background

1.2.1 Crack Growth

Many approaches have been developed for predicting the life of a crack from the initiation to growth stages. These include stress-life and strain-life methodologies for the crack initiation, and linear elastic fracture mechanics (LEFM) principles.

Using the LEFM approach, engineers may assume the existence of flaws in the design of an engineering structure, and from there, they can predict the approximate life before inspection or retirement. LEFM assumes that crack growth is controlled by the cyclic SIF, ΔK. SIF relates loading, crack size, and specimen geometry, and is often given in the form as

$$K = \sigma_o \sqrt{\pi a}\, \beta(a). \tag{1.1}$$

The growth rate of a crack versus cyclic SIF curve shows a sigmoidal shape for many materials (Figure 1-1). The lower asymptote for small ΔK is the threshold region:

Stage I. In this region, the crack growth would arrest for decreasing values of ΔK. The upper asymptote for large ΔK is the fracture region (Stage III), where the SIF at the crack tip approaches the fracture toughness in this region. For the steady state region (Stage II), many fatigue crack growth prediction method are developed to correlate the constant amplitude fatigue growth rates with various loading parameters. Paris Law has been most widely used, where Paris and Erdogan [23] showed that the fatigue crack growth rate (da/dN) is a function of the cyclic change in SIF (ΔK) as

$$\frac{da}{dN} = C\ (\Delta K)^m \tag{1.2}$$

where *C* and *m* are empirical parameters that depend on the material and mean stress of interest.

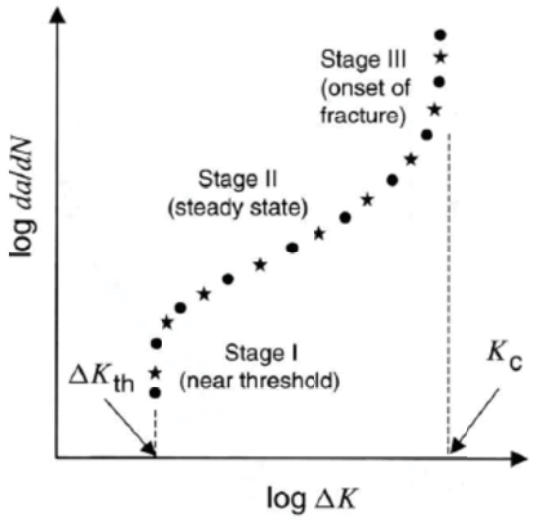

Figure 1-1 Fatigue crack growth rate [6].

1.2.2 Previous Research on Multiple Crack Interaction

The initiation of multiple surface crack is found to be common in many types of material failure, such as fatigue (Kamaya, Miyokawa, and Kikuchi [11], and Soboyejo and Knott [27]), corrosion fatigue (Wang et al. [30]), and stress corrosion cracking (Stonesifer, Brust, and Leis [21]). When such cracks are present in an engineering component or structure, the failure is usually progressed by the interaction and coalescence of those cracks.

Due to the complexity in the analysis, exact solutions which are obtained by analytical methods are only applicable to problems with simple crack configurations [19, 21]. With the rapid advancement of computer technology, extensive studies have been conducted using numerical methods to understand the crack growth behavior under multiple crack interaction [2, 9, 10, 11, 13, 17, 19, 20, 24, 28]. These studies have shown that the degree of the crack interactions is varied depending on the crack configurations: distance between the cracks, size and shapes of the cracks, etc. A lot of the studies have used the finite element method [2, 11, 13, 17, 19, 20, 24, 28] where the body force method [10] and the boundary element method [9] are also considered in solving the multiple cracking problems.

Multiple crack interactions are usually categorized into coplanar and parallel. As shown in Figure 1-2(a), cracks are aligned in their propagation direction for coplanar crack type. For parallel crack type, cracks are aligned perpendicular to their propagation direction and located parallel to each other (Figure 1-2(b)). As shown in the figure, the local stress fields are affected by the presence of neighboring cracks. Previous

researchers have discovered that the relative location and orientation of the adjacent crack can either enhance or diminish the SIF of the crack from the interaction [1, 15].

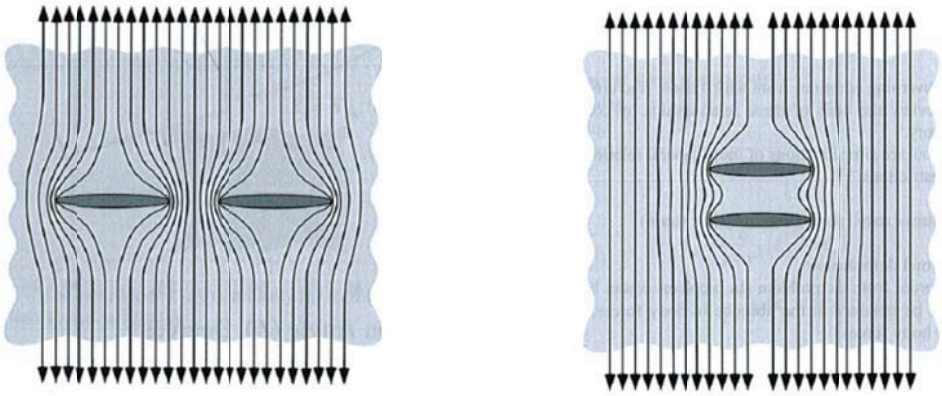

(a) Coplanar (b) Parallel

Figure 1-2 Interaction of multiple cracks under tension. The lines present the effect of the neighboring crack [1].

Figure 1-3 is a plot of the mode I SIF (K_I) solution when two identical coplanar cracks are interacting in an infinite plate under tension [18]. The plot illustrates that K_I can be amplified if the cracks are located in the same plane. At crack tip A, the solution approaches $\sqrt{2}$ as the horizontal distance between two cracks (s) reduces to 0. Since two cracks become a single crack for this case, the length of the single crack also become twice than before. It is also observed that normalized K_I solution increases as a neighboring crack approaches to a crack. In other words, the effect of the crack interaction becomes significant as the horizontal distance between two cracks, s, reduces. From the previous studies, researchers have concluded that the interaction of coplanar cracks may accelerate the crack growth rate and reduce the required time to reach its critical length [5, 7, 9, 15].

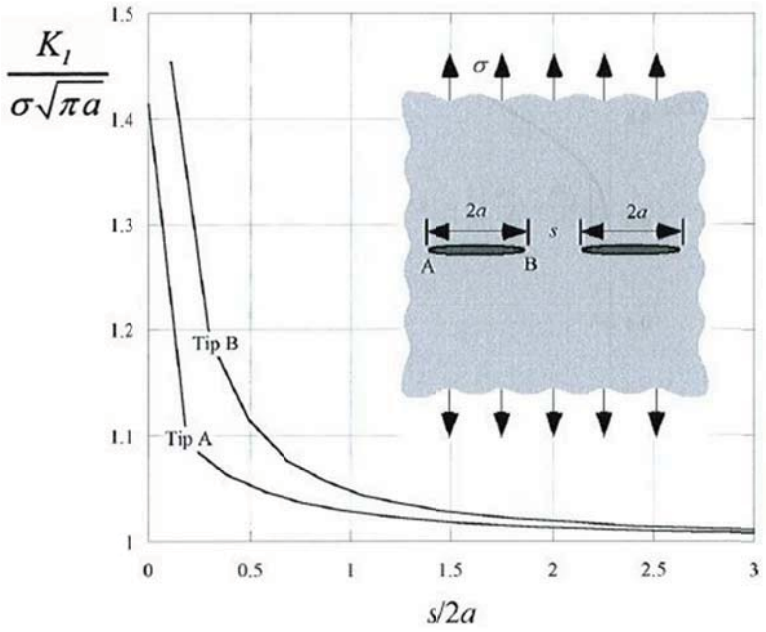

Figure 1-3 Interaction of two identical coplanar through wall cracks in an infinite plate [18].

Figure 1-4 is a plot of the K_I solution for two identical parallel cracks separated by a vertical distance, *s,* under tension [18]. As mentioned in earlier, presence of a neighboring crack created a stress shielding zone around the local stress field. In the figure below, the effect from this stress shieling can be observed when mode I loading is applied to the cracks. As two cracks approaches to each other, K_I at the crack tip decreases due to stress shielding. On the other hand, K_I at the crack tip increases and approaches to that of single crack as the vertical distance between the cracks increases. It is observed that the presence of a neighboring crack causes a shielding effect. It is found that the stress shielding effect reduces the K_I at the crack tip and propagation of the crack which prohibits the cracks from coalescing [1, 4, 11, 13, 28, 30].

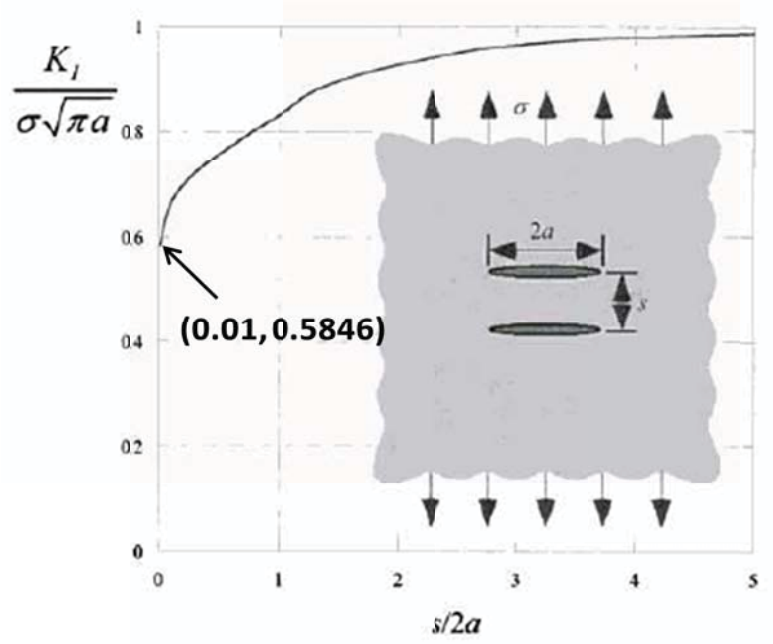

Figure 1-4 Interaction of two identical parallel through wall cracks in an infinite plate [18]. As the vertical distance between two cracks (*s*) increases, the solution approaches 1 (single crack). Note that the minimum of the curve is 0.5846 at $s/2a$ = 0.01.

Several experiments are conducted to investigate changes in crack growth rate due to the interaction and change in crack shape during the coalescence between the cracks under fatigue loading [2, 4, 7, 11, 13, 14, 17, 22, 28, 30]. From these experiments, it is found that when the cracks are closely located from each other, the SIF of interacting coplanar cracks is almost identical to the SIF of coalesced crack [2, 7, 15, 29, 30]. Figure 1-5 is a plot of K_I value at crack tip A when two identical semi-elliptical surface cracks are interacting in an infinite plate. SIF of interacting cracks for various horizontal distances between crack centers (*d*) for different crack shapes (*b*/*a*) are evaluated by Murakami and Nisitani [18]. F_A is the normalized K_I at crack tip A by the following equation

$$F_I = \frac{K_I}{\sigma_o \sqrt{\pi a}}. \tag{1.3}$$

From the figure, it is found that the effect of the crack depth (b) on the SIF of interacting cracks diminishes as the crack depth to length ratio increases. Also, normalized K_I at tip A of interacting cracks (F_A) converges to the SIF of the single equivalent coalesced crack (λ = 1) as the distance between two coplanar cracks decreases. On the other hand, when the two cracks are located very far apart from each other (λ = 0), F_A approaches to that of the single crack solution.

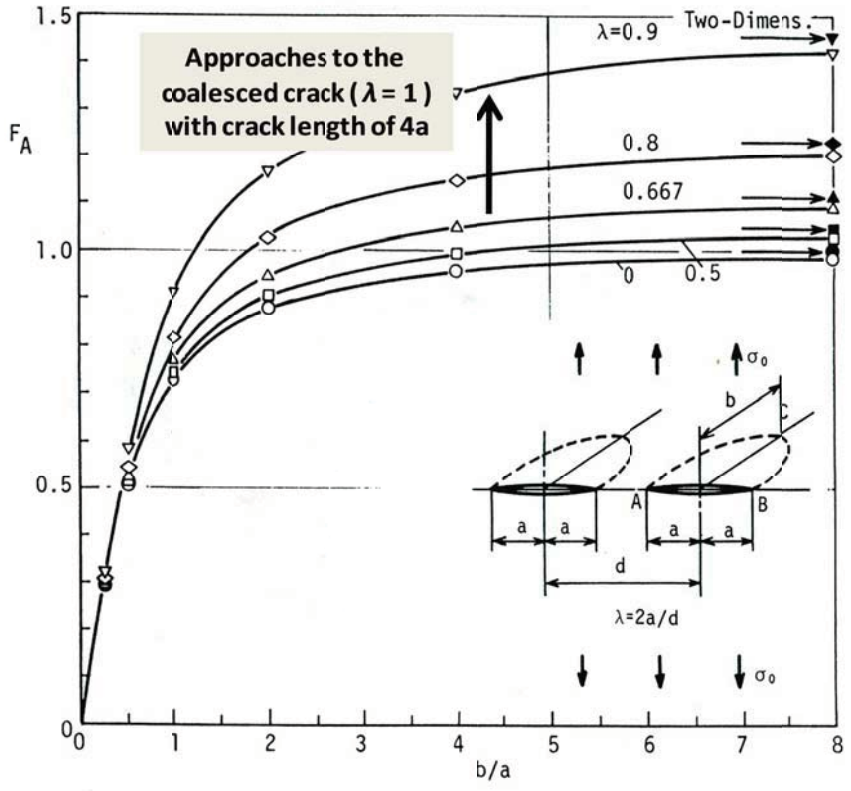

Figure 1-5 Interaction of two identical semi-elliptical surface cracks under tension [18]. Note that as the distance between two cracks increases ($d \rightarrow \infty$), F_A converges to the single crack solution.

Song and Choi [28] performed experimental research to identify the types of parallel through crack interactions. Based on the observations, propagation behavior of the interacting parallel cracks is categorized into three different types: collinear coalescence, parallel coalescence, and bypass (Figure 1-6). When the cracks are located very close to each other vertically, two cracks are coalesced over time as shown in that of coplanar/collinear crack interactions (type 1). When the secondary crack is somewhat close to the first crack, inner tips of two cracks grow towards each other as they overlap (type 2). In the last case, secondary crack is located far from the first crack. The edge crack bypasses the secondary crack while the secondary crack is arrested (type 3).

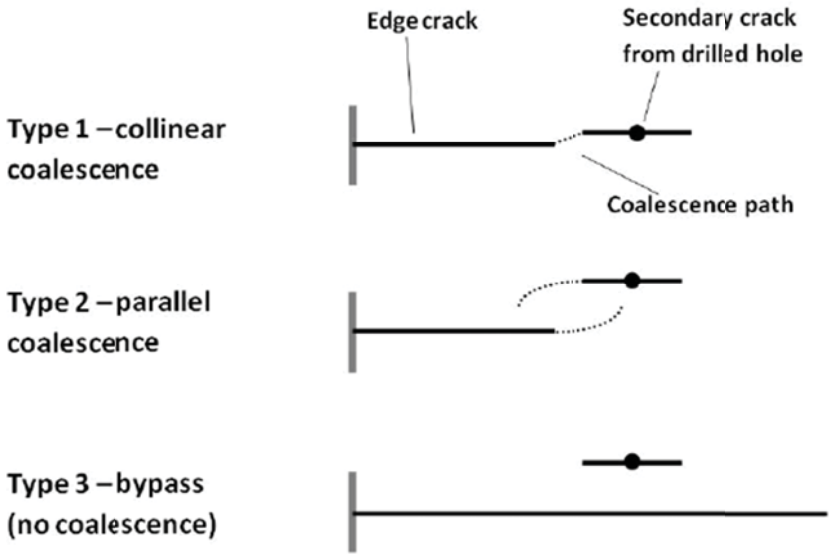

Figure 1-6 Types of parallel cracks interactions [20].

Forsyth [4] and Zezula [31] investigated the effect of inherent inhomogeneities on the initiation and growth of fatigue cracks in semi-circular edge notch specimens of aluminum 7050-T7451 thick plate alloy (Figure 1-7). Fatigue crack growths for several

versions of this alloy with various sizes and number of inhomogeneities are studied in these researches. As shown in Figure 1-7, the width of the rectangular double-edge notch specimen is designed to be large enough (2.00 in) so that the growth of a small crack in one notch is not affected by the presence of the opposite notch (radii = 0.00938 in). Fatigue crack growth is monitored from the point of initiation. In several fatigue tests, small cracks initiated at different locations of the notch, and they grew into the through crack that eventually caused specimen failure. As these cracks are traced in cyclic time, small cracks which would coalesce at a later period in the test are assigned with numbers such as 1.1 and 1.2, indicating that they coalesced into crack number 1.

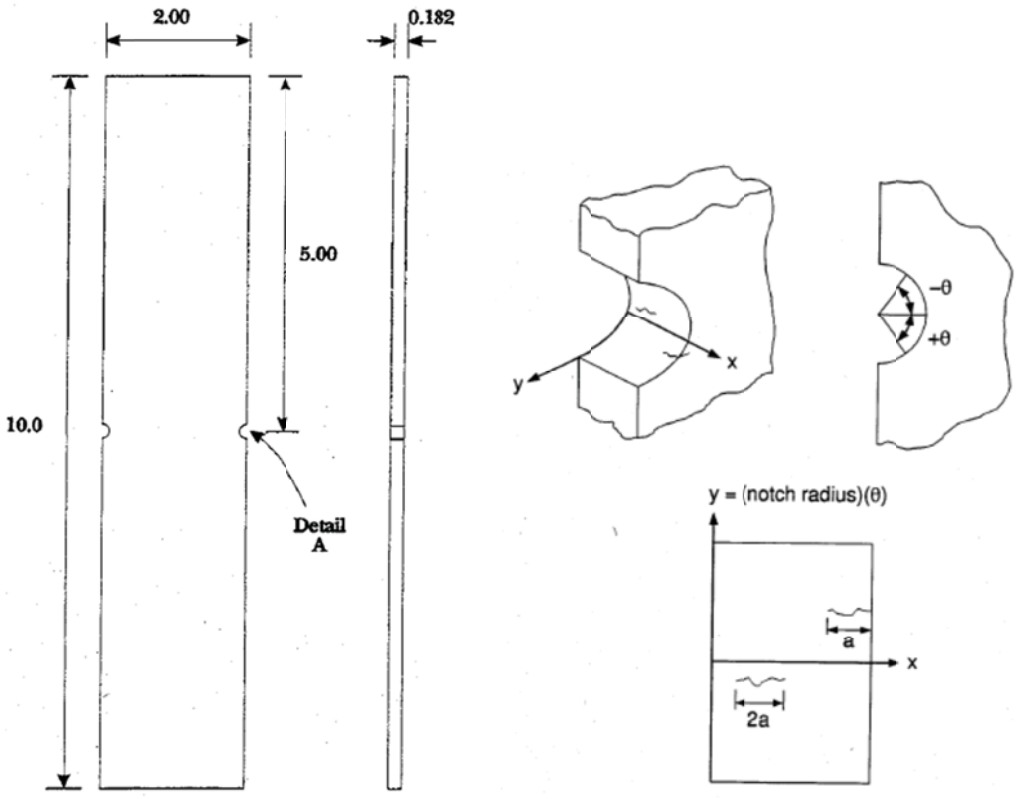

Figure 1-7 Specimen with two notches (Crack are located at notches) [4, 31].

Among the experimental data from Forsyth [4] and Zezula [31], interaction behavior of two parallel cracks, as shown in Figure 1-6, is also found in four test cases: one “collinear coalescence”, two “parallel coalescence”, and one “bypass” type. Sample figures from specimen 7112-a22, front notch data at 53,000, 61,000, 67,000, and 73,000 cycles are provided in Figure 1-8. Here parallel overlapping cracks (type 2) are observed to grow and coalesce as a function of elapsed cycles. It is shown that cracks (crack numbers 1.1 and 1.2) grew independently until about 61,000 cycles. Since the size of the cracks are different, the larger crack (lower right crack) grew faster than the smaller crack (upper left crack), and the smaller crack stopped growing within the stress shielding area of the larger crack. As the crack tips passed each other, coalescence occurred and the direction of progress of inner crack tips of two cracks are changed. Now, crack tips grew toward the opposite crack while the progress directions of outer tips are perpendicular to the loading direction. This implies that the cracks began to interact with each other to coalesce into a larger crack. In the experiment, the cracks did not coalesce before the specimen fractured (measured cycles to failure = 73,730).

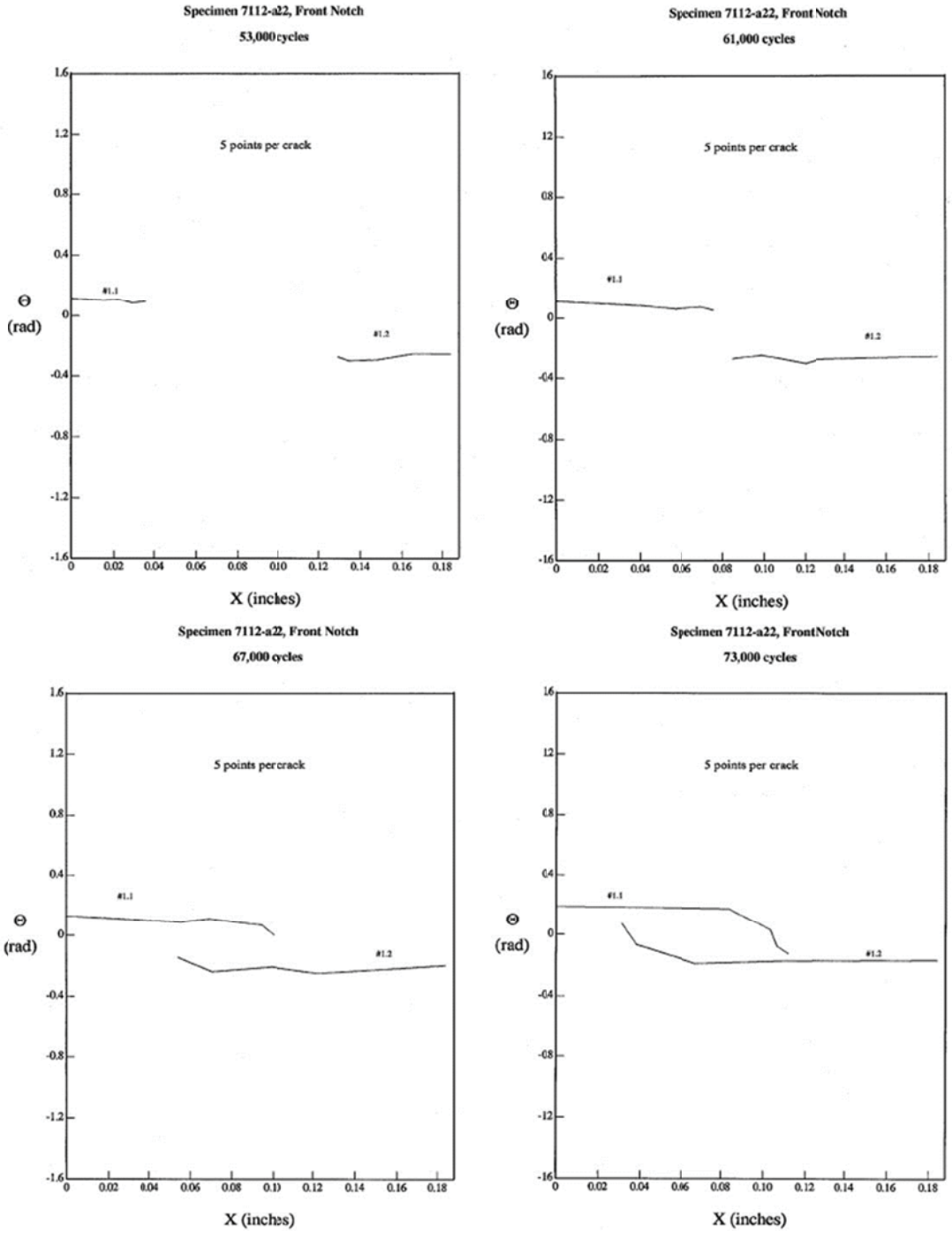

Figure 1-8 Interaction of parallel overlapping cracks over cycles [4, 8, 31].

1.3 Objective

The objectives of this research can be identified as following:

1. characterize interactions of two symmetric parallel semi-elliptical surface cracks with a wide range of crack configurations and determine the SIF along the crack front by the finite element method,
2. characterize interactions of two non-symmetric parallel semi-elliptical surface cracks with a wide range of crack configurations and determine the SIF along the crack front by the finite element method, and
3. validate the results obtained by comparing those with existing experimental and analytical data from Kamaya [13, 14] and Needham [20].

Many engineering structures and components often contain non-coplanar crack configurations. However, relatively few studies are conducted on the interaction behavior of parallel cracks, and majority of those studies are focused on the variation of SIF. Therefore, in order to evaluate the safety of a structure, investigation on the crack growth behavior or fatigue life assessment on a structure containing two parallel cracks are required.

In Chapter 2, crack analysis and stress intensity factor calculations in Abaqus and development of the Abaqus model are introduced. Then, correlation between the crack type and the separation distances are analyzed for symmetric and non-symmetric parallel surface crack in the result chapter (Chapter 3). The result chapter discusses

about the comparison between output results of the FEA and the previous experimental data. Finally, Chapter 4 provides discussion and conclusion of the research and states the recommendation for additional study.

CHAPTER 2. METHOD

In this research, the finite element software package Abaqus, Version 6.10 [25] is used to compare the numerical and experimental results. To develop the models, an iterative process is used to move from simple structures that had known SIF solutions to the complex structure that had unknown stress intensity factor solutions.

2.1 Introduction to Abaqus – Finite Element Analysis

Abaqus is a software for finite element analysis (FEA) and computer-aided engineering (CAE). Abaqus relies on contour integrals which first involves determining the displacement field around the crack tip. The displacement field is then used with a strain energy release rate algorithm to determine the SIF at a defined location [25].

Abaqus offers two different ways to model cracks. The first is based on the conventional FEM, which typically requires the user to conform the mesh to the cracked geometry to explicitly define the crack front and to specify the virtual crack extension direction. The second is based on the extended finite element method (XFEM). This method does not require the mesh to match the cracked geometry. However, contour

integral evaluation with XFEM is currently limited to linear tet and brick elements [26]. Thus, the first method is used in this research.

2.1.1 Stress Intensity Factor Computation Methods in Abaqus

Abaqus uses Stress Intensity Factor to J-integral relationship to calculate the stress intensity factors around the crack tip. In fracture mechanics, J-integral is used to calculate the energy release rate associated with crack growth [1]. The energy release rate is given by

$$J = \int_A \lambda(s)\boldsymbol{n} \cdot \boldsymbol{H} \cdot \boldsymbol{q}\, dA, \tag{2.1}$$

where *dA* is area of the elements around the crack front. ***H*** is given by

$$\boldsymbol{H} = \left(W\boldsymbol{I} - \boldsymbol{\sigma} \cdot \frac{\partial \boldsymbol{u}}{\partial \boldsymbol{x}}\right). \tag{2.2}$$

In linear elastic fracture mechanics, mode I, mode II, and mode III SIFs, K_I, K_{II}, and K_{III}, are used to estimate the stress and displacement around crack tips. For an isotropic and homogeneous material, the relationship between the SIFs and the energy release rate (the J-integral) is given as

$$J = \frac{1}{\bar{E}}(K_I^2 + K_{II}^2) + \frac{1}{2G}K_{III}^2 \tag{2.3}$$

where $\bar{E} = E$ for plane stress condition and $\bar{E} = \frac{E}{(1-\upsilon^2)}$ for plane strain condition in three dimensions.

2.1.2 Crack Growth Direction

Engineering structures are subjected to complex loading condition. Therefore, crack growth under the mixed mode loading condition must be investigated especially when interaction between cracks are existent. Erdogan and Sih [3] proposed a maximum tensile stress criterion which provides the near-tip stress field for a crack subjected to mixed mode fracture. This criterion is the simplest approach in predicting the crack extension direction under the mixed mode loading condition, which is also used in Abaqus to calculate the crack propagation angle. The near tip stress field is given by

$$\sigma_{\theta\theta} = \frac{1}{\sqrt{2\pi r}} \cos\frac{\theta}{2}\left(K_I \cos^2\frac{\theta}{2} - \frac{3}{2}K_{II}\sin\theta\right) \tag{2.4}$$

and

$$\tau_{r\theta} = \frac{1}{\sqrt{2\pi r}} \cos\frac{\theta}{2}\left[\frac{1}{2}K_I \sin\theta + \frac{1}{2}K_{II}(3\cos\theta - 1)\right] \tag{2.5}$$

where *r* and *Θ* are the polar coordinate centered at the crack tip. According to the criterion, the crack propagates in the direction at which $\sigma_{\theta\theta}$takes the maximum with respect to *Θ* near the crack tip ($\partial\sigma_{\theta\theta}/\partial\theta = 0$ or $\tau_{r\theta} = 0$). From this condition, crack propagation angle Ø can be obtained by the following equation

$$\frac{K_{II}}{K_I} = \frac{\sin\emptyset}{1 - 3\cos\emptyset} \tag{2.6}$$

or

$$\emptyset = \cos^{-1}\left(\frac{3K_{II}^2 + \sqrt{K_I^4 + 8K_I^2K_{II}^2}}{K_I^2 + 9K_{II}^2}\right) \tag{2.7}$$

Erdogan and Sih found that K_{II} is closely related to the deviation of the crack growth direction. Considering that crack propagation angle Ø is measured with respect

to the crack plane, a positive K_{II} causes a negative Ø while a negative K_{II} causes a positiveØ. Ø = 0 means mode II stress component is not present ($K_{II} = 0$) and the crack extends straight-ahead direction: purely under mode I loading.

2.2 Model Development

In this research, the SIF of interacting parallel semi-elliptical cracks, which are perpendicular to the loading direction, are evaluated by FEM using Abaqus. The research performed to achieve the objectives falls into three categories. The first is the development of the three dimensional model containing parallel surface cracks in Abaqus. The first part of this research is completed by learning and extending the work that has been done by Kamaya [14] and Needham [20]. Due to the lack of experimental data to verify the three dimensionality of the problem which is studied in this research, the complexity of the finite element model is gradually increased from a two dimensional center crack to two parallel cracks, and then to three dimensional surface cracks. Once three dimensional surface crack modeling methods are validated by comparing the obtained results with Newman and Raju's solution for single cracks [21], three dimensional model containing two parallel surface cracks is constructed. Final model is validated by comparing several solutions with Kamaya [12, 14] and Needham's [20] results. In addition to providing a means of verification, this process also afforded valuable experience and familiarity with the software.

As discussed in the previous section, Abaqus defines the first contour as the ring of elements surrounding the crack front when calculating the J-integral. For each

contour, rings of elements are connected to previous contour recursively. From the previous studies [13, 20], SIFs (J-integral) are converged at the 5th contour for quadratic mesh refinement cases. Thus, SIFs are obtained using 2D 8 node quadratic solid elements (CPS8) and 5th integral in all validation cases.

All analyses are assumed as linear and purely elastic, and stiffness and Poisson's ratio of typical Aluminum (E = 3*10^7 and υ = 0.30) is selected for this study. SIFs obtained from Abaqus are normalized by equation (1.3), and calculated results for each configuration are presented against the results from previous studies.

2.2.1 Two Dimensional Offset Parallel Cracks

Prior to the three dimensional model development, two dimensional parallel cracks in offset positions embedded in a wide plate subjected to tensile loading are investigated. In order to compare the results with the Murakami solutions [18], configuration of these cracks is redefined in Figure 2-1. Here 2a is the thru-crack length, f is the vertical distance between crack planes, while e and d are the horizontal and total distance between crack centers.

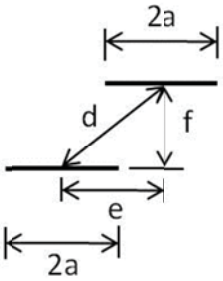

Figure 2-1 Two Offset Parallel Cracks reproduced from [18].

In Figure 2-2, FEM results for various geometries are plotted over results from Murakami handbook [18]. The figure shows a close correlation between the numerical solution obtained from the current Abaqus and the Murakami solutions. Both stress shielding and amplification are observed.

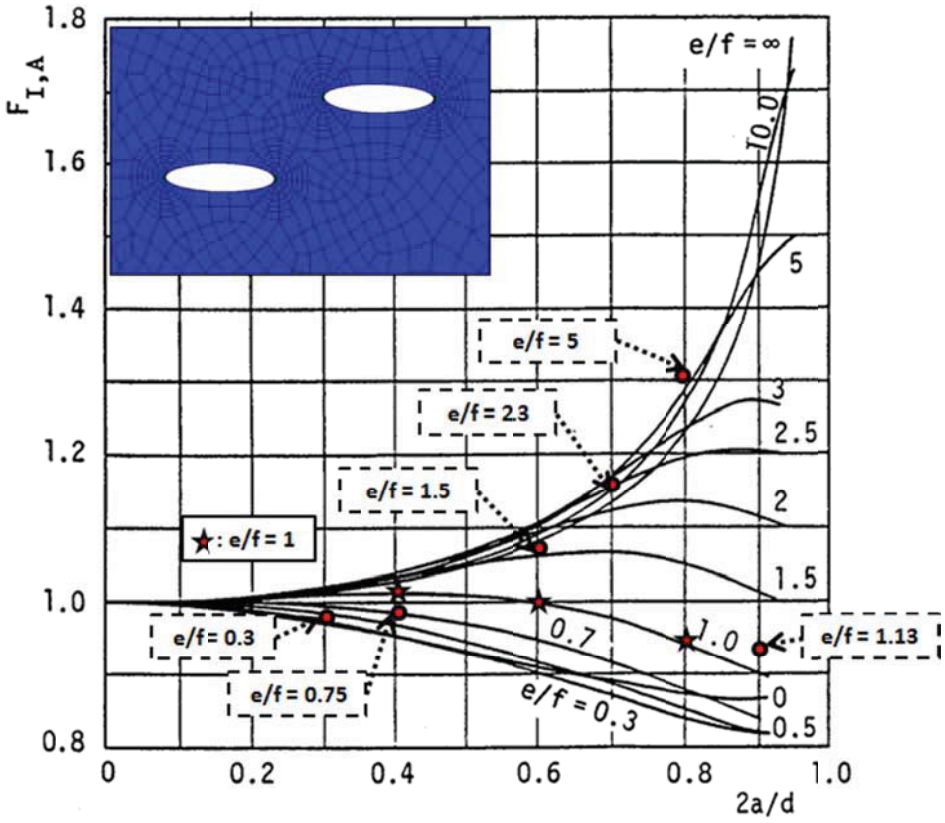

Figure 2-2 Parallel Crack FEM results (symbols) superimposed on Murakami solutions (solid lines) [18].

2.2.2 Three Dimensional Single Semi-Elliptical Surface Crack

As mentioned earlier, complexity of the finite element model is gradually increased. Prior to develop the three dimensional model containing two offset parallel cracks, three dimensional plate with a single semi-elliptical surface crack subjected to tension is modeled. Figure 2-3 below shows the first generation of the three dimensional FEM model containing single surface crack. To simplify the model and reduce the computational time, a half symmetric model is constructed. Since the crack is located at the center of the plate, boundary conditions are symmetric along the crack face. As shown in Figure 2-3 (a), the area around the crack tip is divided into two sections: inner tube and outer tube. By partitioning the crack tip area into two circular tubes, collapsed singularity elements are created in the inner tube region; and structured elements are created in the outer tube region, which to be used in the contour integral evaluations. This partitioning method is recommended by Abaqus to create the finer meshes around a crack tip for more accurate analysis.

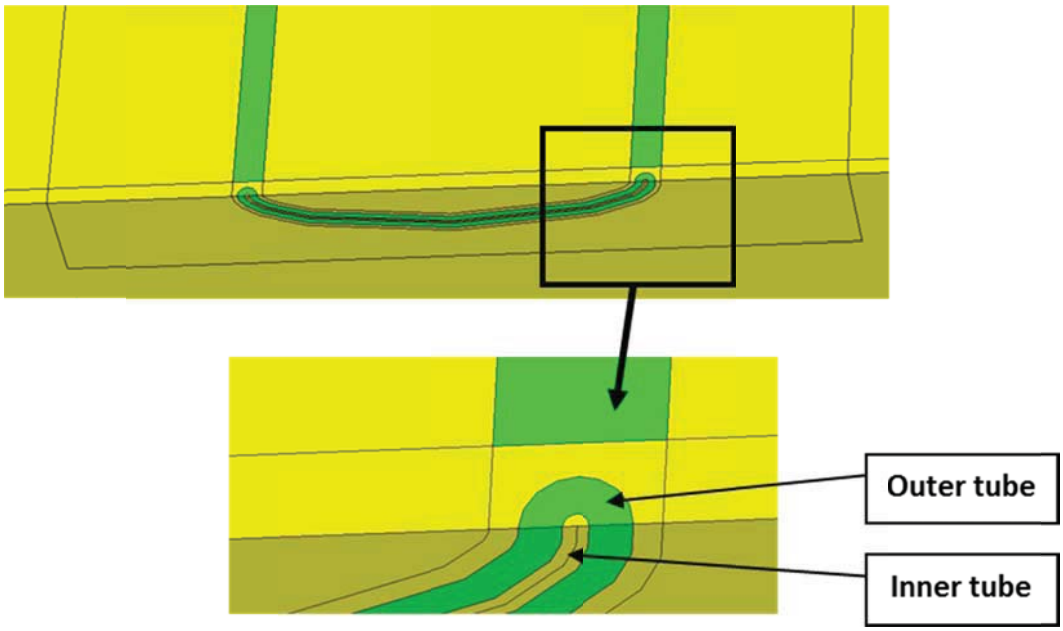

(a) Partitioned model for mesh design

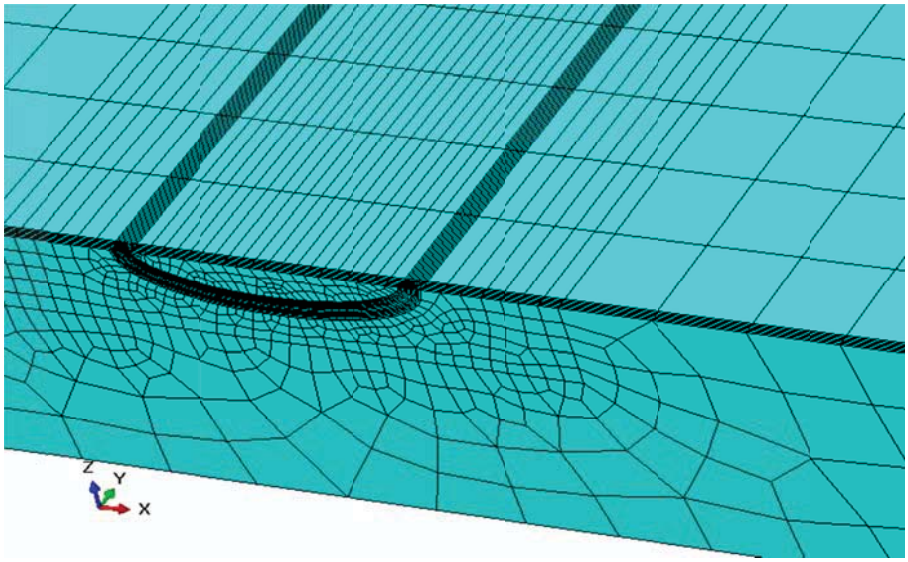

(b) Meshed view

Figure 2-3 First version of the three dimensional FEM model with single surface crack located at the center of the plate. Finer meshes are adopted around the crack.

The mesh partitioning method suggested in the Abaqus documentation has a limitation in the mesh design. As the radius of the inner tube decreases, size of the mesh elements are decreased and finer meshes are formed along the crack front. However, if the size of the inner tube elements is too small, elements in the outer regions connected to those inner tube meshes may be distorted. When the meshes are distorted, quality of the mesh is reduced and Abaqus produces a warning message. Thus, care must be taken to maintain the quality of the mesh within the warning limits.

To select the radius of inner and outer tubes, r and R respectively, various combination of radii are tested on the FEM model shown in Figure 2-3. Identical mesh design (e.g. mesh partition, number of elements for inner and outer tubes along the crack front, etc.), except the tube radii, is used throughout the investigation. KI at free surface and at maximum depth of the crack is then compared with corresponding solutions from Newman and Raju [22]: Table 2-1 summarizes the difference between these K_I solutions for five different tube radii ratio (r/R). As provided in the table, the model with tube radii ratio of 0.1 produced the results which give the lowest average difference between the FEM and Newman and Raju. Thus, tube radii ratio of 0.1 is selected for the final FEM model used in this study.

Table 2-1 Tube radii selection study for three dimensional semi-elliptical surface crack under tension: K_I at free surface and at maximum depth of the crack obtained from five different FEM model is compared with Newman and Raju solution [22].

Model #	Inner tube radius, *r*	Outer tube radius, *R*	Tube radii ratio, *r*/*R*	Difference between FEM and Newman & Raju [%]		
				Free surface	Max depth	Average
1	0.01	0.5	0.020	2.42	2.10	2.26
2	0.01	0.4	0.025	2.40	2.11	2.26
3	0.01	0.2	0.050	1.59	1.31	1.45
4	**0.01**	**0.1**	**0.100**	**1.10**	**0.14**	**0.62**
5	0.01	0.07	0.143	1.47	0.05	0.76

Now, FEM models for various crack geometries are created to validate the final mesh design developed for the three dimensional semi-elliptical surface crack by comparing the results with Newman and Raju's solutions [22]. Normalized K_I along crack front for various crack depths, *c*, and crack lengths, *a*, from the FEM model are plotted against Newman Raju's Solution in Figure 2-4 below. As shown in the figure, FEM results for various crack shapes are compared favorably with Newman and Raju solutions. Maximum difference between the FEM model and Neman and Raju solution is obtained as 4.3 % at the deepest point of the crack for c/w = 0.1 and a/c = 0.3 case (Figure 2-4 (a)) where less than 3% is obtained for other cases.

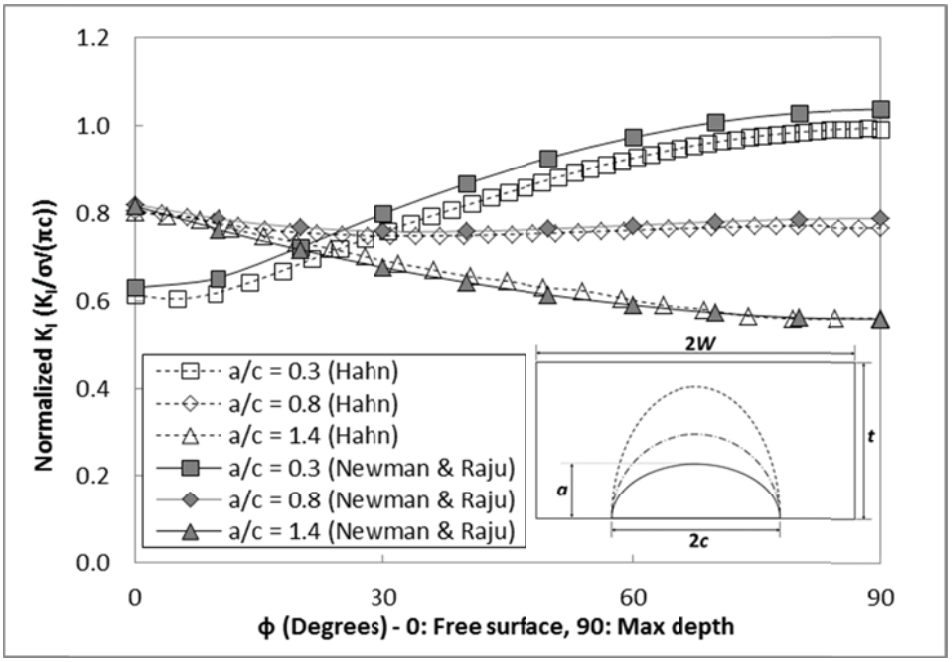

(a) Fixed crack length (c/w = 0.1) for varying crack depth (a/c = 0.3, 0.8, and 1.4)

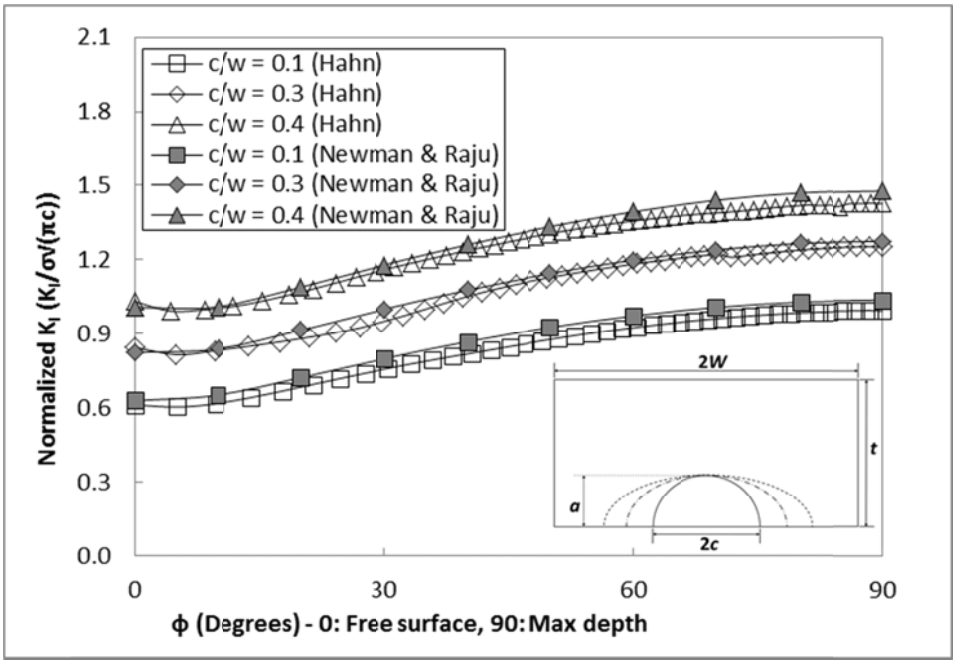

(b) Fixed crack depth (a/c = 0.3) for varying crack length (c/w = 0.1, 0.3, and 0.4)

Figure 2-4 Normalized mode I SIF along crack front for single semi-elliptical surface crack under remote tension. Results obtained for various crack configurations from FEM model are plotted against Newman Raju's Solution [22].

2.2.3 Three Dimensional Overlapping Parallel Surface Cracks

The mesh design of the final model, which contains offset parallel cracks, is adapted from a design used in the Needham's [20] study. As the design of the three dimensional mesh is evolved and redesigned as the complexity is added to the model throughout the study, another mesh modeling technique is introduced. It is discussed in the previous section that finer meshes must be adopted around crack tips to get accurate results in Abaqus. Also, when multiple overlapped cracks are present in a model, mesh patterns of those cracks also overlap each other. Finer meshes and overlapping mesh patterns cause the mesh structure to be complex, which makes it difficult to connect the meshes around the cracks. Therefore, as shown in Figure 2-5, Needham constructed three separate blocks to overcome this problem: two crack blocks and one intermediate block which is inserted between the cracked blocks. Then, by using the "Tie" function in Abaqus, these three blocks with mismatching mesh patterns are assembled as a whole block.

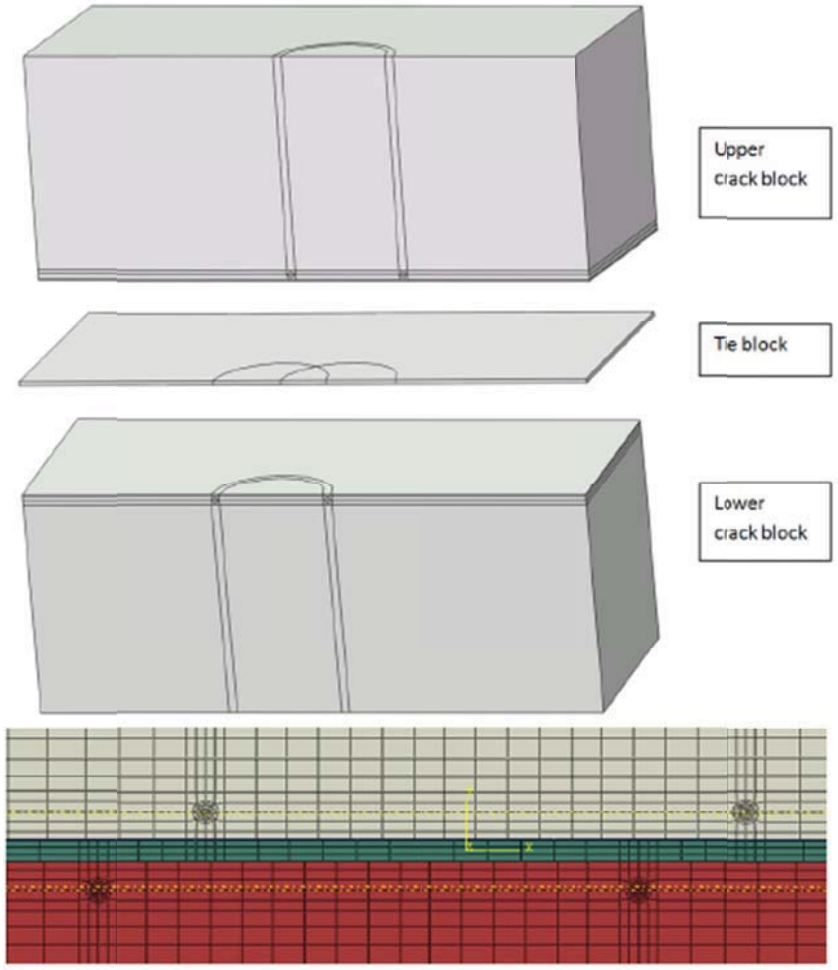

Figure 2-5 FEM model for overlapping parallel surface cracks [20].

The essential mesh design applied for this study is almost the same as the one used in the Needham's study where validity and convergence study of the mesh design is discussed in Needham [20]. Major modification made on the model is the mesh design around the crack tips. Base on the inner and outer tube radius sensitivity study from chapter 2.2.2, radius of the inner tube is modified to be $1/10^{th}$ of the outer tube radius where $1/4^{th}$ is used for the Needham's model. Finer meshes are adopted around the crack tip to increase the accuracy of the analysis and to handle shallower cracks also.

Schematic of the final FEM model constructed for the author's study is provided in the figure below.

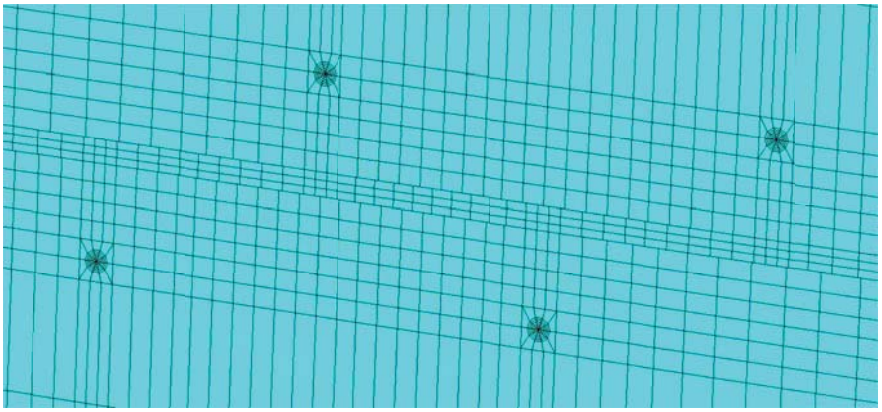

Figure 2-6 Final design of the three dimensional FEM model with overlapping parallel semi-elliptical surface cracks.

To verify the robustness of the final FEM model developed for this study, a series of overlapping parallel crack cases are compared with existing solutions from Kamaya [14] and Needham [20]. Kamaya provided SIF profiles along the crack front for various crack overlapping distances, S/a, at a fixed vertical distance, H/a, of 0.3 (Figure 2-7 (a)). Results obtained using the author's FEM models are plotted against the Needham's results in Figure 2-7 (b). As shown in the figure, FEM results for various crack interaction configurations compare favorably with Kamaya and Needham. Thus, the final mesh design is found to be robust.

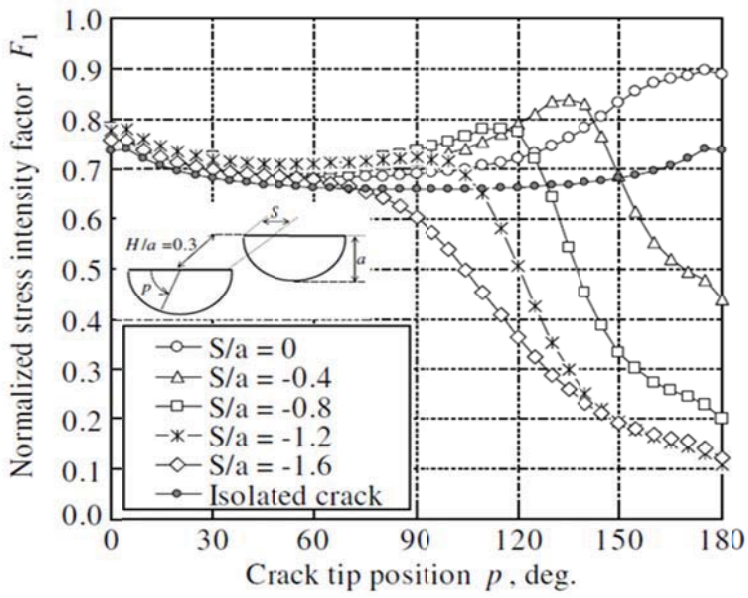

(a) Results from Kamaya [14]

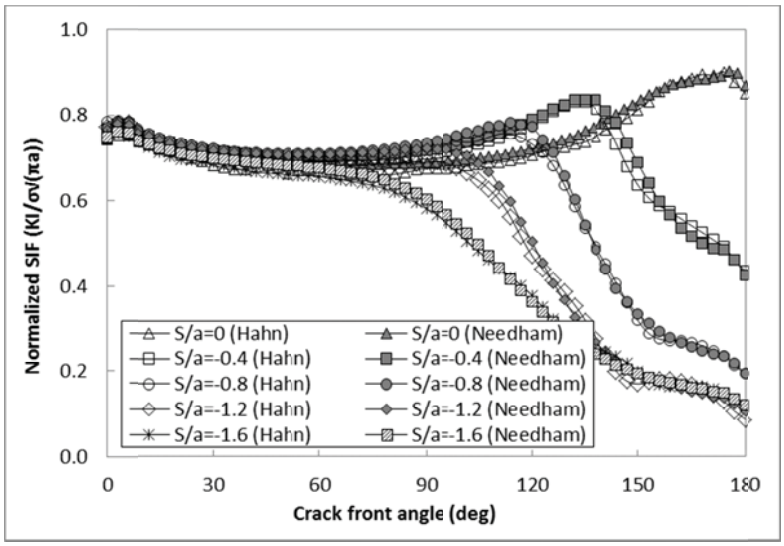

(b) Results from Needham and the author

Figure 2-7 Comparison of normalized mode I SIF along crack front for two identical parallel cracks for varying horizontal separations (S/a).

In this chapter, FEM modeling method and some background information related to the crack analysis in Abaqus are discussed. As the model is evolved from

simple two dimensional model to advanced three dimensional model, result from each model are compared with existing solution. The output from the final model is also compared with Needham and Kamaya's results. Good agreements between the solutions are observed, and it is validated that the final FEM developed is robust and suitable to be used for this study.

CHAPTER 3. RESULTS

3.1 Symmetric Crack Shapes

SIF are obtained from Abaqus for various elliptical crack shapes as a function of the parametric angle, θ. The dimensions of the crack are defined in the figure below.

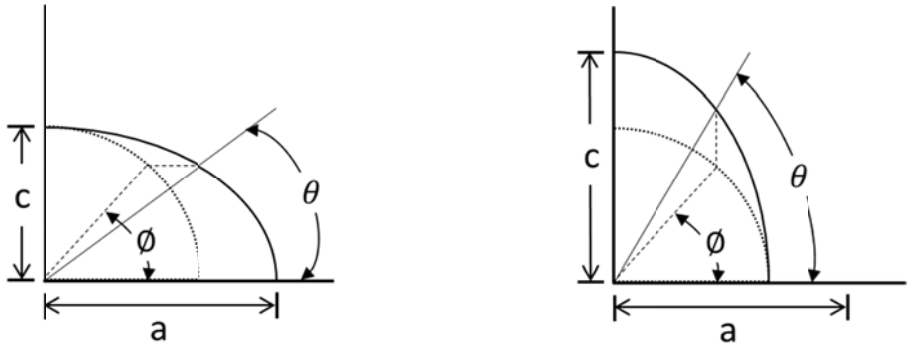

Figure 3-1 Definition of parametric angle.

Since two cracks have identical crack shape, stress profiles of the cracks are equal in opposite direction. Thus, results for the bottom crack are only provided in this section. The SIF result obtained from the finite element analysis is normalized against the thickness of the model to compare the SIF of different crack shapes as

$$\frac{K_I}{\sigma\sqrt{t}} \tag{3.1}$$

where σ is the applied tensile stress and t is the thickness of the plate.

3.1.1 Selection of Parallel Crack Configurations

The test cases used for this research are expanded from the Needham's [20] test case for the semi-elliptical crack shape (c/a) of 0.9. Parameters for the parallel overlapped surface cracks used in this study are described in the figure below.

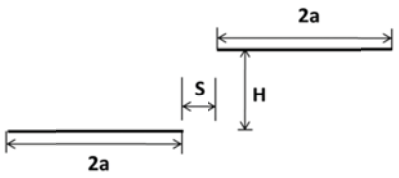

(a) Non overlapped (S > 0)

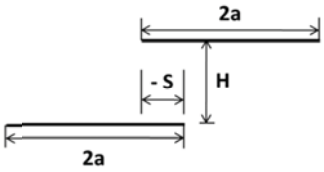

(b) Overlapped (S < 0)

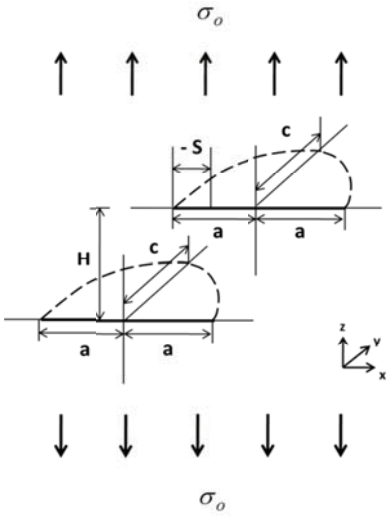

(c) Overlapped (S < 0) cracks in 3D

Figure 3-2 Definition of parallel overlapped semi-elliptical surface cracks.

Needham's study is focused on the cases where two cracks are overlapped over small vertical distances. However, in order to investigate the full effect of relative distance between cracks, cases with wider range of crack spacing are needed. The test cases for this research are shown in Figure 3-3. The developed test cases deals with multiple vertical separations (H/a) between 0.3 and 2 where horizontal separations (S/a) are varied from -2 to 2 for four different crack shapes (c/a = 0.7, 0.9, 1, and 1.2).

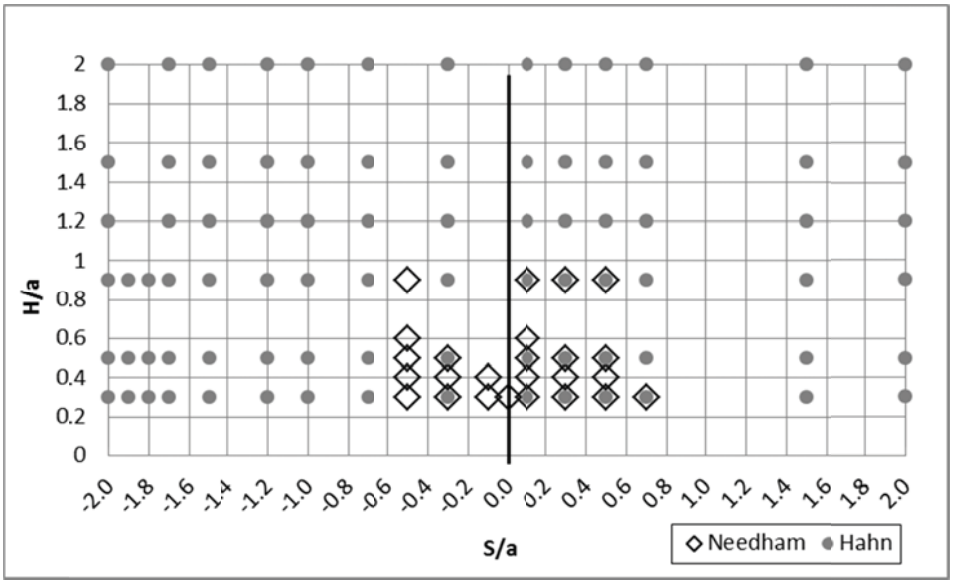

Figure 3-3 Test matrix for symmetric parallel overlapped surface cracks.

Total of 268 models are developed for the identical parallel crack interaction study. Few test cases for c/a = 0.9 and 1 have identical crack geometries to the Needham's [20] and Kamaya's [14] test cases so that the results obtained from this study can be compared with those previous studies.

3.1.2 Mode I Stress Intensity Factor

3.1.2.1 Effect of the horizontal separation

Figure 3-4 below shows the normalized mode I SIF, K_I, profile along the crack front of a semi-elliptical surface crack (c/a = 0.7). The figure illustrates comparatively the behavior of K_I for varying horizontal separations (S/a) at a fixed vertical separation (H/a) of 0.3.

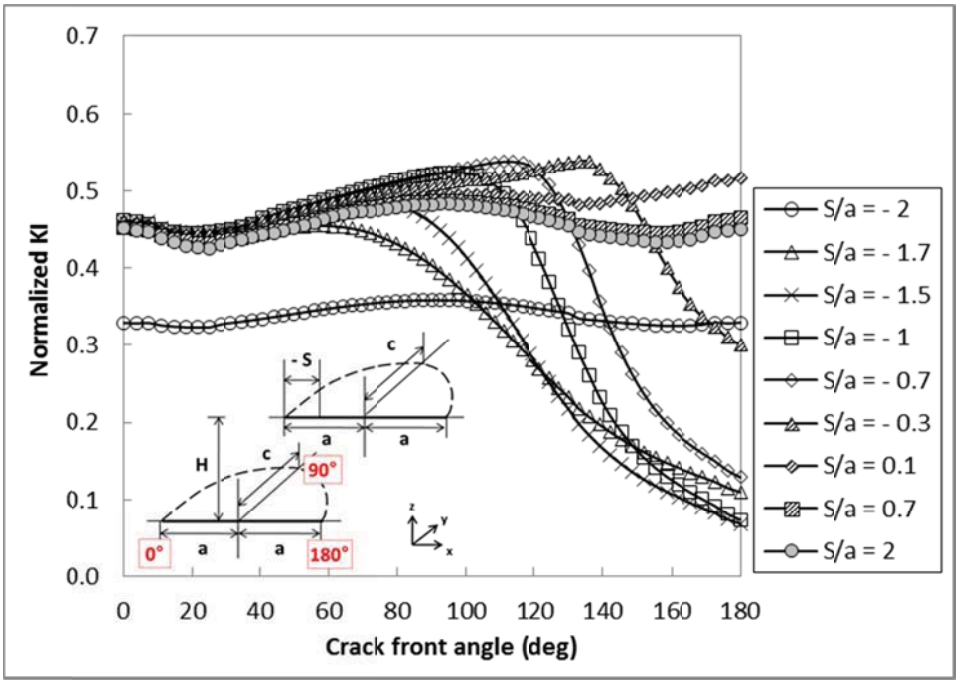

Figure 3-4 Normalized mode I SIF along the crack front for varying horizontal separations (S/a) at a fixed vertical separation (H/a) of 0.3 (c/a = 0.7).

While vertical separation between the cracks is fixed, normalized K_I profile along the crack front, which is varied from -2 to 2, are plotted on the same figure. As shown in the figure above, SIF near inner crack tip (180°) is amplified as the neighboring crack approaches. The maximum K_I is located around the inner crack tip before two cracks are overlapped. Once two cracks start to overlap (S < 0), the stress field of the bottom crack is shielded from the adjacent crack, and the SIF near the inner crack tip are decreased. Due to the stress shielding effect, the location of the maximum K_I location is also shifted along the crack front near the point where two crack fronts are intersected. Top view of two cracks' relative position for various horizontal separations is illustrated in Figure 3-5.

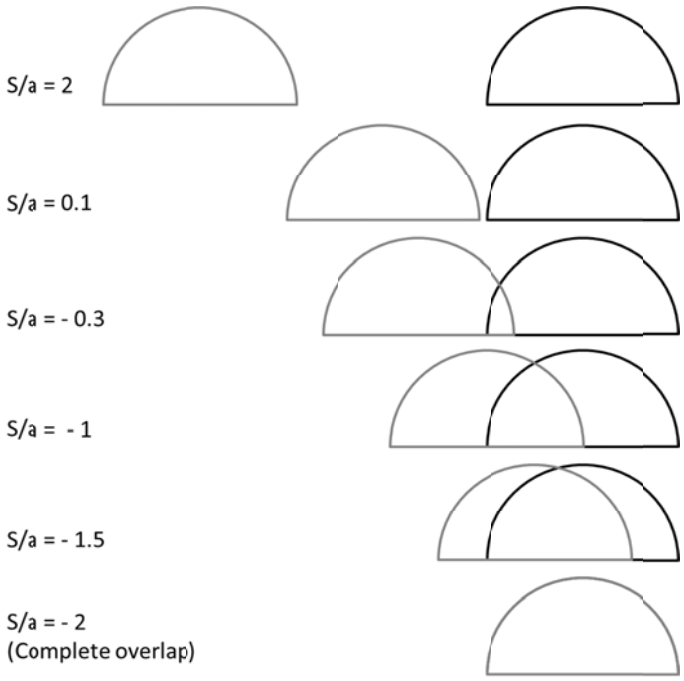

Figure 3-5 Top view of two interacting cracks with varying horizontal separation (S/a).

As majority of the cracks are overlapped (S/a $\geq$ -1.7), SIF near the inner crack tip started to increase again as shielding effect of the top crack diminished. It is found that the K_I profile of the completely overlapped cracks (S/a = -2) is identical to the profile of the isolated cracks (S/a = 2), but the SIFs for the completely overlapped cracks are smaller than the isolated cracks due to the shielding effect. K_Is around the outer crack tip remained almost the same as that of the isolated crack as the horizontal separation between two cracks is varied.

Crack interaction behaviors for the different vertical distances are plotted in Figure 3-6: H/a = 0.5, 0.9, 1.2, and 2. As the vertical distance between two cracks increases, both stress amplification and shielding effects caused by the adjacent crack

are reduced. As shown in Figure 3-6(d), when the cracks are separated far apart, the K_I profiles are converged, and the effect of horizontal separation is minimal.

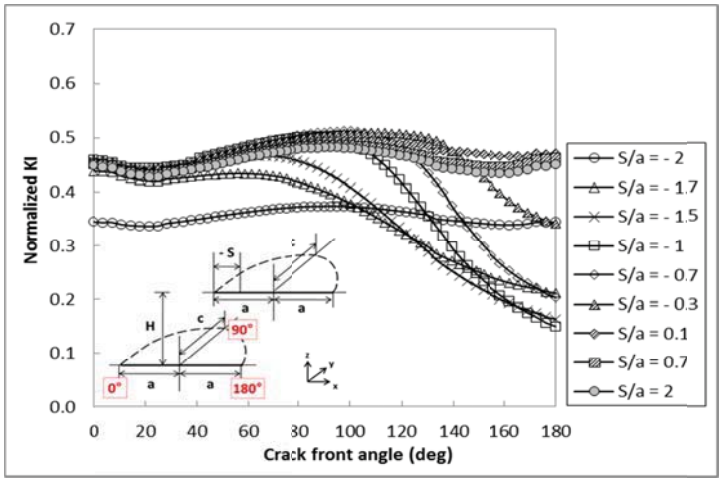

(a) H/a = 0.5

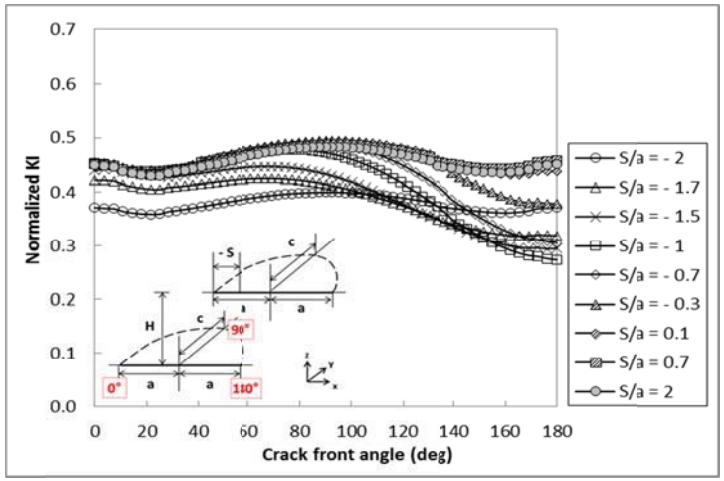

(b) H/a = 0.9

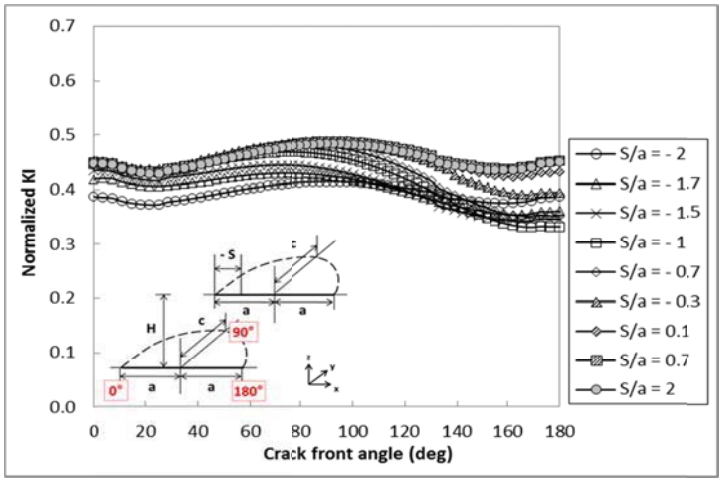

(c) H/a = 1.2

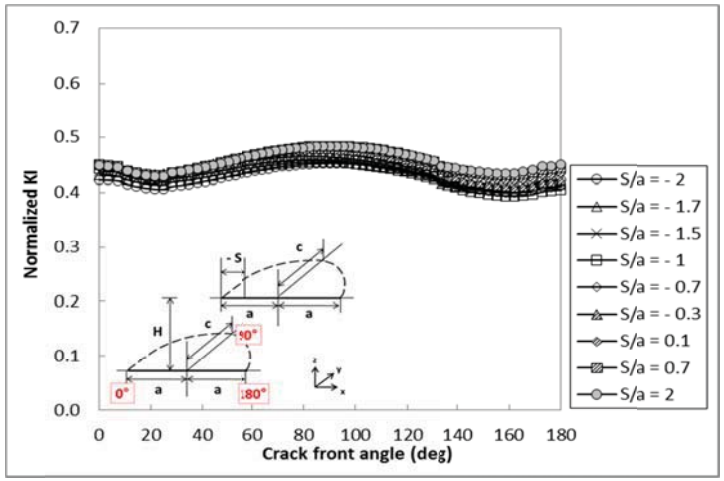

(d) H/a = 2

Figure 3-6 Normalized mode I SIF along crack front for varying horizontal separations (S/a) at fixed vertical separations (H/a) (c/a = 0.7).

3.1.2.2 Effect of the vertical separation

When a crack is isolated from its adjacent crack, (S/a = 2), stress field around the crack is not effected by the presence of the second crack regardless of the vertical separation. There is no sign of stress amplification and shielding effect where SIF profile is symmetric along the crack front. Same results are obtained for all cases developed for the horizontal separations of 2, and the magnitude of K_I are also identical between these cases (Figure 3-7).

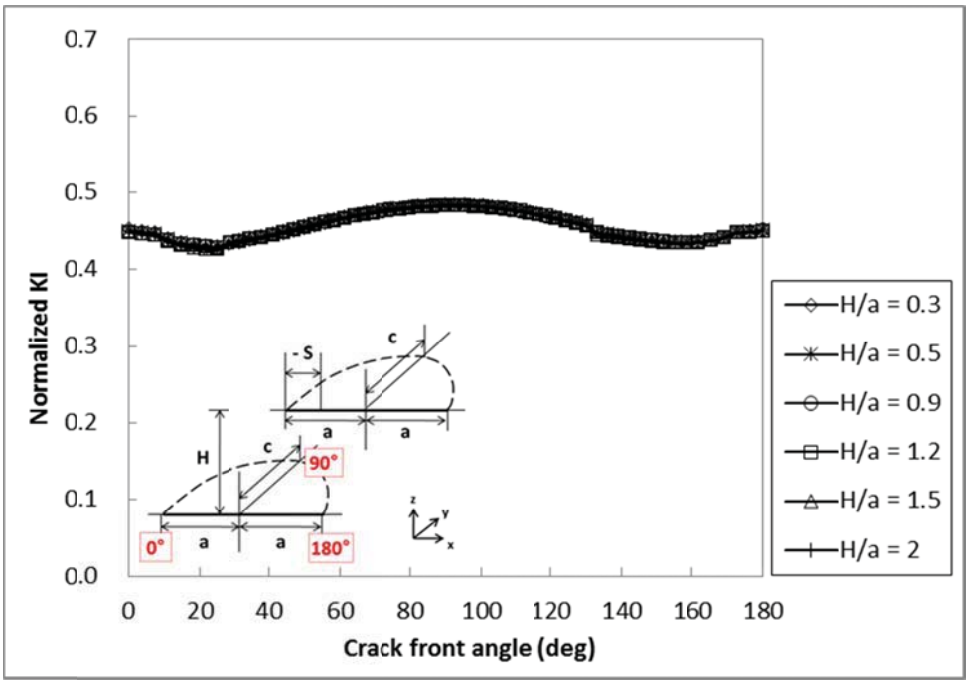

Figure 3-7 Normalized mode I SIF along the crack front for varying vertical separations (H/a) at a fixed horizontal separation (S/a) of 2 (c/a = 0.7).

For the cases where two cracks are completely overlapped (S/a = -2), K_I profile is also symmetric along the crack front as shown in Figure 3-8. However, when the adjacent crack is located right on top of the bottom crack, stress field of the crack is

interfered by the second crack. The bottom crack is under the stress shielding effect caused by the adjacent crack, and SIFs along the crack front are decreased. The stress shielding effect is significant for the smallest vertical separation between the cracks (H/a = 0.3): K_I at the crack tips are dropped by 27% from the isolated crack's solution. SIF for H/a of 0.3 is found to be the lowest among the five cases of the completely overlapped crack geometry. As the vertical separation between two cracks increases, stress shielding effect is reduced, and SIF profiles are converged to the isolated crack's SIF profile.

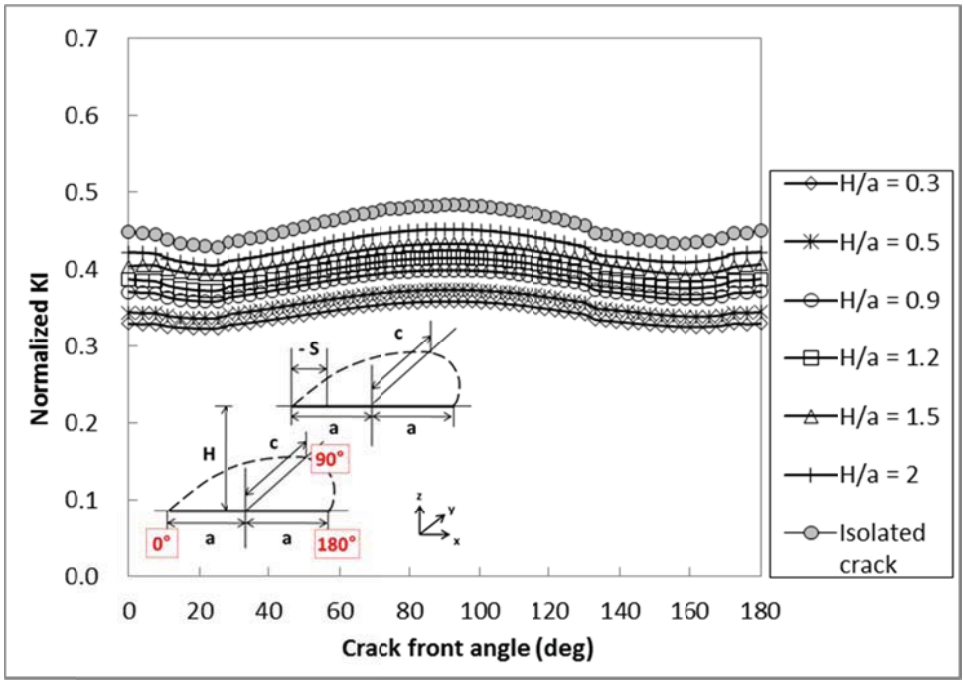

Figure 3-8 Normalized mode I SIF along the crack front for varying vertical separations (H/a) at a fixed horizontal separation (S/a) of -2 (c/a = 0.7).

Normalized K_I profiles for a fixed horizontal separation (S/a) of -1 are plotted for vertical separations between 0.3 and 2 in Figure 3-9. Stress amplification and shielding

effects are observed as two cracks are overlapped, and these effects are more obvious when cracks are located closer vertically. As shown in the figure, crack front regions under the stress shielding effect are about the same when the horizontal spacing between the cracks is the identical. It is also found that the stress amplification and shielding effects are significant when the adjacent crack is closely located from the bottom crack vertically. K_I for H/a = 0.3 is reduced by 84% at the inner crack tip (θ = 180°) from that of the isolated case where K_I for H/a = 2 is only reduced by 10%. Stress amplification is observed for H/a = 0.3 and 0.5 only. For these cases, the location of the maximum SIF is near two cracks' overlapping point. When the vertical separation is greater than 0.5, SIFs along the non-overlapped crack front region are about the same as that of H/a = 2. As the vertical distance between the cracks increases, stress shielding effect is decreased and the SIF profiles are converged to the isolated crack case.

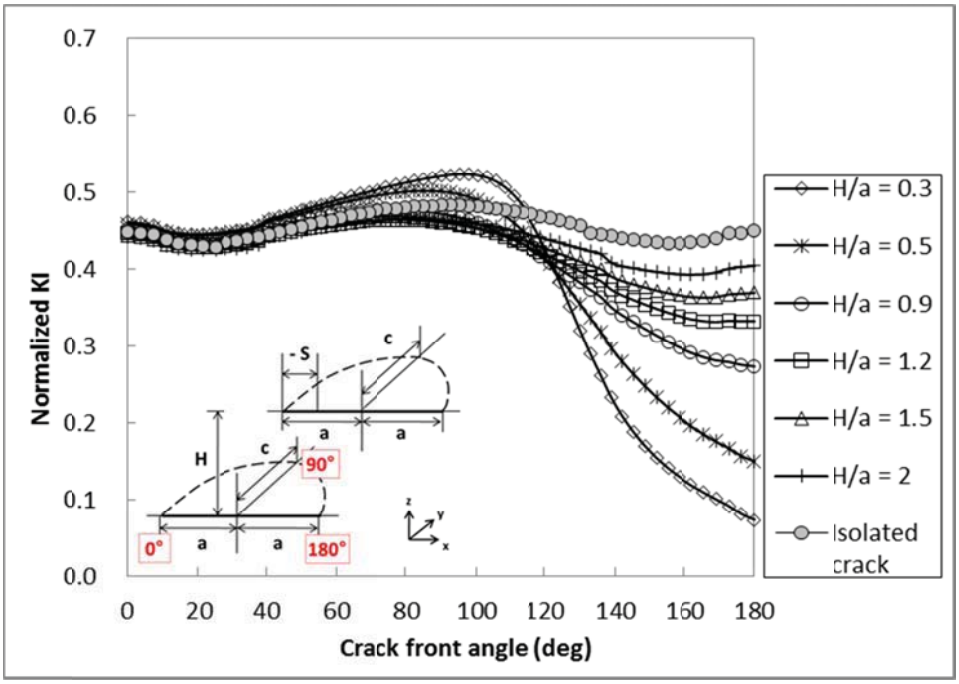

Figure 3-9 Normalized mode I SIF along the crack front for varying vertical separations (H/a) at a fixed horizontal separation (S/a) of -1 (c/a = 0.7).

Normalized K_I along crack front for varying vertical separations (H/a) are plotted in Figure 3-10 for fixed horizontal separations (S/a) of 0.1, -0.3, -0.7, and -1.5. Before two cracks are overlapped (see Figure 3-10(a)), SIFs of the bottom crack near the inner crack tip are amplified by the presence of the adjacent crack: 15% for H/a = 0.3 and 5% for H/a = 0.5. When two cracks are overlapped (s/a < 0), both stress amplification and shielding behaviors are observed in the plot. For all cases, these effects are reduced as the vertical separation increases, and SIF profiles are converged to the profile of isolated crack. Normalized K_I profiles for the crack shapes of 0.9, 1, and 1.2 are provided in Appendix A.

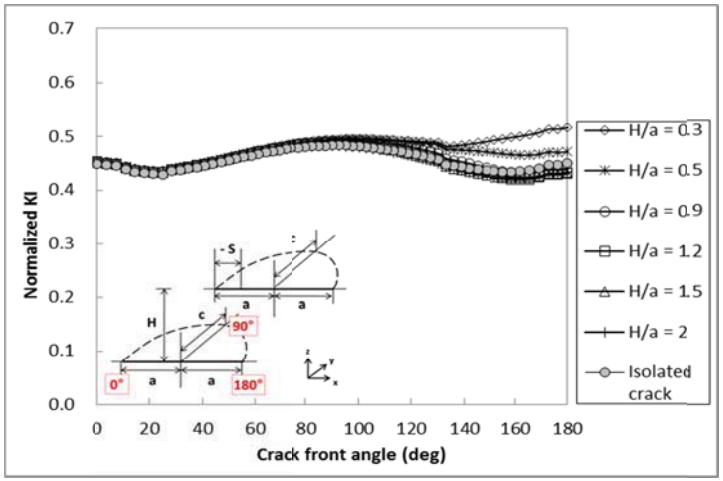

(a) S/a = 0.1

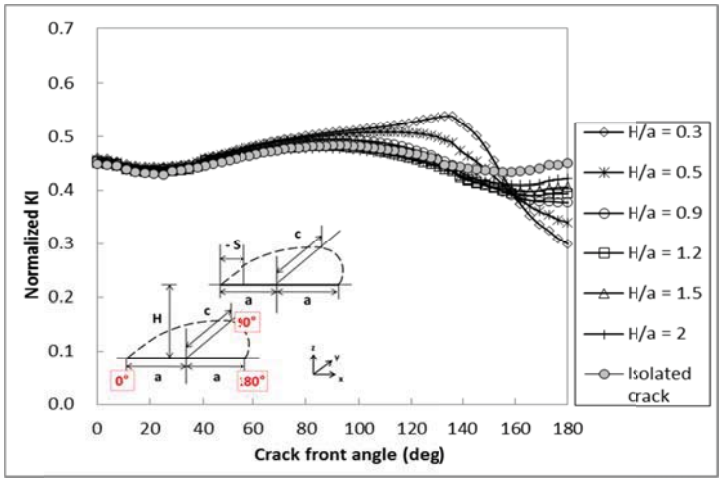

(b) S/a = - 0.3

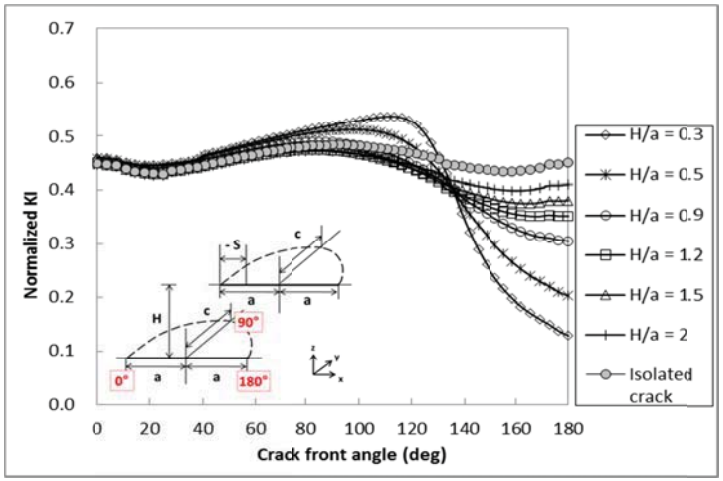

(c) S/a = -0.7

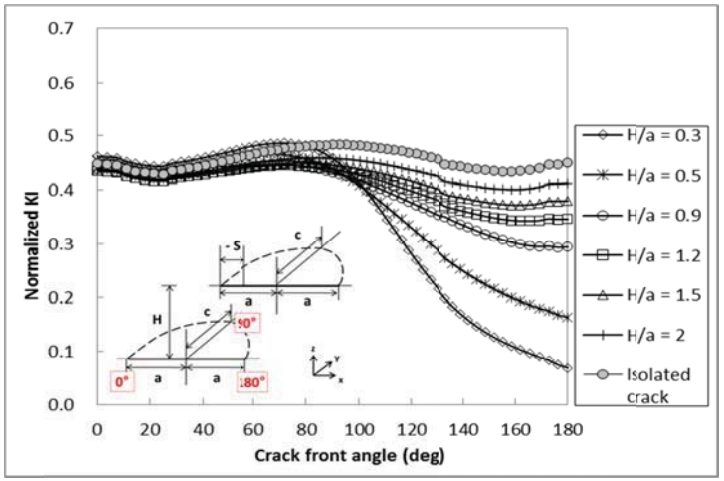

(d) S/a = -1.5

Figure 3-10 Normalized mode I SIF along crack front for varying vertical separations (**H**/a) at fixed horizontal separations (S/a) (c/a = 0.7).

3.1.2.3 Variation of the mode I stress intensity factor

Normalized mode I SIFs at inner and outer crack tips of the bottom crack are plotted in Figure 3-11 for a better understanding of the effect of the horizontal separation. SIFs for the crack shape (c/a) of 0.9 are presented in this section since the most test cases are developed for c/a of 0.9. Also, horizontal separations in the range of $-2 \leq S/a \leq 2$ at vertical separation of 0.3 are selected because the stress shielding and amplification effects are significant when the distance between two cracks is close.

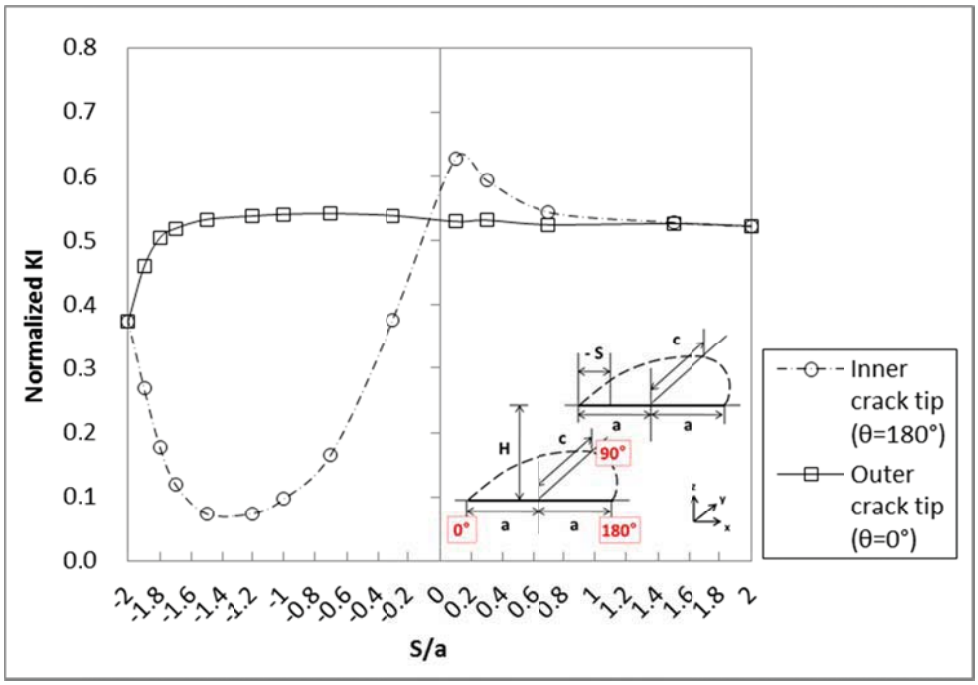

Figure 3-11 Normalized mode I SIF at inner and outer crack tips for varying horizontal separations (S/a) at a fixed vertical separation (H/a) of 0.3 (c/a = 0.9).

In Figure 3-11, it is clear that the inner tip of the crack is more sensitive to the crack overlap than the outer crack tip. The outer crack tip does not experience significant SIF variations until S/a is smaller than -1.7. However, the inner crack tip

experienced both stress amplification and shielding effects while K_I at the outer crack tip remained about the same until majority of two cracks are overlapped. For both tips, K_I converges to that of isolated crack when the horizontal separation between two cracks (S/a) is large. It is found that the K_I is the highest just before the cracks overlap at the inner crack tip. As two cracks overlap, SIF at the inner crack tip decreased dramatically by 86% from that of isolated crack until more than half of the crack area (S/a > -1.5) is overlapped. Once majority of the crack area is overlapped, K_I is increased again and converged to that of completely overlapped case. As shown in the previous section (Figure 3-7 and Figure 3-8), K_I profile of S/a = -2 and 2 are symmetric along the crack front. Thus, K_I at the inner crack tip and outer crack tip for both s/a = -2 and 2 are the same.

Variations of K_I at inner and outer crack tips for various vertical separations are plotted in Figure 3-12 and Figure 3-13. It is clear that SIFs are most sensitive for H/a = 0.3 and least sensitive for H/a = 2 among the results provided. Mode I interaction is diminished and SIF profile is converged as the vertical separation is increased. For the outer crack tip (see Figure 3-13), mode I interaction is not observed when cracks are overlapped; and only small amount of mode I interactions are observed for S/a less than 0. Interestingly, stress amplification effects are observed for H/a of 0.3 and 0.5 where S/a is between -1.2 and 0.3. When S/a is less than -1.2, stress shielding is effective for all vertical separations.

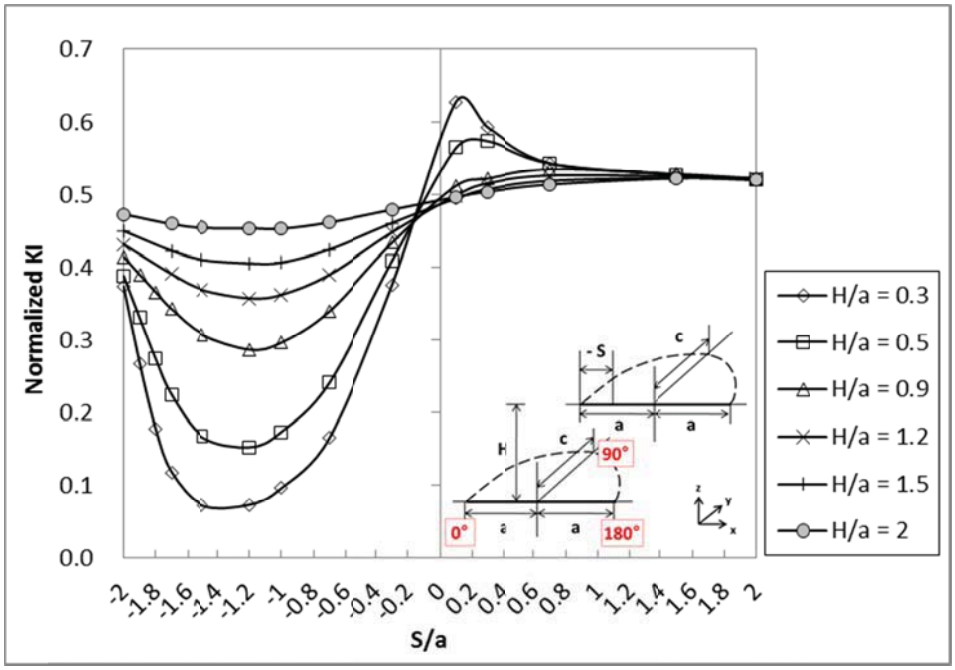

Figure 3-12 Variation of normalized mode I SIF at inner crack tip ($\theta = 180°$) for various vertical separations.

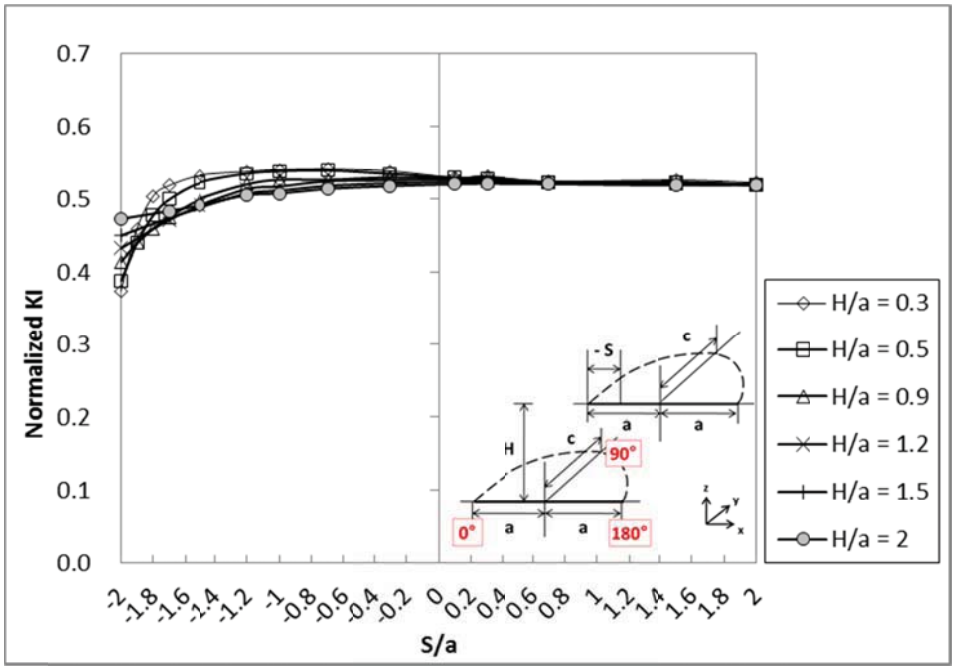

Figure 3-13 Variation of normalized mode I SIF at outer crack tip ($\theta = 0°$) for various vertical separations.

In this chapter, variation of K_I along the crack front is discussed for two parallel symmetric surface cracks with various horizontal and vertical separation distances. It is found that K_I around inner crack tip is amplified as two parallel cracks approach to each other. Then, once two cracks are overlapped, K_I started to decrease due to the stress shielding effects. These SIF variations are observed to be significant when vertical separation distance between two cracks is small, and SIF profiles are converged as vertical separation increases.

3.1.3 Mode II Stress Intensity Factor

Engineering structures are subjected to complex loading condition. Therefore, crack growth under the mixed mode loading condition must be investigated especially when interaction between cracks are existent. In this chapter, mode II stress intensity factor (K_{II}) is analyzed the same way as the mode I stress intensity factor (K_I) in Chapter 3.1.1.

3.1.3.1 Effect of the horizontal separation

Figure 3-14 shows the normalized mode II SIF profile along the crack front of a semi-surface crack (c/a = 0.7) over the range of $-0.3 \leq H/a \leq 2$ at S/a of 2. When the horizontal distance between two cracks is greater than 0.3, mode II interaction between the cracks are minimal. Especially when two cracks are isolated from each other (S/a = 2), K_{II} is essentially zero, and the crack opening is purely under mode I. However, as the

cracks approach each other, the crack front experiences mixed mode loading condition near the inner tip: K_{II} around inner crack tip decreases and becomes negative where crack will be deflected in a positive direction due to a negative K_{II} value (refer to Chapter 2.1.2). Then, K_{II} near the inner crack tip starts to increase as about 1/3 of the crack length is overlapped (S/a = - 0.7). When the half of the crack length is overlapped (S/a = -1), K_{II} around crack front overlapping point (~120°) also starts to increase and becomes positive: crack propagation direction will be switched to a negative direction. As the majority of the cracks are overlapped (S/a < -1.5), K_{II} along the entire crack front increases and becomes positive, and the SIF profiles are converged to the SIF profile of completely overlapped crack configuration (S/a = -2). It is found that when two cracks are completely overlapped, K_{II} interaction is observed in the entire crack front area and is symmetric along the crack front.

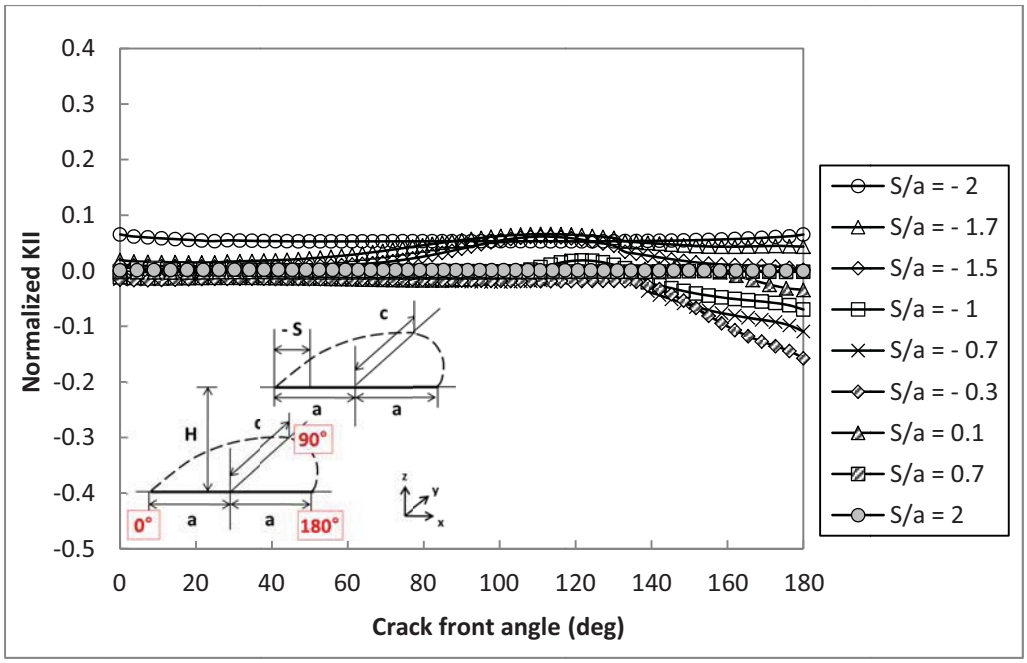

Figure 3-14 Normalized mode II SIF along the crack front for varying horizontal separations (S/a) at a fixed vertical separation (H/a) of 0.3 (c/a = 0.7).

In Figure 3-15, profiles of the normalized K_{II} are plotted in the same way as the mode I SIF as shown in the previous chapter. Crack interaction behaviors for H/a of 0.5, 0.9, 1.2, and 2 are provided. As the vertical distance between two cracks increases, mode II loading effect is diminished and the K_{II} profiles are converged to zero.

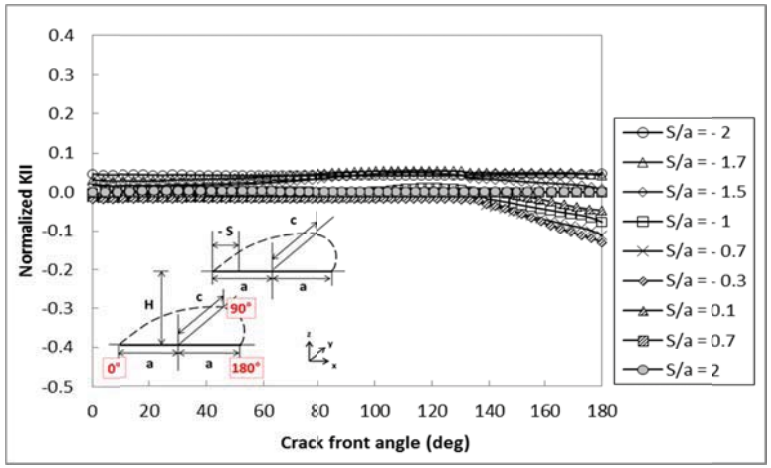

(a) H/a = 0.5

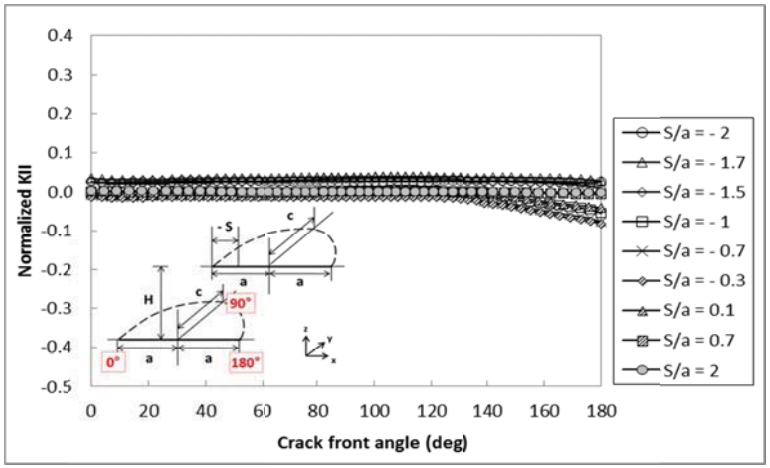

(b) H/a = 0.9

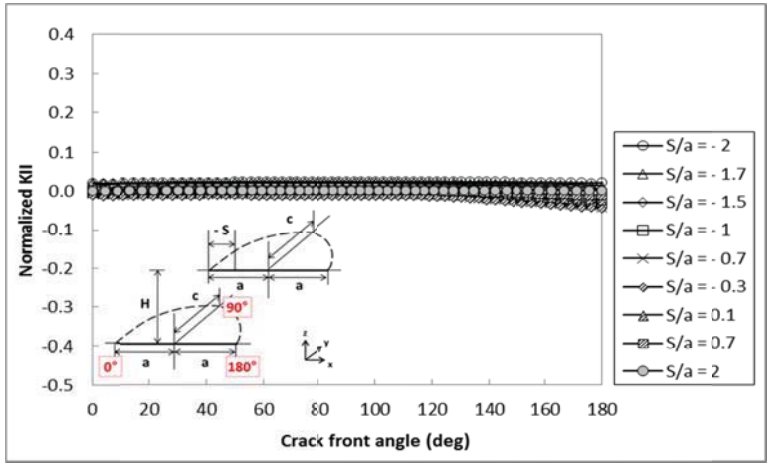

(c) H/a = 1.5

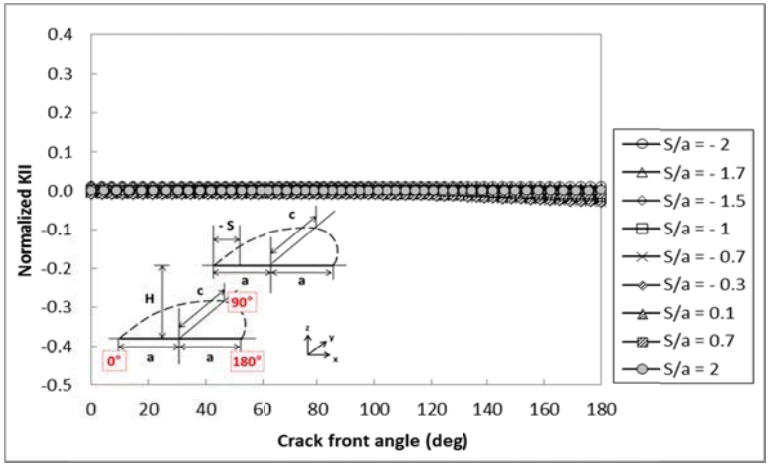

(d) H/a = 2

Figure 3-15 Normalized mode II SIF along crack front for varying horizontal separations (S/a) at fixed vertical separations (H/a) (c/a = 0.7).

3.1.3.2 Effect of the vertical separation

Normalized K_{II} along the crack front at S/a of 2 for various vertical separation distances within the range of -0.3 ≤ H/a ≤ 2 are shown in Figure 3-16. When two cracks are isolated from each other (S/a = 2), K_{II} is essentially zero regardless of the vertical separation distance between two cracks, and mode II loadings are not observed.

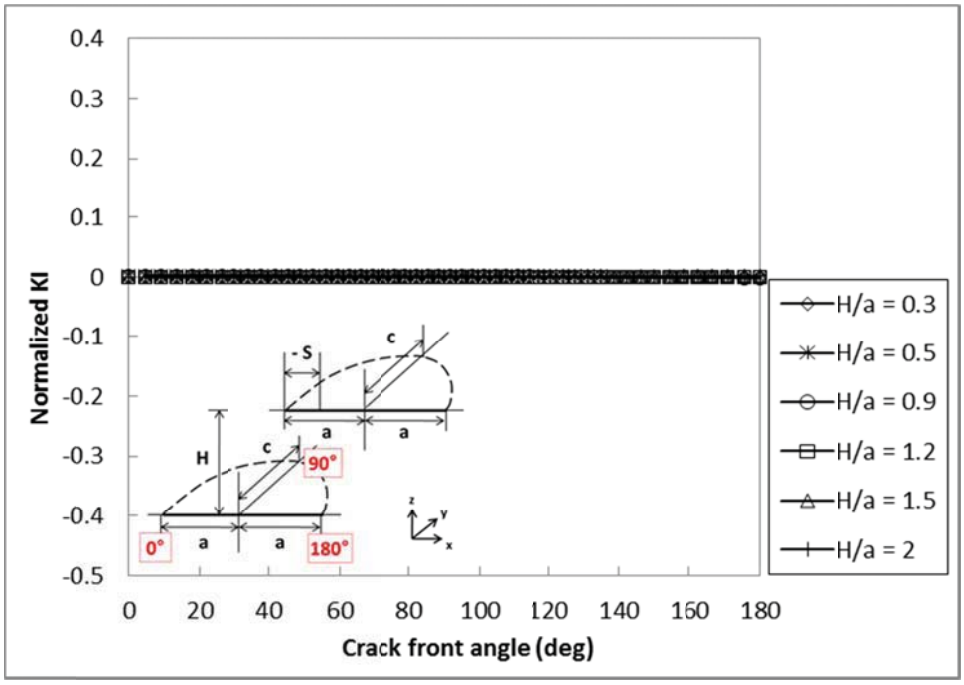

Figure 3-16 Normalized mode II SIF along the crack front for varying vertical separations (H/a) at a fixed horizontal separation (S/a) of 2 (c/a = 0.7).

Normalized K_{II} along crack front for varying vertical separations (H/a) are plotted for fixed horizontal separations (S/a) of 0.1, -0.3, -1, and -1.5. It is shown that the K_{II} interaction begins around S/a = 0.1 and increased its effect as the overlap increase. Therefore, plots for four horizontal separation cases in which S/a is in the rage of -2 < S/a ≤ 0.1 are included in Figure 3-17.

Similar to K_I interactions, K_{II} interactions are more obvious when cracks are located closer vertically. However, the effect of vertical separations on K_{II} interactions is not as significant as seen in K_I interactions. For all cases, mode II loading effects are reduced as the vertical separation increases, and SIF profiles are converged to the profile of the isolated crack.

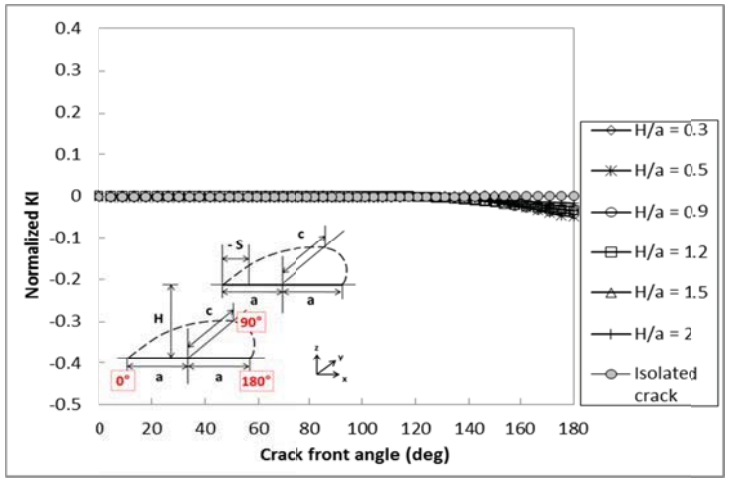

(a) S/a = 0.1

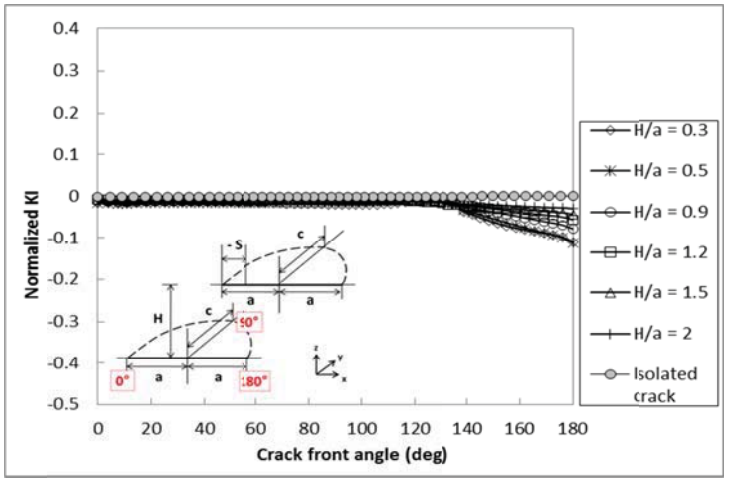

(b) S/a = - 0.3

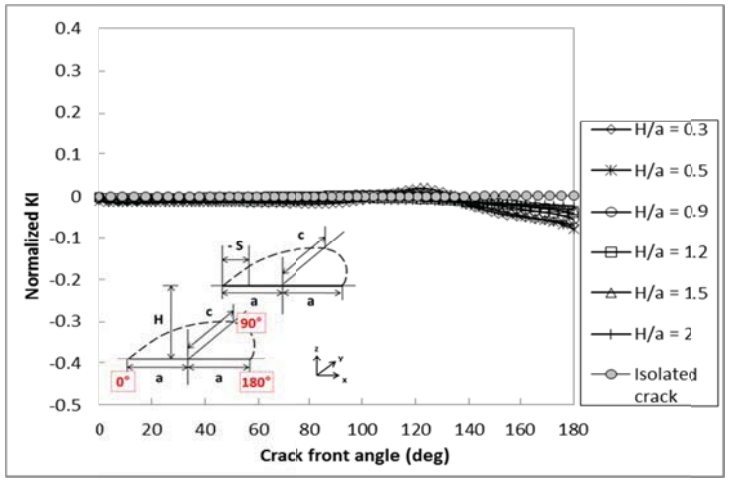

(c) S/a = - 1

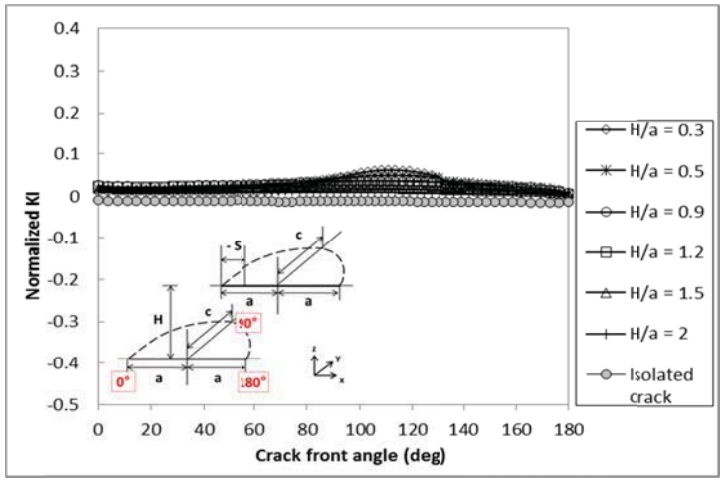

(d) S/a = -1.5

Figure 3-17 Normalized mode II SIF along crack front for varying vertical separations (H/a) at fixed horizontal separations (S/a) (c/a = 0.7).

Figure 3-18 shows K_{II} along the crack front for various vertical separation distances within the range of -0.3 ≤ H/a ≤ 2 at a fixed horizontal separation of S/a = -2. As shown in the figure. K_{II} profiles are symmetric along the crack front for all cases when two cracks are completely overlapped. As the vertical separation between two cracks increases, mode II loading effect diminishes, and KII along the crack front is converged to zero.

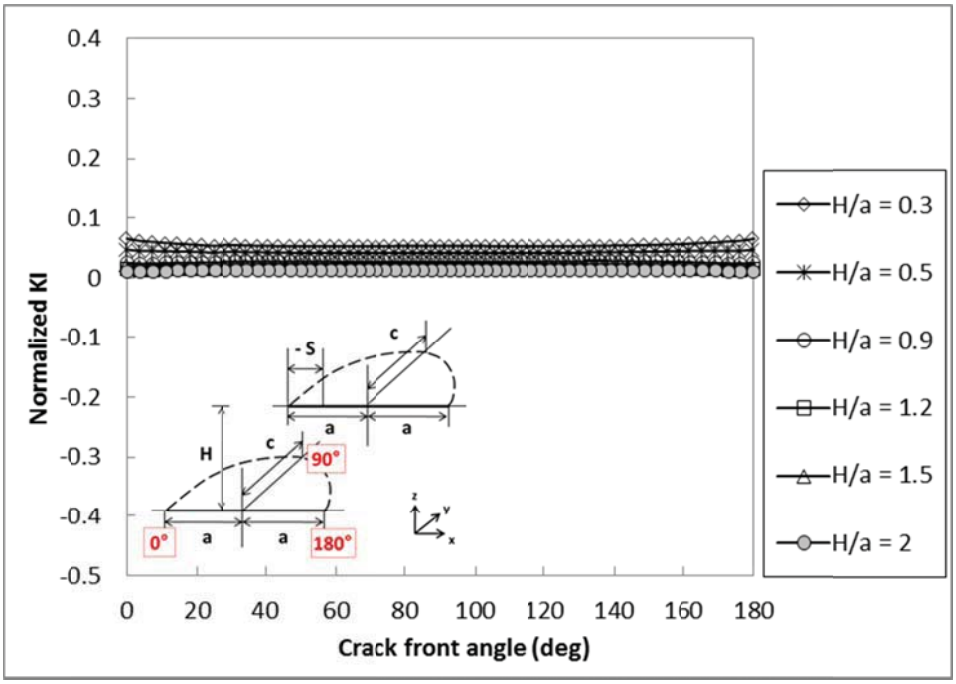

Figure 3-18 Normalized mode II SIF along the crack front for varying vertical separations (H/a) at a fixed horizontal separation (S/a) of -2 (c/a = 0.7).

3.1.3.3 Variation of the mode II stress intensity factor

The mode II SIFs are extracted from the models for the inner and outer tips and plotted in Figure 3-19. The plot shows that K_{II} of the inner tip begins to decrease at S/a = 0.3 and K_{II} is minimum at S/a = -0.3. Then, it increases as the tips pass, and the sign

changes from negative to positive at S/a = -1.5. K_{II} of the outer tip within the horizontal separation range of -1.5 < S/a ≤ 2 is essentially zero, indicating that the mode II interaction is not introduced while the inner crack tips approach and then pass one another. At the outer crack tip, the interaction begins when majority of the cracks are overlapped (S/a ≤1.5). In other words, crack grows straight at the outer crack tip for most cases, and crack grows in negative direction only when the inner crack tip of the adjacent crack is near the outer tip of the bottom crack. It is clear that the inner tip of the crack is more sensitive to the overlap than the outer crack tip.

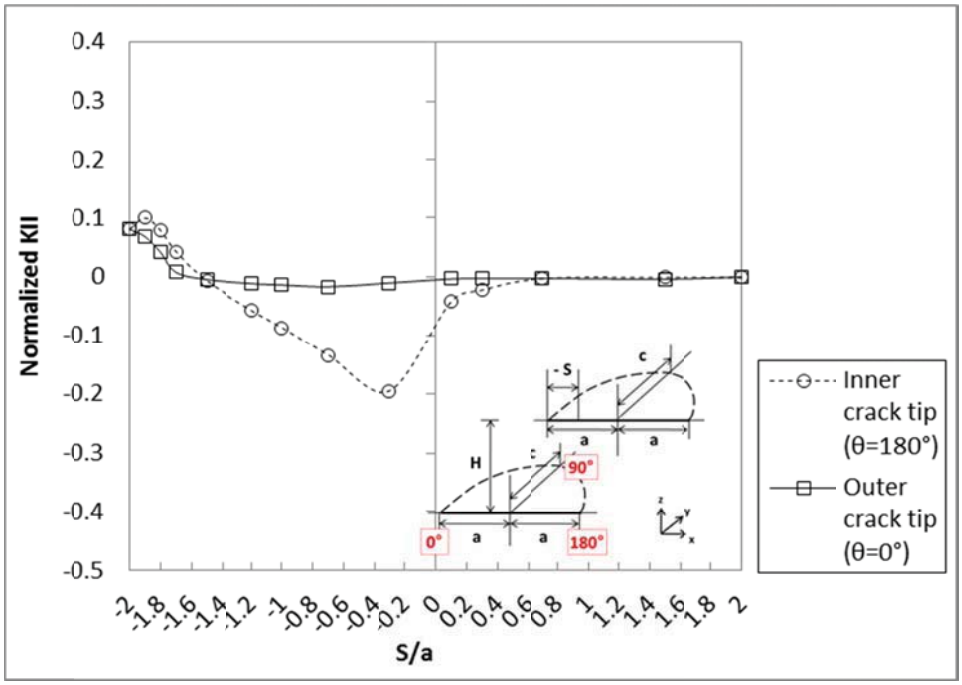

Figure 3-19 Normalized mode II SIF at inner and outer crack tips for varying horizontal separations (S/a) at a fixed vertical separation (H/a) of 0.3 (c/a = 0.9).

Variations of mode II SIF at inner and outer crack tips for various vertical separations are plotted in Figure 3-20 and Figure 3-21. Similar to mode I interactions,

mode II interactions are most observed for H/a = 0.3 least observed for H/a = 2. As the vertical separation distance between the cracks is increased, mode II interaction is diminished and K_{II} profiles are converged.

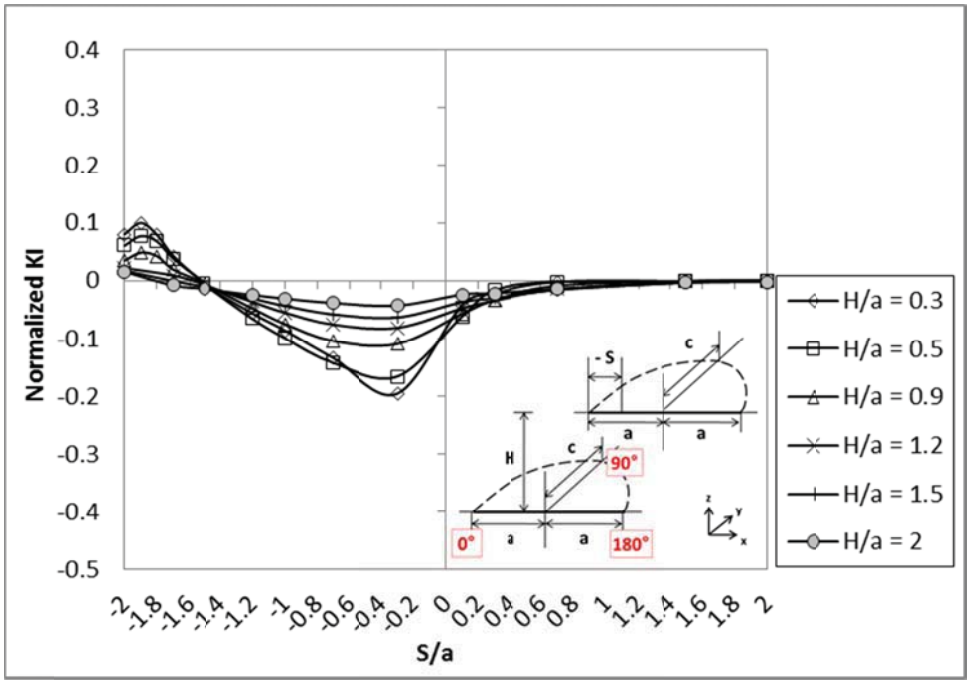

Figure 3-20 Variation of normalized mode II SIF at inner crack tip ($\theta = 180°$) for various vertical separations (c/a = 0.9).

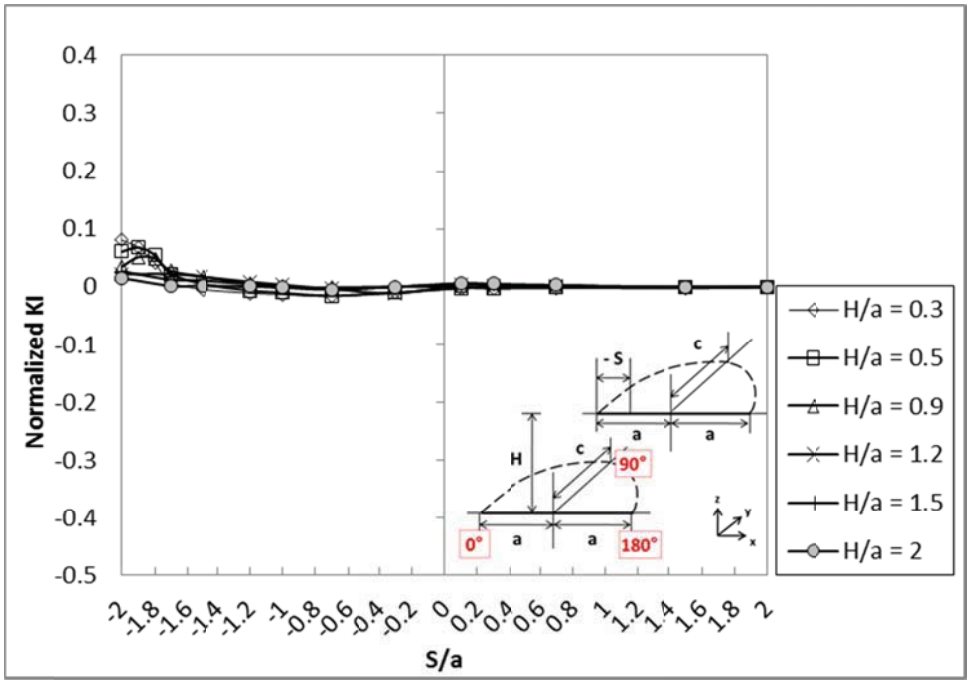

Figure 3-21 Variation of normalized II SIF at outer crack tip ($\theta = 0°$) for various vertical separations.

Changes in K_{II} along the crack front are discussed for interacting two parallel symmetric surface cracks when horizontal and vertical separation distances are varied. It is observed that K_{II} is zero when the cracks are isolated from each other. Magnitude of K_{II} around inner crack tip is increased (sign of K_{II} is negative) as two parallel cracks approach to each other. Then, magnitude of K_{II} is decreased where sign of K_{II} is changed from negative to positive as two cracks' overlapping area increases. Mode II interaction is not as significant as seen in Mode I interaction. However, as sign of K_{II} determines the direction of crack growth path, variation of K_{II} for various crack configurations are also discussed in this chapter.

3.1.3.4 Effect of the crack depth

Figure 3-22 shows the normalized mode I SIF for four different crack shapes over various vertical separations ($0.3 \leq H/a \leq 2$) for completely overlapped crack configuration (s/a = -2). The length of the cracks, *a*, are the same as 10, but the depth of cracks, *c*, are different as 7, 9, 10, and 12. SIF solutions for two parallel thru-wall cracks from Murakami's Stress Intensity Factors Handbook [18] are also plotted in the figure to find the effect of the crack depth in mode I crack interactions. As shown in the figure below, SIF increases and converges to thru-wall crack results as the depth of crack deepens regardless of the vertical separation distance.

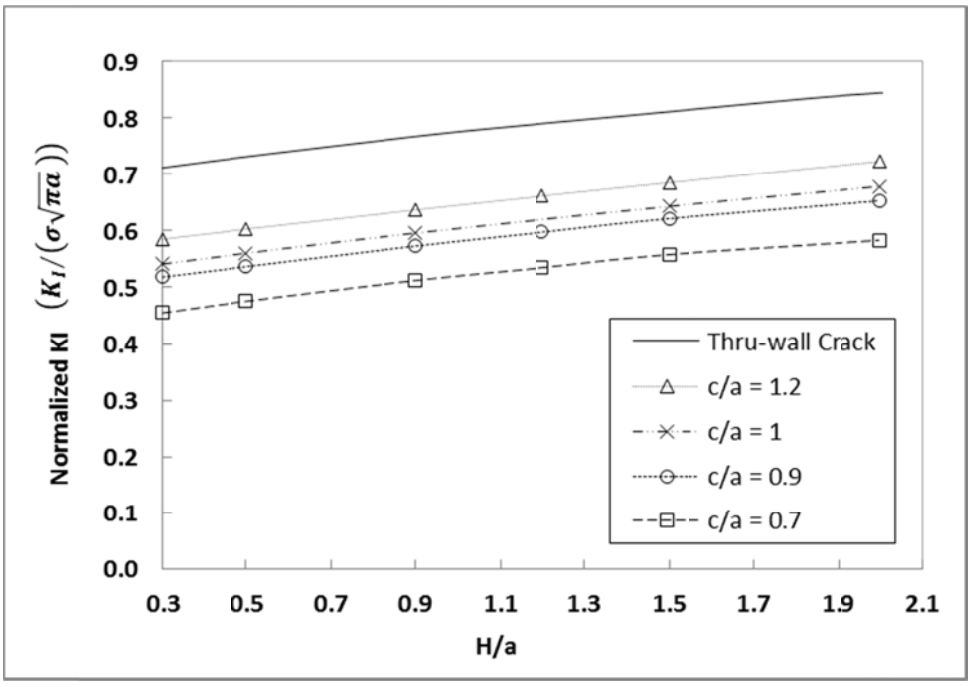

Figure 3-22 Normalized mode I SIF for different crack depths with various vertical separations at a fixed horizontal separation (S/a = -2).

In Figure 3-23, variations of mode I SIF over the range of $-2 \leq S/a \leq 2$ at vertical separation of 0.3 for four crack shapes are plotted. As shown in the figure, similar mode I crack interaction behaviors are observed for all crack shapes: c/a = 0.9, 1, and 1.2. Magnitudes of the SIFs are increased as the size of the crack is increased as expected where similar SIF profiles are found for all crack shapes. It is shown that the effect of crack depth on mode I interaction is greater before two cracks are overlapped (S/a > 0).

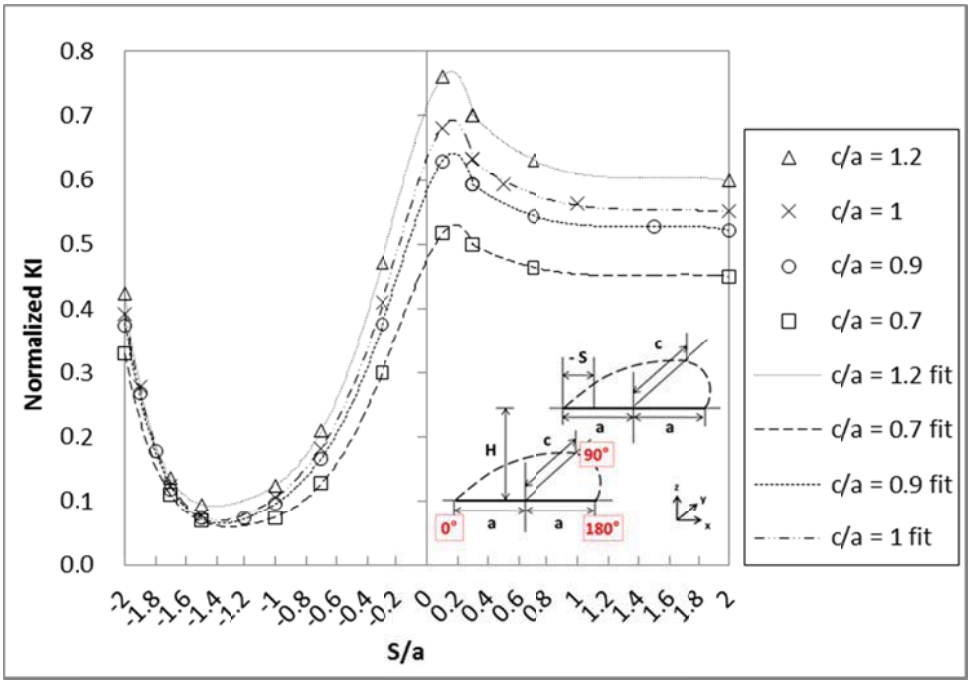

Figure 3-23 Normalized mode I SIF for two identical parallel cracks with various crack depths 1.2 at a fixed vertical separation of 0.3.

3.1.4 Polynomial Fits

In order to interpolate between the obtained results, relationships for normalized K_I and K_{II} with respect to the horizontal separation (S/a) and vertical separation (H/a) at the inner tip are determined for the crack shapes (c/a) of 0.7, 0.9, 1,

and 1.2. Figure 3-24 Curve fit for the normalized mode I SIF with varying horizontal distance (S/a) at a fixed vertical distance (H/a) for c/a = 0.7, 0.9, 1, and 1.2 and Figure 3-25 show the fitted polynomials of normalized K_I and K_{II} at fixed vertical separations within the range of $0.3 \leq H/a \leq 2$ for each crack shape.

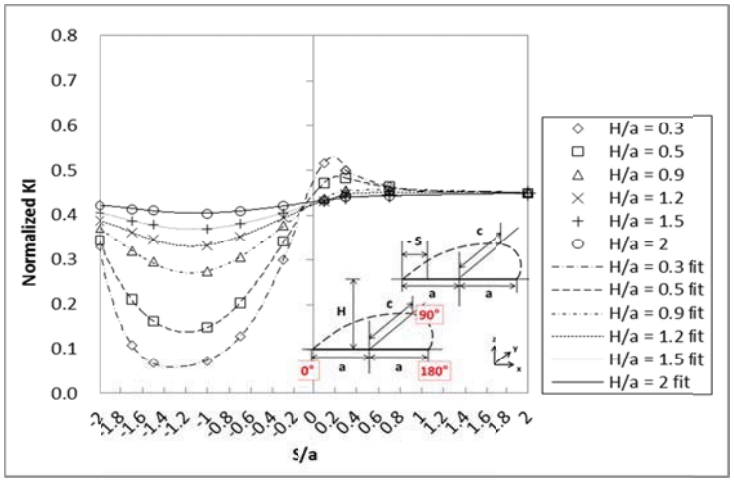

(a) c/a = 0.7

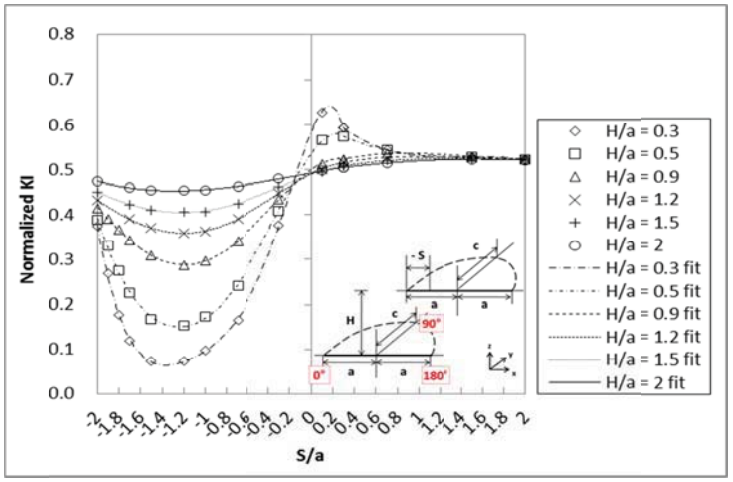

(b) c/a = 0.9

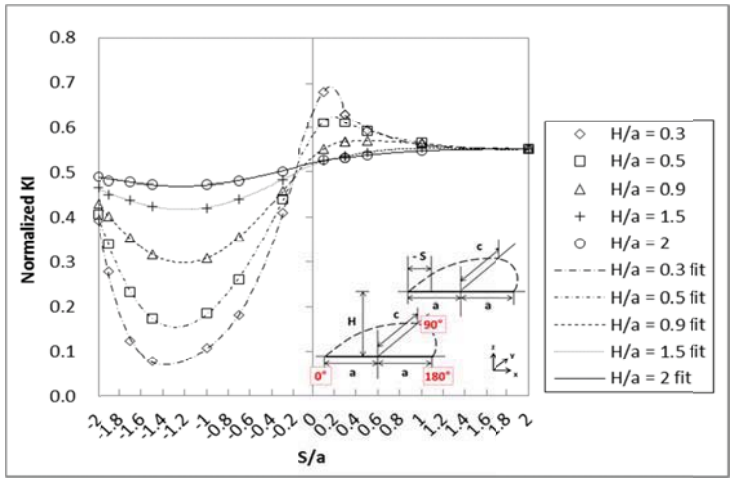

(c) c/a = 1

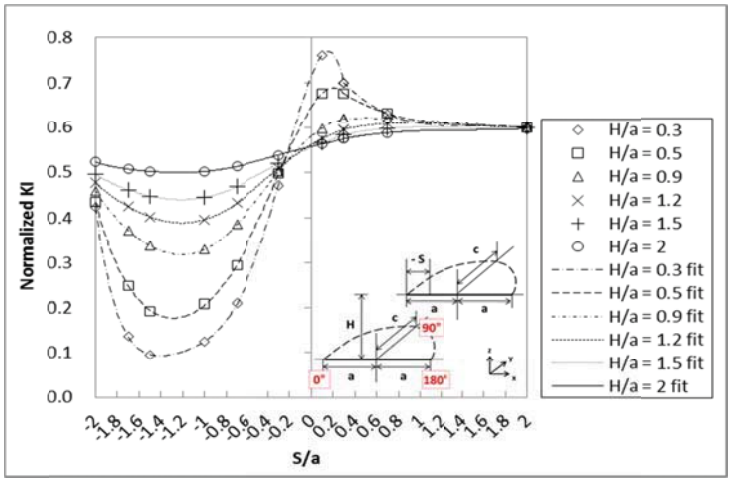

(d) c/a = 1.2

Figure 3-24 Curve fit for the normalized mode I SIF with varying horizontal distance (S/a) at a fixed vertical distance (H/a) for c/a = 0.7, 0.9, 1, and 1.2.

As seen in Figure 3-12 in chapter 3.1.2.3 and Figure 3-20 in chapter 3.1.3.3, SIF variations are irregular over the range of -2 ≤ S/a ≤ 2, it is not possible to obtain good regression line over the entire range. Thus, horizontal separation range is divided into two separate regions:

- K_I: $-2 \leq \mathrm{S/a} \leq 0.3 \;\&\; 0.3 < \mathrm{S/a} \leq 2$ for all crack shapes
- K_{II}: $\begin{cases} -2 \leq \mathrm{S/a} \leq 0.1 \;\&\; 0.1 < \mathrm{S/a} \leq 2 & \text{for c/a = 0.7, 0.9, 1} \\ -2 \leq \mathrm{S/a} \leq 0.3 \;\&\; 0.3 < \mathrm{S/a} \leq 2 & \text{for c/a = 1.2} \end{cases}$

The difference between the FEM results and the resulting curve fit solutions are less than 1 percent for all cases. Coefficients of the polynomial fits and coefficient of determination, r^2, of the regression lines for normalized K_I and K_{II} determined for each region are listed in Table 3-1 and Table 3-2, respectively. As an example, polynomial equation of normalized K_I value for c/a = 0.9 and H/a = 2 over the range of $-2 \leq \mathrm{S/a} \leq 2$ is reconstructed using the coefficients listed in Table 3-1:

$$\mathrm{Norm}\, K_I = -0.0094\left(\frac{S}{a}\right)^3 - 0.0008\left(\frac{S}{a}\right)^2 + 0.0452\left(\frac{S}{a}\right) + 0.4921 \qquad \text{for } -2 \leq \frac{S}{a} \leq 0.3$$

$$\mathrm{Norm}\, K_I = -0.0005\left(\frac{S}{a}\right)^3 - 0.0103\left(\frac{S}{a}\right)^2 + 0.0353\left(\frac{S}{a}\right) + 0.4949 \qquad \text{for } 0.3 < \frac{S}{a} \leq 2$$

Normalized K_I value for the horizontal distance (S/a) of -1.5 can be calculated as 0.4542 from the equation provided above.

Table 3-1 Coefficients of the polynomial fits and r^2 of normalized K_I for varying horizontal distance (S/a) between cracks at fixed vertical distances (H/a). Variable *x* in the table represents the horizontal distance (S/a).

		H/a											
		-2 ≤ S/a ≤ 0.3						0.3 < S/a ≤ 2					
		0.3	0.5	0.9	1.2	1.5	2	0.3	0.5	0.9	1.2	1.5	2
c/a = 0.7	x^6	-0.0329											
	x^5	-0.3914	-0.0513	0.0141	0.0185	0.0072	0.0072						
	x^4	-1.2943	-0.2774	0.0171	0.0543	0.0177	0.0177						
	x^3	-1.7561	-0.5993	-0.1151	-0.0038	-0.0173	-0.0173	-0.0301	-0.0148	0.0033	0.0053	0.0063	0.0003
	x^2	-0.7298	-0.3786	-0.1297	-0.0413	-0.0228	-0.0228	0.1358	0.0672	-0.0155	-0.0224	-0.0255	-0.0024
	x	0.4919	0.2928	0.1411	0.0894	0.0594	0.0594	-0.1996	-0.1045	0.0178	0.0287	0.0341	0.0095
	C	0.4763	0.4472	0.4270	0.4239	0.4249	0.4249	0.5476	0.5083	0.4512	0.441	0.4326	0.4383
	r^2	1	1	0.9993	0.9994	0.9978	0.9978	1	1	1	1	1	1
c/a = 0.9	x^6	-0.0835											
	x^5	-0.6878	-0.0541										
	x^4	-1.9205	-0.2910	-0.0520	-0.0264	-0.0129							
	x^3	-2.3440	-0.6567	-0.2528	-0.1288	-0.0670	-0.0094	-0.0468	-0.0242	0.0175	0.0118	0.0072	-0.0005
	x^2	-0.9343	-0.4509	-0.2332	-0.1041	-0.0494	-0.0008	0.2022	0.1078	-0.0769	-0.0532	-0.0377	-0.0103
	x	0.5803	0.3348	0.1705	0.1250	0.0845	0.0452	-0.2875	-0.1653	0.0946	0.0708	0.0608	0.0353
	C	0.5832	0.5353	0.4993	0.4906	0.4885	0.4921	0.6623	0.6148	0.5008	0.4994	0.4930	0.4949
	r^2	0.9998	0.9993	0.9999	0.9995	0.9994	0.9969	1	1	1	1	1	1

Table 3-1 Continued.

		H/a											
		-2 ≤ S/a ≤ 0.3						0.3 < S/a ≤ 2					
		0.3	0.5	0.9	1.2	1.5	2	0.3	0.5	0.9	1.2	1.5	2
c/a = 1	x^6	-0.0946	-0.0515										
	x^5	-0.7730	-0.3357										
	x^4	-2.1553	-0.8346	-0.0488		-0.0194	-0.0094						
	x^3	-2.6347	-1.0872	-0.2433		-0.0916	-0.0422	-0.0374	-0.0064	0.0179		0.0155	0.0034
	x^2	-1.0701	-0.5489	-0.2147		-0.0715	-0.0283	0.1751	0.0517	-0.0612		-0.0673	-0.0219
	x	0.6156	0.3855	0.2039		0.0937	0.0526	-0.2742	-0.1229	0.0480		0.0919	0.0460
	C	0.6340	0.5808	0.5324		0.5152	0.5197	0.6967	0.6420	0.5579		0.5122	0.5189
	r^2	0.9998	0.9998	1		0.9986	0.9937	0.9876	0.9983	0.9982		1	0.9988
c/a = 1.2	x^6		0.0051	0.0286	0.0194	0.0149	0.0109						
	x^5	-0.3458	-0.0664	0.1486	0.1065	0.0819	0.0553						
	x^4	-1.5770	-0.4237	0.2142	0.1719	0.1380	0.0880						
	x^3	-2.5215	-0.9241	-0.0867	-0.0116	0.0224	0.0225	-0.0554	-0.0278	0.0112	0.0173	0.0177	0.0120
	x^2	-1.2696	-0.6265	-0.2264	-0.1171	-0.0542	-0.0190	0.2536	0.1337	-0.0443	-0.0752	-0.0740	-0.0518
	x	0.6100	0.3854	0.2045	0.1443	0.1039	0.0577	-0.3836	-0.2227	0.0370	0.0944	0.0964	0.0763
	C	0.7145	0.6458	0.5798	0.5613	0.5547	0.5571	0.7949	0.7322	0.6132	0.5733	0.5602	0.5556
	r^2	1	0.9999	1	1	1	1	1	1	1	1	1	1

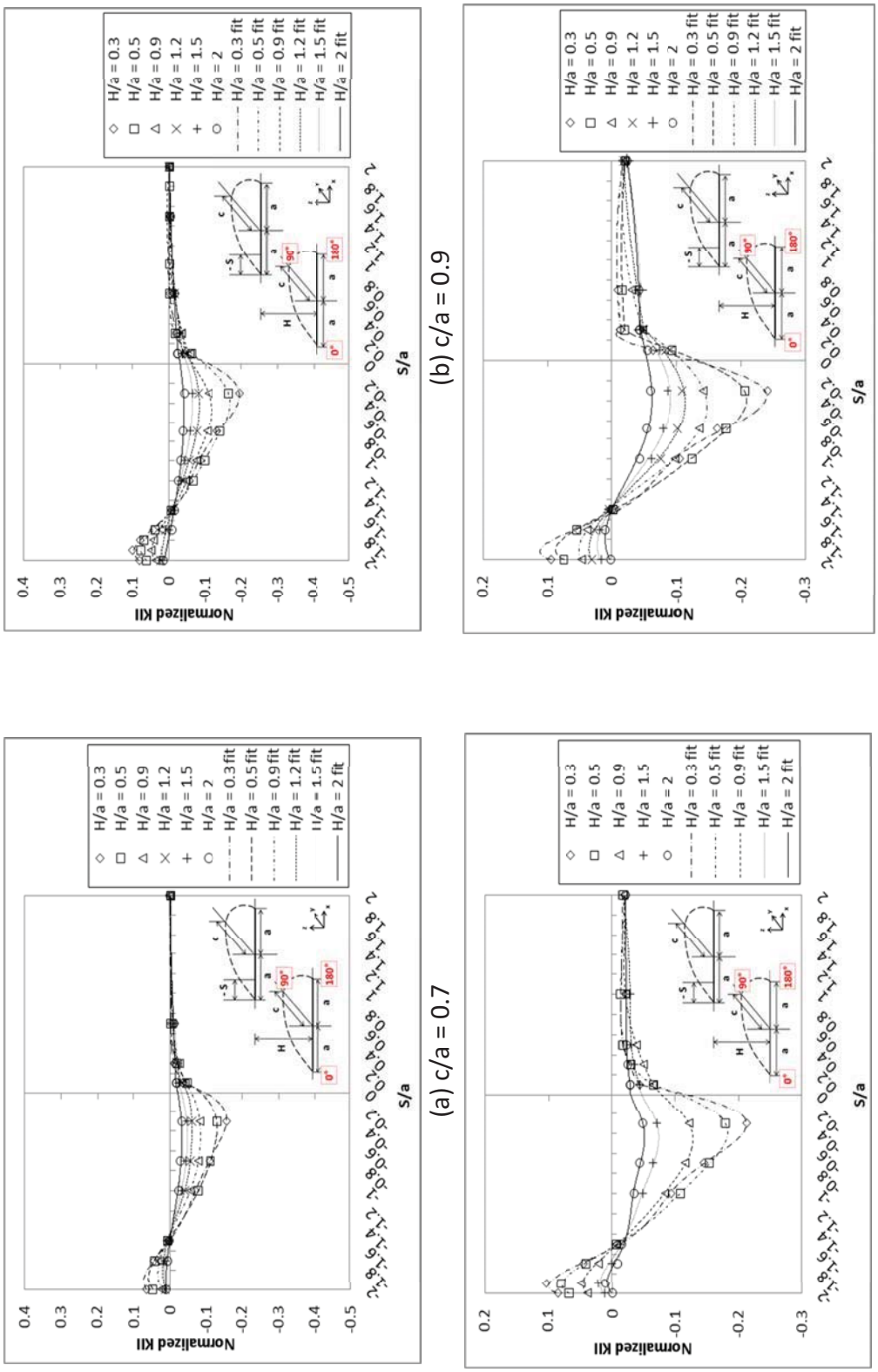

Figure 3-25 Curve fit for the normalized mode II SIF with varying horizontal distance (S/a) at a fixed vertical distance (H/a) for c/a = 0.7, 0.9, 1, and 1.2.

Table 3-2 Coefficients of the polynomial fits and r^2 of normalized K_{II} for varying horizontal distance (S/a) between cracks at fixed vertical distances (H/a). Variable *x* in the table represents the horizontal distance (S/a).

		H/a											
		-2 ≤ S/a ≤ 0.1						0.1 < S/a ≤ 2					
		0.3	0.5	0.9	1.2	1.5	2	0.3	0.5	0.9	1.2	1.5	2
c/a = 0.7	x^6	-0.0513	-0.0302	0.0267	0.0406								
	x^5	-0.1306	-0.0923	0.1757	0.2533			0.0356	0.0151				
	x^4	0.2459	0.0181	0.3997	0.5649	-0.0164	-0.0072	-0.2171	-0.1092	-0.0114			
	x^3	1.1208	0.3719	0.4245	0.5722	-0.0260	-0.0060	0.5033	0.3089	0.0655	0.0138	-0.0023	
	x^2	1.3249	0.5990	0.3201	0.3284	0.0571	0.0478	-0.5507	-0.4250	-0.1402	-0.0552	0.0013	-0.0026
	x	0.5002	0.3004	0.1421	0.1012	0.0652	0.0475	0.28430	0.2816	0.1367	0.0746	0.0206	0.0141
	C	-0.0987	-0.0846	-0.0591	-0.0472	-0.0317	-0.0212	-0.0577	-0.0724	-0.0539	-0.0367	-0.0264	-0.0176
	r^2	1	1	1	1	0.9977	0.9946	1	1	0.9978	0.9079	0.9951	0.9888
c/a = 0.9	x^6	-0.3386	-0.1623	-0.0701	-0.0216	-0.0208			-0.0434				
	x^5	-1.8133	-0.8428	-0.3619	-0.1282	-0.1291			0.3271				
	x^4	-3.3663	-1.5265	-0.6711	-0.2886	-0.2918		-0.0042	-0.9975		0.0045		
	x^3	-2.2642	-0.9824	-0.4727	-0.2574	-0.2568	0.0032	0.0415	1.5720	0.0247	-0.0109	0.0015	-0.0037
	x^2	0.1435	0.2075	0.0807	0.0301	0.0079	0.0333	-0.1241	-1.3498	-0.1085	-0.0203	-0.0161	0.0070
	x	0.5032	0.3443	0.1739	0.1020	0.0793	0.0309	0.1432	0.5996	0.1539	0.0755	0.0471	0.0125
	C	-0.0923	-0.0972	-0.0742	-0.0583	-0.0450	-0.0322	-0.0548	-0.1098	-0.0714	-0.0552	-0.0421	-0.0257
	r^2	0.9981	0.9993	0.9971	0.9998	0.9995	0.9697	1	1	0.9997	1	0.9987	0.9989

Table 3-2 Continued.

		H/a											
		-2 ≤ S/a ≤ 0.1 for c/a = 1 -2 ≤ S/a ≤ 0.3 for c/a = 1.2						0.1 < S/a ≤ 2 for c/a = 1 0.3 < S/a ≤ 2 for c/a = 1.2					
		0.3	0.5	0.9	1.2	1.5	2	0.3	0.5	0.9	1.2	1.5	2
c/a = 1	x^6	-0.2018	-0.1254	-0.0907		-0.0905	-0.0999						
	x^5	-0.9414	-0.6243	-0.5088		-0.5084	-0.5571		0.0434				
	x^4	-1.2745	-1.0434	-1.0595		-1.0483	-1.1295	-0.0106	-0.2643	0.0092		-0.0123	-0.0047
	x^3	0.0410	-0.4896	-0.929		-0.9251	-0.9765	0.0645	0.6210	-0.0256		0.0633	0.0243
	x^2	1.2554	0.4437	-0.1272		-0.2275	-0.2620	-0.1419	-0.7079	-0.0118		-0.1107	-0.0447
	x	0.6506	0.3880	0.1641		0.0676	0.0461	0.1295	0.3921	0.0764		0.0825	0.0350
	C	-0.1205	-0.1086	-0.0788		-0.0472	-0.0296	-0.0552	-0.0987	-0.0724		-0.0511	-0.0318
	r^2	0.9990	0.9997	0.9990		0.9954	0.9846	0.9796	1	0.9999		0.9993	0.9963
c/a = 1.2	x^6	-0.3585	-0.1329										
	x^5	-1.9106	-0.6734										
	x^4	-3.5069	-1.1823	-0.0440	-0.0324	-0.0242	-0.0236						
	x^3	-2.2558	-0.6799	-0.0759	-0.0553	-0.0372	-0.0523						
	x^2	0.3187	0.3493	0.1452	0.1028	0.0836	0.0205	-0.0098	-0.0076	-0.0196	-0.0052	0.0088	0.0059
	x	0.5922	0.3761	0.1644	0.1068	0.0763	0.0331	0.0206	0.0170	0.0619	0.0306	-0.0078	-0.0024
	C	-0.1245	-0.1334	-0.1083	-0.0900	-0.0753	-0.0539	-0.0183	-0.0234	-0.0641	-0.0572	-0.0419	-0.0418
	r^2	0.9975	0.9998	0.9996	0.998	0.9941	-0.0092	1	1	1	1	1	1

3.1.5 Crack Propagation Angle

Changes in crack propagation angle with respect to horizontal and vertical separation distance are discussed in this chapter. As discussed in Chapter 2.1.2, crack propagation angle can be calculated from K_I and K_{II}. From the fitted equations of K_I and K_{II} determined in the previous chapter (Chapter 3.1.4) and equations 2.6 and 2.7, crack propagation angles of c/a = 0.7 at the inner tip over the ranges of $-2 \le S/a \le 2$ are calculated for H/a = 0.3, 0.5, 0.9, 1.2, 1.5. The calculated results are plotted in Figure 3-26. In Figure 3-26(a), change in K_{II}/K_I ratio is illustrated as a function of the relative location between two cracks. The ratio can be used to calculate a crack propagation direction so that the crack growth path, positive, straight, or negative, at crack tips can be estimated. As discussed in Chapter 2.1.2, when crack is under pure mode I loading, the crack grows in straight direction ($\phi = 0$ when $K_{II}/K_I = 0$). However, when mode II loading is introduced as two cracks approach each other, mixed-mode loading condition is applied to the crack tips, and the tips start to twist in either positive (counterclockwise: $\phi > 0$ when $K_{II}/K_I < 0$) or negative (clockwise: $\phi < 0$ when $K_{II}/K_I > 0$) direction as they grow.

As discussed in the previous chapters, SIFs variations are strongly dependent on the relative separation distance between the cracks. The magnitude of the K_{II}/K_I ratio is affected by K_I while the shape of the ratio changes is similar to that of K_{II}. K_{II}/K_I ratio significantly decreases as the adjacent cracks approach and then passes the inner crack tip. In this region, cracks will propagate in a convergent path: crack tips are twisted toward each other and crack deviation angle ϕ is increased. While two cracks are overlapping, the magnitude of K_{II}/K_I ratio reaches its maximum, and then decreases until

S/a ≈ -1/5. At around S/a = -1/5, the sign of the ratio changes from negative to positive, which crack propagation angle ϕ is converted from positive (counterclockwise) to negative (clockwise) direction. The magnitude of the ratio increases until it decreases again as two cracks are completely overlapped. As the crack deviation angles are obtained from the relationship between K_I and K_{II} by applying equation 2.6 or 2.7, the changes in the magnitude of the K_{II}/K_I ratio over the crack's relative location are also reflected in Figure 3-26(b). Almost same trends are observed for other crack shapes (c/a = 0.9, 1, and 1.2), and thus, the crack propagation angle plots for c/a = 0.7 are only included in this paper.

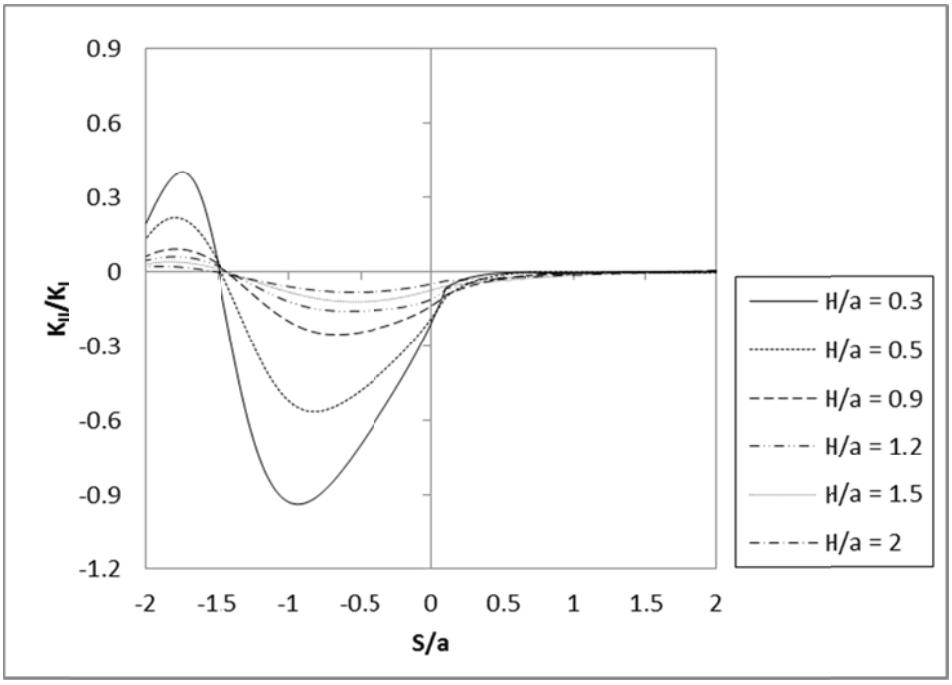

(a) Change in the K_{II}/K_I ratio (Equation 2.5)

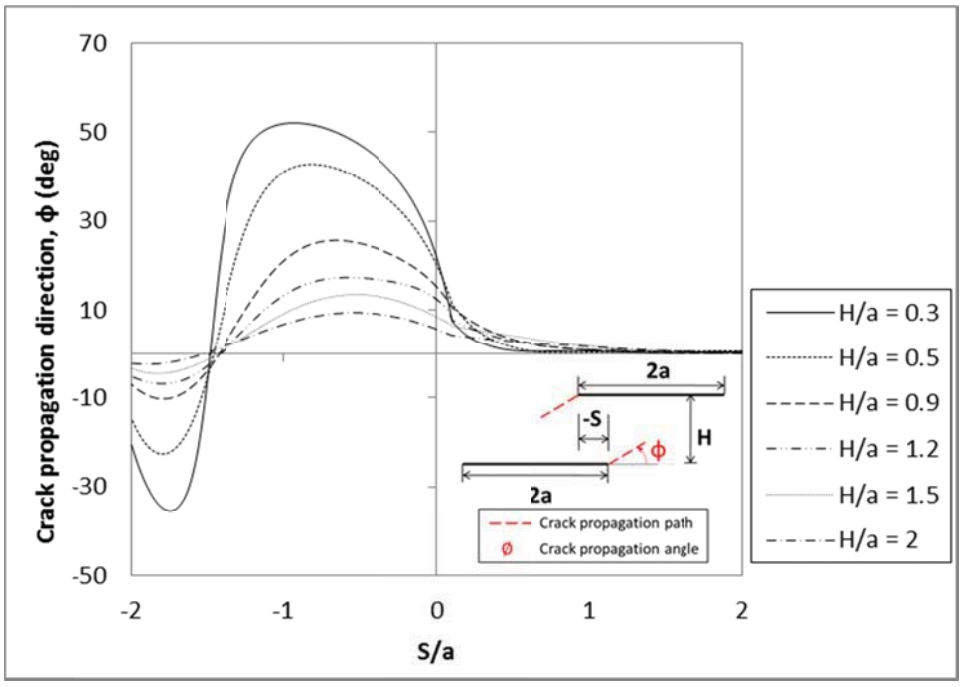

(b) Change in the crack propagation angle ϕ (Equation 2.7).

Figure 3-26 Direction of crack growth at the inner crack tip under mixed mode I and II conditions for various horizontal separations at fixed vertical distances (c/a = 0.7).

3.2 Non-symmetric Crack Shapes

In this chapter, interaction of the two cracks with non-symmetric crack shapes is studied. Two different types of non-symmetric crack shapes are chosen as follows:

1. Type I: semi-circular shape versus semi-elliptical shape with various crack depths (Figure 3-27)
2. Type II: semi-circular shape versus semi-elliptical shape with various crack lengths (Figure 3-28)

For both types, shape of the crack#1 is fixed as semi-circular with crack length of 2a (a = 10). As shown in Figure 3-27, length of the crack#2 is also fixed as 2a while depth of the crack (c_2) is varied from 3 to 10 for type I crack shapes. Four different cracks are chosen to study the effect of crack depth on the interaction of two cracks. For type II crack shapes, depth of the crack#2 (c_2) is fixed as 5 ($c_2 = 0.5a_1$) while length of the crack#2 (a_2) is varied from 2.5 to 12. Five cracks shapes are selected to study the effect of crack length on the interaction of two cracks.

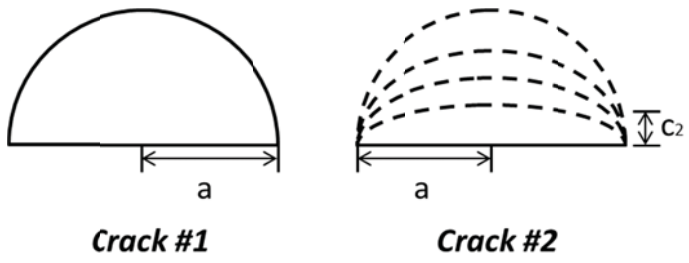

Figure 3-27 Type I non-symmetric crack shape: variation of crack depth (c_2/a = 0.3, 0.5, 0.7, 1).

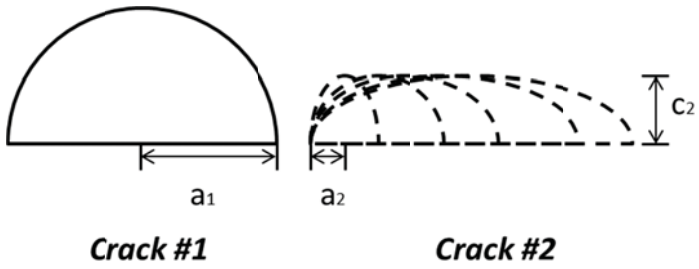

Figure 3-28 Type II non-symmetric crack shape type II: variation of crack length (a_2/a_1 = 0.25, 0.5, 0.7, 1, 1.2, $c_2 = 0.5a_1$).

The test cases used for the non-symmetric crack study are similar to the test cases selected for the symmetric crack study and are shown in the figure below (Figure 3-29). Selected test cases also deal with multiple vertical separations (H/a) between 0.3 and 2 where horizontal separations (S/a) are varied from -2 to 2 for all crack shapes categorized under type I and type II crack cases.

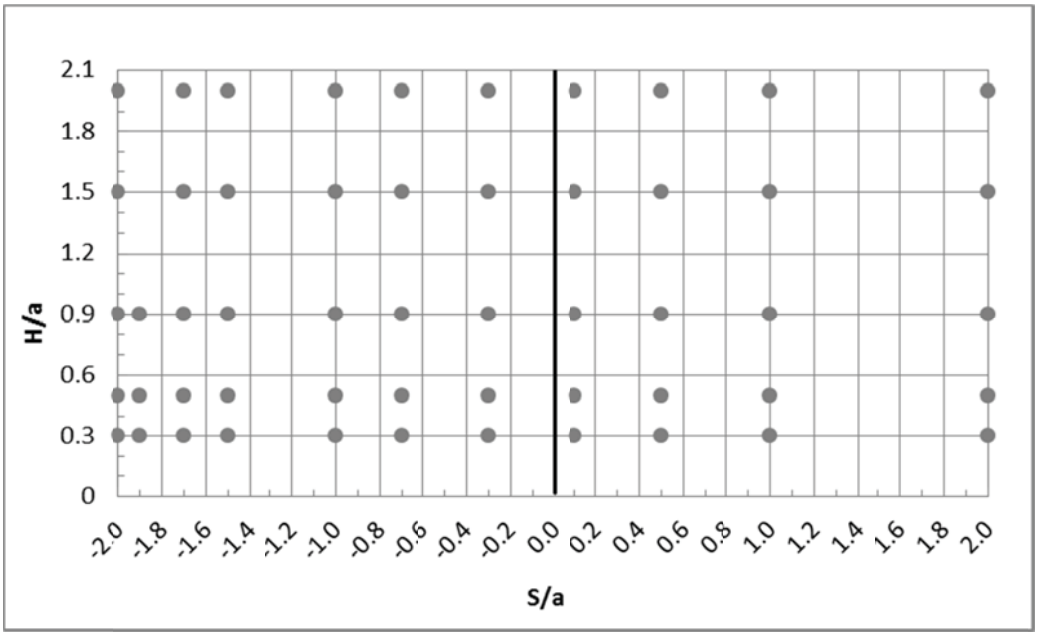

Figure 3-29 Test matrix for non-symmetric parallel overlapped surface cracks.

From Chapter 3.1, it is found that stress field interference is significantly observed when the vertical distance between two cracks are small. Therefore, only the stress profiles from the crack interaction cases at vertical separation (H/a) of 0.3 are presented in this Chapter.

3.2.1 Effect of the crack depth (Type I)

Effect of the neighboring crack's depth is studied by observing the changes in SIF profile of crack #1 when the depth of crack#2 is varied. First, mode I SIF profiles of isolated crack cases (S/a = 2) are considered. In Figure 3-30, K_I profiles along the crack front of crack #1 are plotted for Type I cracks (c_2/a = 0.3, 0.5, 0.7, 1). As discussed in Chapter 3.1.1, SIF profile of the crack is symmetric along the crack front, and the profile is identical regardless of the vertical separation distance or the neighboring crack's shape.

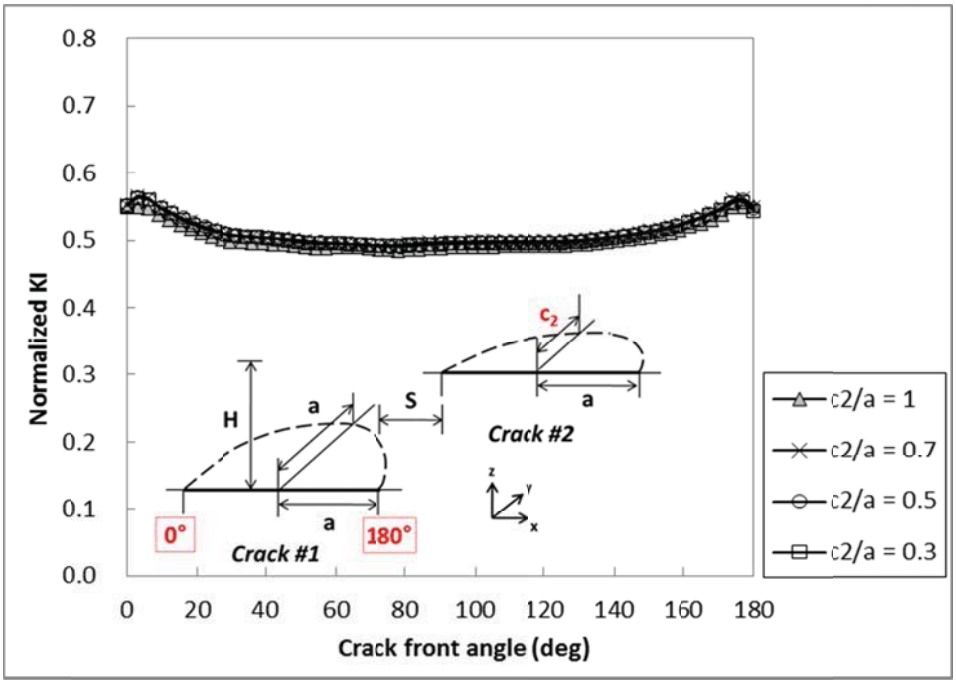

Figure 3-30 Normalized mode I SIF along the crack front of crack#1 for varying crack depth (c_2/a) (S/a = 2 &H/a = 0.3).

However, as two cracks approach each other, K_I profiles are obtained differently. As expected, stress amplifications are observed near the inner crack tip of crack #1 (Θ = 180°), and the magnitude of the amplification is increased as the depth of crack#2 deepened. Figure 3-31 shows K_I profiles of crack#1 when two cracks are closely located (S/a = 0.1) at a vertical separation distance of 0.3. Stress around the outer crack tip is identical for all crack shapes; stress around the inner crack tip is varied according to the crack depth. At the inner crack tip, stress is highest for c_2/a = 1 and is converged to c_2/a = 0.3 as the depth of crack#2 decreases. Also, stress profile is symmetric along the crack front for c_2/a = 0.3 case. From these observations, it is found that the stress interference

from the neighboring crack is negligible when c_2/a is less than 0.3 even if two cracks are located closely located horizontally and vertically.

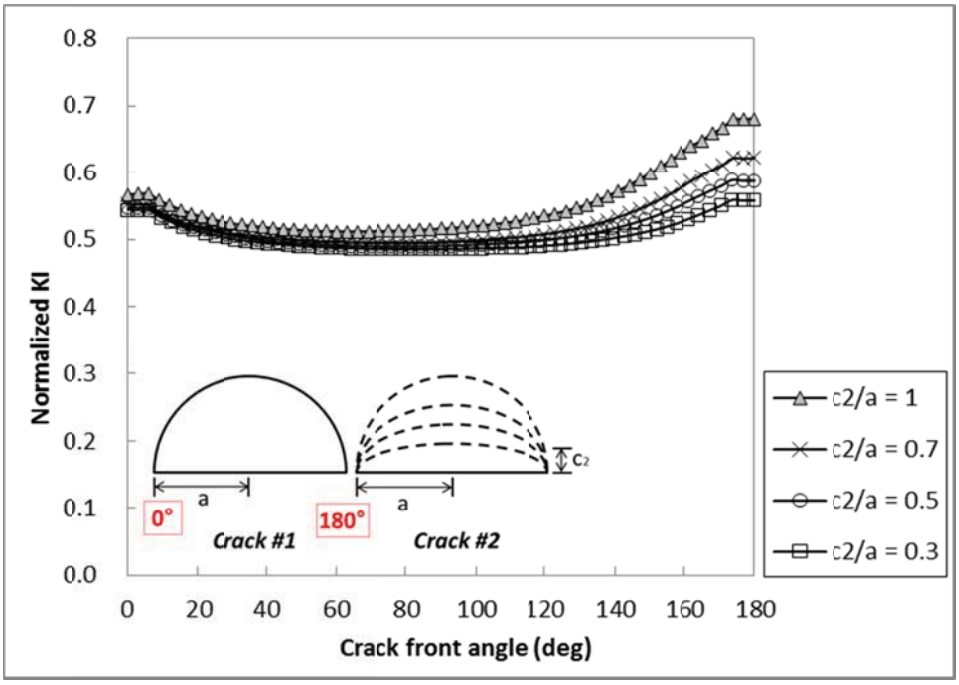

Figure 3-31 Normalized mode I SIF along the crack front of crack#1 for varying crack depth (c_2/a) (S/a = 0.1 &H/a = 0.3).

Figure 3-32 illustrates two interacting cracks with non-symmetric crack shapes overlapped with horizontal separation distance of -1.5 viewed from the top. Crack fronts are intersected at about Θ = 165° for c_2/a = 0.3; Θ = 150° for c_2/a = 0.5; Θ = 135° for c_2/a = 0.7; Θ = 105° for c_2/a = 1. As shown in the figure, size of the overlapped crack front area are reduced and location of two crack front's intersecting point shifts toward the crack#1's inner crack tip (Θ = 180°) as the depth of crack#2 decreases. Due to these facts, stress field of crack#1 is interrupted at different crack front areas for each crack shape type (c_2/a) of 0.3, 0.5, 0.7, and 1.

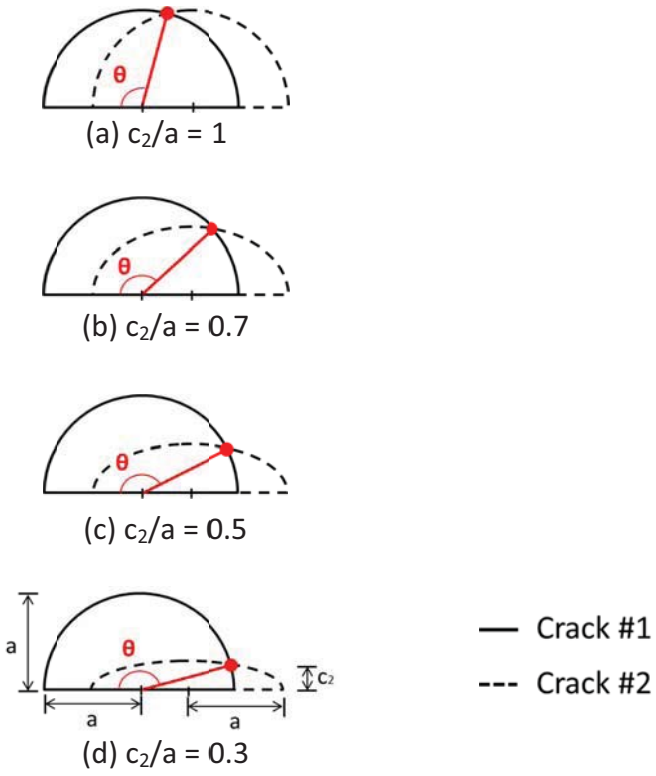

Figure 3-32 Top view of two overlapped cracks with non-symmetric crack shapes at fixed horizontal separation (S/a) of -1.5.

In Figure 3-33, K_I profiles of crack #1 are plotted for which the horizontal separation distance between two cracks is -1.5. As shown in Figure 3-31, stress around the outer crack tip is identical for all crack shapes. However, stress shielding is in effect near inner crack tip for all crack cases. When the depth of the neighboring crack is varied while the length is fixed, overlapping crack front area is increased as the depth is deepened. From the figure below, it is observed that crack front area in which two crack fronts are overlapped is affected by the shielding effect and stress for this region is decreased. In addition, stress shielding effect becomes more significant as the depth of

crack#2 increases: largest SIF decrease over the widest range of crack front angle is observed for c_2/a = 1 case.

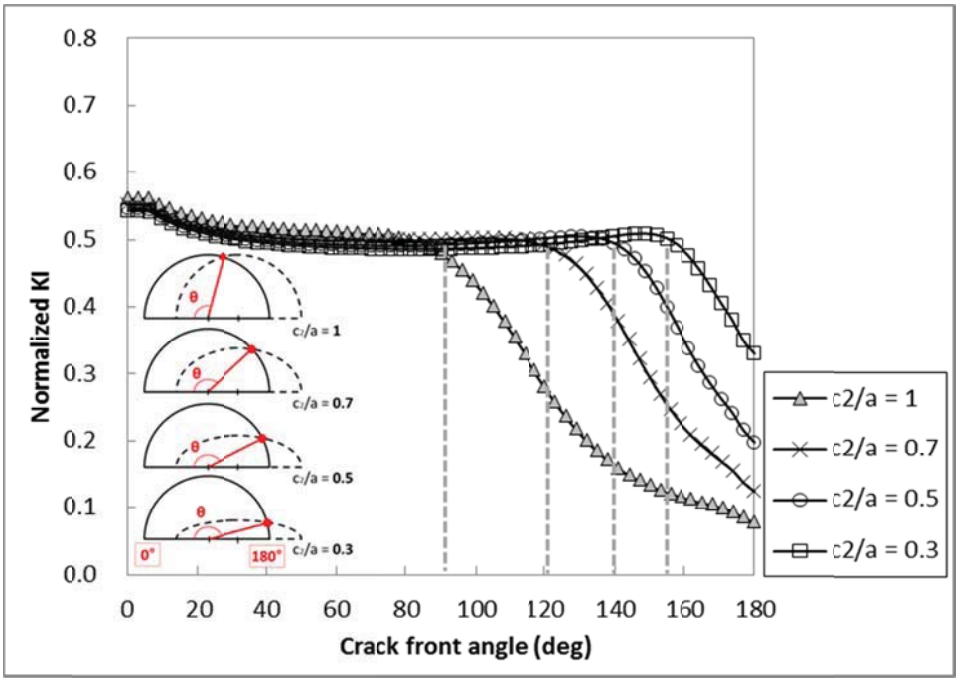

Figure 3-33 Normalized mode I SIF along the crack front of crack#1 for varying crack depth (c_2/a) (S/a = -1.5 &H/a = 0.3).

Now, K_I profiles where two cracks are completely overlapped (S/a = -2) are plotted in Figure 3-34. SIF profiles are symmetric along the crack front for all crack shapes as shown in the previous chapters. However, K_I profiles show different trends from previous K_I profile figures. In the figure, only the profile of c_2/a = 1 shows similar trend observed before: SIF profile is similar to that of isolated crack's profile AND magnitude of K_I along the crack front are lower than that of isolated crack's K_I. From the plot, it is found that stress shielding is only effective near the crack tips (Θ = 0, 180°) for Type I cracks. Even though the lengths of two cracks are the same, the depth of the

crack shapes of c2/a = 0.3, 0.5, and 0.7 are shallower than the depth of crack#1. Thus, crack fronts are partially overlapped around the inner and outer crack tips, and only K_I around these tips are decreased from the stress shielding. Near the crack tips, effect of the stress shielding is increased as the depth of crack#2 deepens, and SIFs converged to that of c2/a = 1.

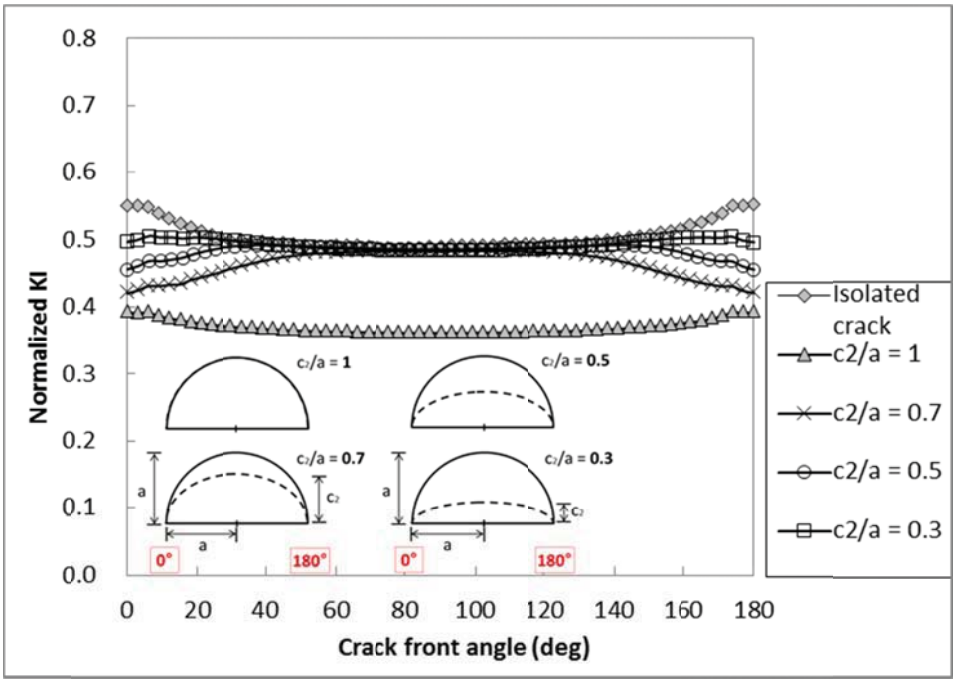

Figure 3-34 Normalized mode I SIF along the crack front of crack#1 for varying crack depth (c_2/a) (S/a = -2 &H/a = 0.3).

In this chapter, effects of the neighboring crack's relative depth on the interaction of two cracks are discussed. It is seen that stress amplification and shielding effects are stronger when the depth of the second crack is deeper. On the other hand, if the depth of neighboring crack is shallow (i.e. $c_2/a \leq 0.3$), stress interference from the

adjacent is found to be negligible. Also, it is observed that the crack front region which is under the stress shielding effect is shifted along two cracks' overlapping point.

3.2.2 Effect of the crack length (Type II)

In this chapter, effect of the neighboring crack's length is studied using the SIF profiles obtained for Type II crack interactions. First, mode I SIF profiles of crack#1 for overlapped distance of -1.5 are considered for Type II cracks. Top view of Type II crack shapes at horizontal separation distance of -1.5 are illustrated in Figure 3-35 below. Depth of crack#2, c_2, is fixed as the half crack length of crack#1 (c_2/a_1 = 0.5), and length of crack#2, a_2, is varied (a_2/a_1 = 0.25, 0.5, 0.7, 1, and 1.2). As shown in the figure, size of crack#2 for cases (a), (b), and (c) are smaller than crack #1, and thus, crack fronts of two cracks are not intersected when S/a = -1.5. Only the crack fronts for cases (d) and (e) are intersected at Θ = 150°.

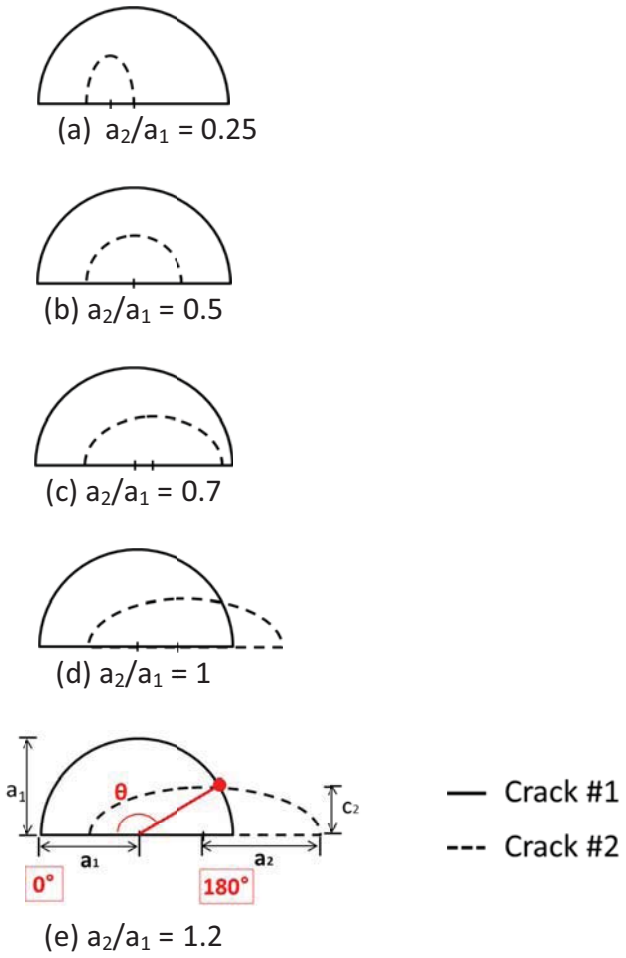

Figure 3-35 Top view of two overlapped cracks with non-symmetric crack shapes at fixed horizontal separation (S/a) of -1.5 (c_2/a_1 = 0.5).

K_I profiles of crack#1 at S/a = -1.5 are plotted in the figure below (Figure 3-36). Similar to Type I crack interactions, trend in K_I profile along the crack front differs between the crack shapes depending on whether the crack fronts of two cracks are intersected or not. When cracks fronts are intersected as shown in Figure 3-35 (d) and (e), stress field of crack#1 is interfered by the presence of crack #2, and K_I near the inner crack tip decreased significantly due to the stress shielding effect. However, for cases (a) and (b), crack#2 is located inside of crack#1's crack front area. Since crack fronts of the

cracks are not intersected, stress interference is not occurred between the crack and KI profile is found to be symmetric along the crack front. Little interference is observed at the inner crack tip for a_2/a_1 = 0.7 case. This happened because even though crack#2 is smaller than crack #1 and is located within crack#1's crack front, the outer tip of crack#2 is closely located from the inner crack tip of crack#1 and caused interference on the stress field.

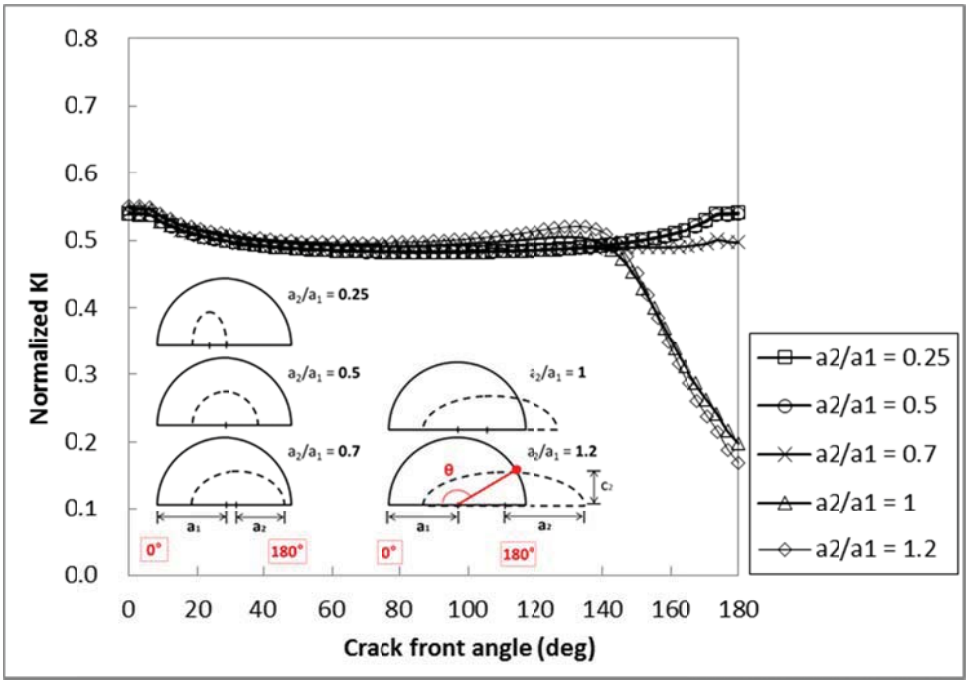

Figure 3-36 Normalized mode I SIF along the crack front of crack#1 for varying crack length (a_2/a_1) at a fixed horizontal separation distance of -1.5 (H/a = 0.3).

K_I profiles for Type II cracks are plotted for horizontal separation distance within the range of -1.9 ≤ S/a ≤ 0.1 in Figure 3-37. In the figure, changes in the stress profile of crack#1 can be observed. Same as the other types of crack interactions discussed in the previous chapters, stress filed of crack#1 is not affected by the presence of the

neighboring crack regardless of its size and vertical location: stress profile is symmetric along the crack front, and the profile is identical for all Type II crack shapes. Therefore, K_I plot at S/a = 2 is omitted in this chapter.

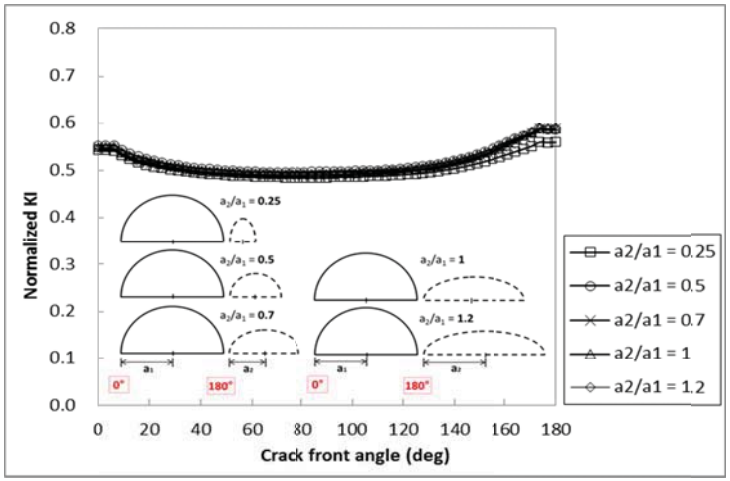

(a) S/a = 0.1

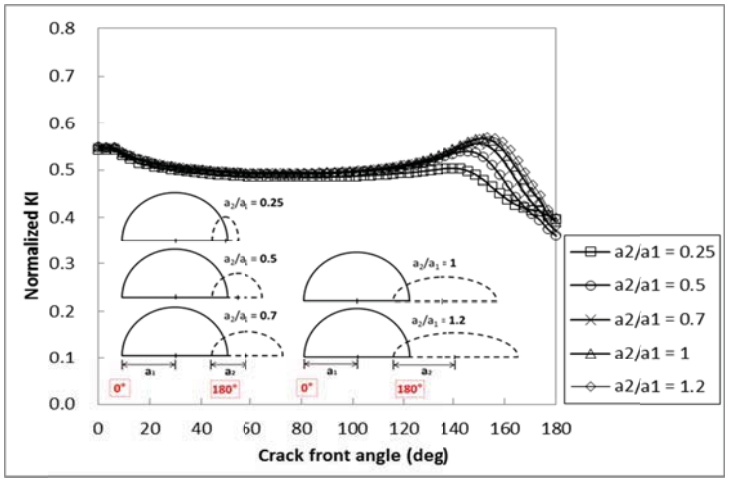

(b) S/a = -0.3

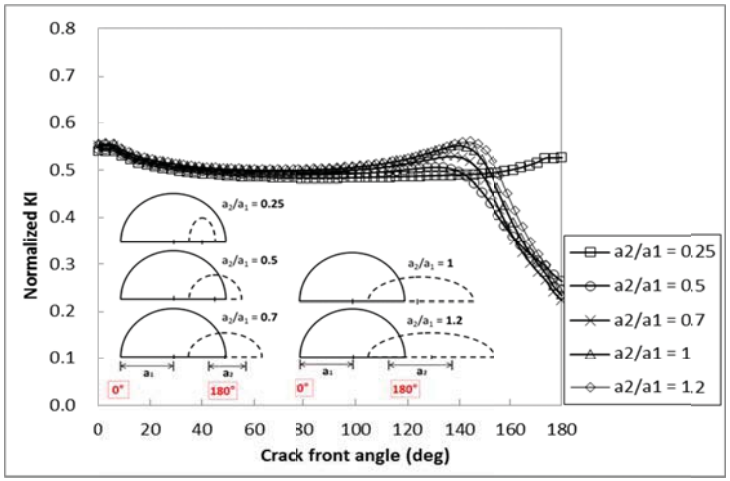

(c) S/a = -0.7

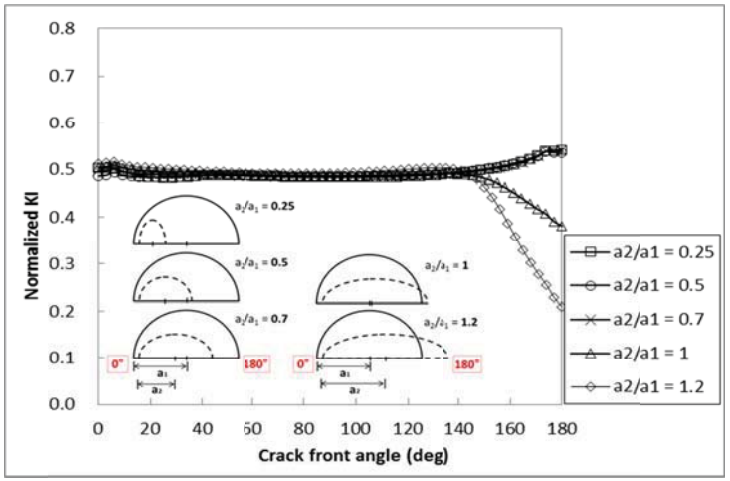

(d) S/a = -1.9

Figure 3-37 Normalized mode I SIF of crack#1 along crack front for varying crack length (a_2/a_1) at various horizontal separation distances (H/a = 0.3).

As crack#2 approaches to crack#1 (see Figure 3-37(a)), stress near the inner crack tip is increased about 3% for a_2/a_1 = 0.5, 0.7, 1, and 1.2 and 1% for a2/a1 = 0.25. Compare to other crack interaction cases observed before, stress interference is detected to be minimal when two cracks are not overlapped (Note that the depth of crack#2 is fixed as half of crack#1's crack length). It is found that the amount of stress amplification does not differ when the length of crack#2 (crack length ratio, a_2/a_1) is in between 0.5 and 1.2. For a_2/a_1 = 0.25, almost no stress amplification (less than 1%) is occurred at S/a = 0.1, and thus, it is concluded that when two cracks are not overlapped, influence from the neighboring crack is even negligible if a_2/a_1 is less than 0.25.

Figure 3-37(b) shows K_I profiles for overlapped cracks with a horizontal separation distance of -0.3 are illustrated. Similar to the previous crack interactions, both stress shielding and amplification effects are observed when two cracks are overlapped (S/a < 0). Stress near the inner crack tip is amplified, but the locations of the highest K_I are shifted to Θ = 150° to 155° except a_2/a_1 = 0.25: stress amplification effect is not observed for a_2/a_1 = 0.25 case regardless of the horizontal separation distance (refer to Figure 3-36, Figure 3-37, and Figure 3-38). Also, K_I profiles of crack#1 beyond the crack intersection angle, in which the cracks are overlapped, are reduced due to stress shielding for all crack cases. When S/a is reduced from -0.3 to -0.7, crack overlapping area is increased, and thus, stress shielding effect from the crack interactions is enhanced. As a result, K_I near the inner crack tip decreased even more (Figure 3-38(c)).

When crack#2 is approached near the outer crack tip of crack#1 (S/a = -1.9), interference on the stress field is caused by crack #2, and K_I around the outer crack tip is decreased by 10% or less (Figure 3-38) from that of the isolated crack. On the other hand, stress shielding effect near the inner crack tip of crack#1 is 1) not existent for a_2/a_1 = 0.25 and 0.5 cases since crack#2 is located far from the inner crack tip and 2) reduced for a_2/a_1 = 1 and 1.2 cases as the overlapping area between two cracks are decreased.

Figure 3-38 illustrates the K_I profiles of completely overlapped cases (S/a = -2). Except a_2/a_1 = 1 case, SIF profiles of Type II cases at S/a = -2 is not symmetric along the crack front as shown in other crack interaction cases. In previous chapters, the length of the cracks is the same for both cracks whether the shape of two interacting cracks is identical (Chapter 3.1) or not (Chapter 3.2.1). Consequently, stress interference behavior at both inner and outer crack tips is obtained to be identical. However, for type II crack interactions, only a_2/a_1 = 1 case has the same crack length, which produced symmetric K_I profile along the crack front. Normalized K_I near the outer crack tip (Θ = 0°) is decreased about 15% to 20% from that of the isolated crack. The behavior of mode I interaction near the inner crack tip (Θ = 180°) for a_2/a_1 = 0.25 and 0.5 cases are found to be identical to the trend shown for S/a = -1.9 (Figure 3-38(c)): no stress shielding effect. Stress shielding is observed for a_2/a_1 = 1 and 1.2 cases, but the effect from the shielding is reduced, and KI is increased from that of S/a = -1.9 case since the crack front overlapping area is 1) diminished for a_2/a_1 = 1 case and 2) reduced for a_2/a_1 = 1.2.

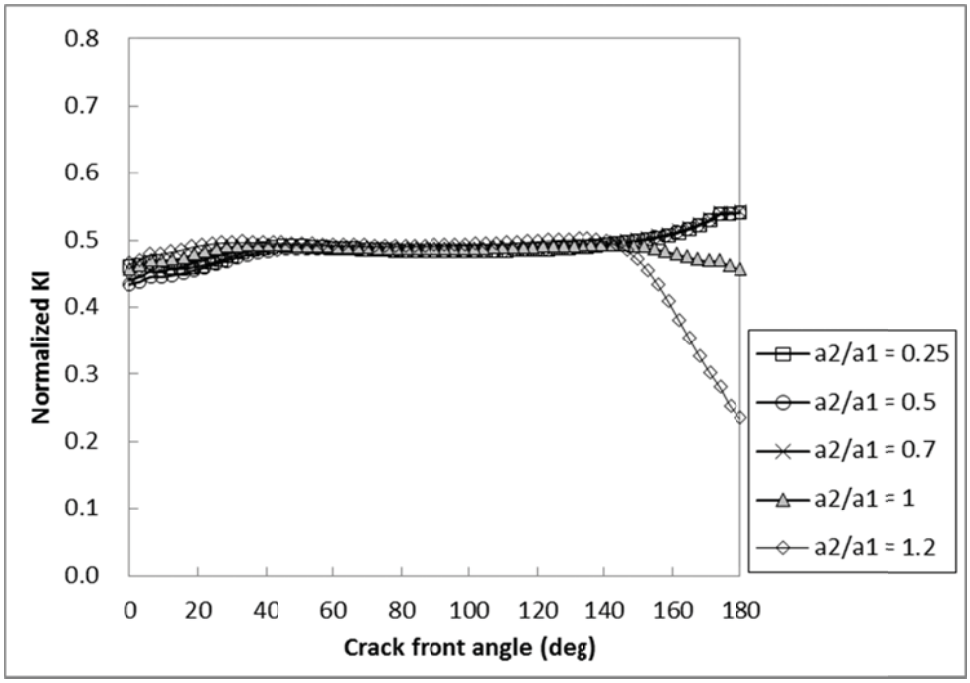

Figure 3-38 Normalized mode I SIF along the crack front of crack#1 for varying crack length (a_2/a_1) at a fixed horizontal separation distance of -1.5 (H/a = 0.3).

In Figure 3-37 and Figure 3-38, it is observed that stress transition point between amplification and shielding occurs around two cracks' intersection point. As shown in the figure below (Figure 3-39), for Type II crack interactions, depth of crack#2 is fixed as $c_2/a_1 = 0.5$. As a result, the minimum angle of crack front intersection is obtained as 150° except when two cracks are completely overlapped (S/a = -2). Therefore, for all S/a cases shown in Figure 3-37, stress amplification and shielding is significantly observed around 150° and higher.

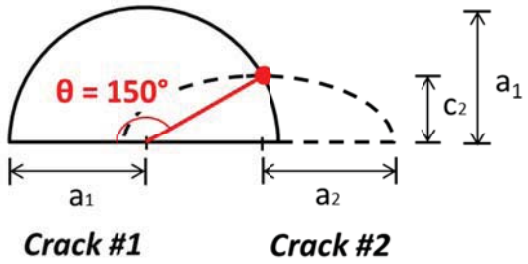

Figure 3-39 Minimum angle of crack front intersection for Type II crack interactions when the horizontal separation distance (S/a) is greater than -2 (c_2/a_1 = 0.5).

From the Type II crack study, it is found that the stress variation from varying the length of the neighboring crack is minimal. In addition, when crack fronts of two cracks are not intersected even though the cracks are overlapped (i.e. Figure 3-35 (a)), stress interference is not observed between the crack. Similar patterns of SIF variation are observed for all crack lengths except a_2/a_1 = 0.25.

In this chapter, effects of the adjacent crack's relative depth and length on mode I interaction of two parallel surface cracks are investigated. However, as mode II interaction is not as significant as mode I interaction (only small amount of stress shielding and amplification are observed), and SIF variation similar to symmetric crack study is observed. Therefore, plots of mode II SIF profiles along the crack front for non-symmetric crack shapes are omitted from this paper. However, coefficients of the polynomial fits for both K_I and K_{II} from Type I and Type II crack shapes are provided as a table in Appendix B.

3.3 Crack Growth Simulations and Comparisons with Previous Experimental Results

As discussed in Chapter 1.2, previous studies have investigated the changes in a shape of surface crack contained in a plate made of various materials with various initial crack sizes as they grow under cyclic loading. Experiments on predicting crack shape changes are performed including few cases which concern two interacting surface crack as studied in the current research [4, 13, 14, 31]. To validate the applicability of the current solutions, i) growth of interacting parallel surface cracks are predicted using the stress intensity factor results obtained from the same Abaqus finite element model developed in this study, and then, ii) the results from the predictions are compared to the data from those experimental studies.

In this research, crack growth is simulated based on the fatigue crack growth prediction method for a single surface crack proposed by Newman and Raju [21], which is a standardized method in fatigue crack growth predictions. This method assumed a fatigue crack growth Paris law (equation 1.2) is valid for surface cracks, and that the surface fatigue cracks maintain their semi-elliptical shape as they grow and only the aspect ratio of the crack changes. These assumptions are widely used in other surface growth prediction studies and are supported by experimental evidence [13, 14, 24, 27]. Based on these assumptions, the following relations are used to calculate the growth of the crack:

$$\frac{da}{dN} = C_a(\Delta K_a)^m, \qquad \frac{dc}{dN} = C_c(\Delta K_c)^m, \tag{3.2}$$

where

a = crack length,

c = crack depth,

N = number of fatigue cycles,

m = material constant,

C_a, C_c = material resistances at the surface and deepest points, and

ΔK_a, ΔK_c = ranges of SIF at the surface and deepest point.

Material constants *m* and C_c are obtained from standardized test, and C_a is calculated by the empirical correlation $C_a = 0.9^m C_c$. Using this correlation, the changes in surface crack shapes are defined as

$$\frac{dc}{da} = \left[0.9\sqrt{\frac{c}{a}}\left(1.1 + 0.35\left(\frac{c}{t}\right)^2\right)\right]^{\frac{1}{m}} \text{ for } \frac{c}{a} \leq 1.0,$$

and $$\frac{dc}{da} = \left[0.9\sqrt{\frac{c}{a}}\left(1.1 + 0.35\left(\frac{c}{t}\right)^2\left(\frac{c}{a}\right)\right)\right]^{\frac{1}{m}} \text{ for } \frac{c}{a} > 1.0. \quad (3.3)$$

First step of the crack growth simulation process is to select a crack growth increment Δ*c* and calculate Δ*a* from equation 3.3 to determine the new dimensions of the crack c_1 and a_1: $c_1 = c_0 + \Delta c$ and $a_1 = a_0 + \Delta a$. Secondly, SIF distribution for a crack along crack front is calculated using Abaqus. Now, the number of fatigue cycles, *N*, is the only unknown parameter in the Paris law (equation 3.2), and *N* can be determined by numerically solving the Paris law with evaluated SIF and material constants. For each crack growth increment, this process is repeated until the final crack depth has been reached. As descried in the simulation process, SIF is the essential parameter of the predictive method.

Kamaya conducted experiments containing two semi-circular surface cracks with same size which are located at the center of the specimen [13, 14]. Among the experiments, test conditions for Specimen B-H5 and B-H10 found to be closely related to the current research: two symmetric semi-circular cracks are located at the center of a plate parallel to each other. Identical test conditions are applied both specimen except the vertical separation distance between two cracks. Therefore, the crack growth of B-H5 and B-H10 are simulated using the experiment condition identified by Kamaya. Then, the results obtained from the simulation are compared with Kamaya's results: i) crack growth at the deepest point of the crack over the cycles (Figure 3-40) and ii) crack growth shape on the surface of the specimen (Figure 3-41 and Figure 3-42). Initial dimensions of the surface crack and experimental conditions of B-H5 and B-H10 are summarized in Table 3-3 below.

Table 3-3 Experiment conditions for Specimen B-H5 and B-H10 [13].

Stress Range, Δσ [MPa]	Stress Ratio, *R*	Plate Thickness, *t* [mm]	Crack Length, *a* [mm]	Crack Depth, *c* [mm]	Horizontal Separation, S [mm]		Vertical Separation, H [mm]	
					B-H5	B-H10	B-H5	B-H10
120	0.1	15	5	5	0	0	5	10

Starting from the initial crack shape (a_0 = 5 mm, c_0 = 5 mm), five additional crack growth patterns are simulated for both crack cases. The material constants used in this crack growth prediction study are $C_c = 3.5*10^{-11}$ and m = 2.52, which are obtained from a compact tension specimen test using the same material by Kamaya. First, crack growth

at the deepest point of the crack is simulated using Newman and Raju's fatigue crack growth prediction method [21]. The step size of the crack growth length at the deepest point, Δc, is chosen as 0.94 mm, which is about 6% of the plate thickness. The growth length at the surface, Δa, is calculated using equation 3.3. SIF is evaluate by Abaqus for the grown crack, and then, the number of fatigue cycles, N, is calculate using the Paris law (equation 3.2). This process is repeated for five times, and the result obtained from the simulation is plotted with Kamaya's results from the simulation and experiment in Figure 3-40. The curves with filled markers are the experimental results obtained by Kamaya from the two parallel cracks tests. The curves with open markers are the results obtained from the simulation performed by Kamaya and the author. Kamaya also used the crack growth prediction method proposed by Newman and Raju except average K values are used instead of the local K values in the simulation. As shown in the figure, simulated results for multiple interacting cracks using the fatigue crack growth prediction method for a single crack by Newman and Ragu [21] agreed well with the experimental results.

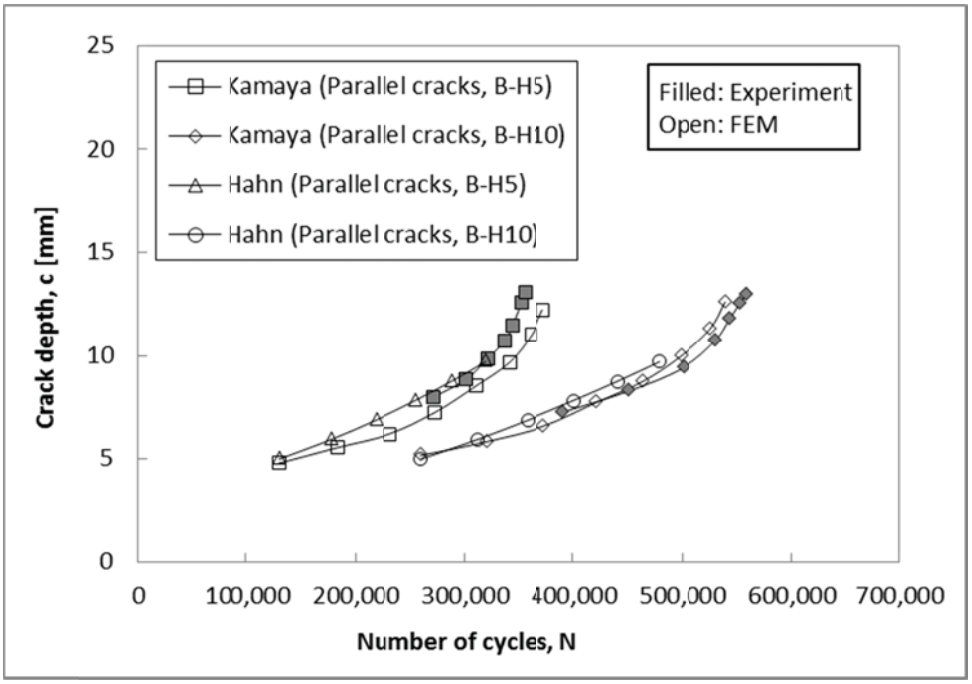

Figure 3-40 Comparison of simulated crack growth with Kamaya's simulated and experimental crack growth for parallel cracks [13, 14]. Crack growth curves at the deepest point of the crack are plotted.

Second, crack growth shape at the plate surface is predicted using the results obtained from the first simulation: incremented crack lengths over cycles and K_I and K_{II} calculated for each crack length. As discussed in Chapter 2.1.2, direction of crack growth under a mixed loading condition can be estimated from the maximum tensile stress criterion. By plugging in K_I and K_{II} calculated for each grown crack shape into equation 2.7, crack growth path of the specimens B-H5 and B-H10 are determined. Simulated results are provided over few loading cycles to show how the cracks are curved as they grow over time (Figure 3-41(a) and Figure 3-42(a)). In this study, simulation is simplified by i) applying the SIF solutions calculated for interacting cracks where the tips of the

cracks remained straight, and ii) assuming the crack growth rate at both inner and outer tips of the crack are the same.

At the inner crack tips, deviation of the crack growth path is observed for the specimens as two cracks overlap each other. Curving of the crack tip is more obvious for the specimen B-H5 since the vertical separation distance between the cracks is smaller for B-H5. On the other hand, crack growth at the outer crack tips are almost straight as their stress field is not disturbed by the adjacent crack.

Figure 3-41(b) and Figure 3-42(b) are photos of the crack shape development on the surface of specimen B-H5 and B-H10 obtained during the experiment conducted by Kamaya, Miyokawa, and Kinuchi [12]. From the comparisons between the simulation results and experimental results on i) the crack growth at the deepest point of the crack and ii) crack shape development on the surface of the specimen, it is concluded that there is a good correlation between the results obtained by the author and the results obtained by Kamaya from both experiments and simulations.

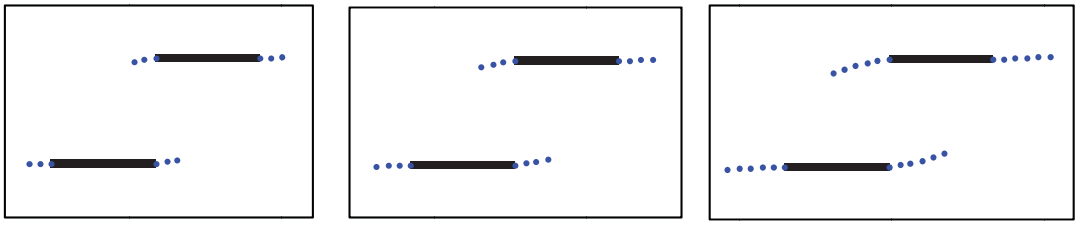

N = 357,245 cycles N = 440,548 cycles N = 478,639 cycles

(a) Simulation result from the author

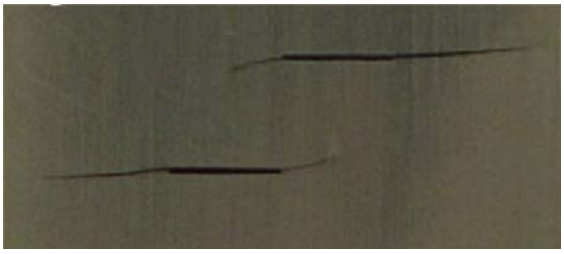

(b) Experimental result from Kamaya [12]

Figure 3-41 Crack growth shape on the surface of the specimen B-H10 (H/a = 2).

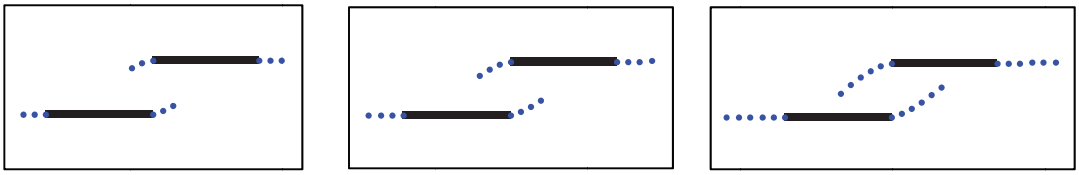

N = 217,998 cycles N = 254,565 cycles N = 318,654 cycles

(a) Simulation result from the author

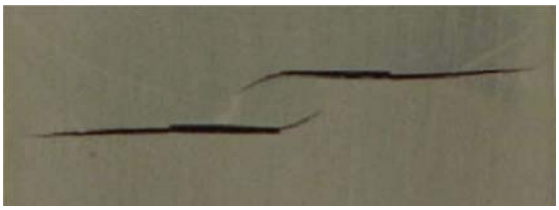

(b) Experimental result from Kamaya [12]

Figure 3-42 Crack growth shape on the surface of the specimen B-H5 (H/a = 1).

CHAPTER 4. CONCLUSIONS AND RECOMMENDATIONS

4.1 Conclusion

FEM is used to analyze the interaction between two semi-elliptical surface cracks which are located in offset positions perpendicular to the loading direction. Since fatigue crack growth is controlled by the cyclic Stress Intensity Factor (SIF), effects of relative positions and shapes of the interacting cracks on variation of SIF along the crack front are discussed. SIFs of 619 crack interaction configurations with various horizontal and vertical separation distances are evaluated in this study.

It is seen that mode II SIF (K_{II}) along the crack front is essentially zero and crack is purely under mode I when two cracks are located far from each other. As two cracks approach each other, mode I SIF (K_I) near the inner crack tip are amplified and K_{II} is introduced around the neighboring crack tips. Cracks are now under a mixed mode I and mode II loading condition. When two cracks start to overlap, stress shielding effects are observed around the overlapping crack front, and both K_I and K_{II} near the inner crack tip is decreased. Due to stress shielding, SIF of interacting cracks are decreased, and crack growth rate is reduced.

SIF variations are found to be significant when the vertical separation between two cracks (H/a) is small. More stress disturbance (amplification or shielding) along the

crack front is observed as H/a reduces. However, when two cracks are located far from each other, effect from the vertical separation is found to be minimal or negligible.

By varying the shape of the neighboring crack, effects of the adjacent crack's relative depth and length on the interaction of two non-symmetric cracks are also investigated. From the depth variation study, it is seen that stress field interference from the neighboring crack increases as the depth of the adjacent crack increases while length of the crack is fixed. Location of the stress shielding effect is shifted along the crack front because the size and the location of the overlapped crack front area are varied depending on the depth of the second crack.

From the crack length variation study where the depth of the neighboring crack is now fixed, it is also found that the location of crack front region under the stress shielding effect shifts along area of the overlapped crack front. Effect from the crack length is found to be negligible when the depth of the neighboring crack is fixed. Therefore, it is concluded that in addition to the horizontal separation distance between the cracks, the location of two crack fronts' intersecting point is also causing a great impact on the interaction between two parallel surface cracks.

Throughout the study, it is seen that mode II interaction is not as significant as mode I interaction. K_{II} is found to be less sensitive to crack separation distance than K_I. However, it is important to note that sign of K_{II} changes (from zero to negative, then to positive) as two cracks' horizontal separation distance (S/a) decreases. When two parallel surface cracks are interacting under the fatigue loading, propagation direction of the crack is determined by the sign of K_{II}. When K_{II} is introduced as two cracks

approach each other, crack propagation direction is twisted, and crack growth path starts to converge/diverge towards the adjacent crack. It is found that crack propagation is retarded when two cracks are overlapped.

Using the SIFs of various crack interaction configurations obtained by FEM, change in crack growth propagation path is predicted by using the maximum tangential stress criterion proposed by Egan and Sih [3]. Also, fatigue crack growth is simulated and compared with the results from previous experiments conducted by Kamaya, Miyokawa, and Kinuchi [12]. From the comparisons, it is confirmed that the direction of crack growth under mixed loading conditions (mode I & mode II) can be reasonably predicted by applying the results obtained from Abaqus to the maximum tangential stress theory.

For all K_I and K_{II} profiles for various relative spacing and shapes are curve fitted, and polynomials of the fitted curve equations are provided in the table so that the values between the data points can be interpolated. The tabulated data can easily be reconstructed into a polynomial equation, which can be integrated in conventional fatigue life prediction software.

4.2 Recommendations

In this study, interaction between parallel offset semi-elliptical surface cracks are only considered for a limited number of crack shapes. Also, both cracks are located perpendicular to the loading direction. Therefore, further investigation on additional crack configurations and different loading conditions are required to complete the analysis on the parallel offset crack interactions. Also, further research on identifying

the conditions for crack propagation behavior of the interacting parallel cracks (collinear coalescence, parallel coalescence, or no coalescence) is also recommended.

LIST OF REFERENCES

LIST OF REFERENCES

1. Anderson, T.L. Fracture Mechanics - Fundamentals and Applications. Taylor and Francis, third edition, 2005.

2. Bayley, C.J. and Bell, R. Experimental and Numerical Investigation of Coplanar Fatigue Crack Coalescence. *International Journal of Pressure Vessel and Piping,* 1997, Vol. 74, pp. 33-37.

3. Erdogan, F., and Sih, G. C., On the Crack Extension in Plates under Plane Loading and Transverse Shear," *ASME Journal of Basic Engineering*, 1963, Vol. 85(4), pp. 519 – 527.

4. Forsyth, E.N. Initiation, Growth, and Coalescence of Small Fatigue Cracks at Notches. Master's Thesis - Purdue University, West Lafayette, May 1993.

5. Frise, P.R. and Bell, R. Fatigue Crack Growth and Coalescence at Notches. *International Journal of Fatigue*, 1992, Vol. 14, pp. 51-56.

6. Grandt Jr., A.F. Fundamentals of Structural Integrity - Damage Tolerant Design and Nondestructive Evaluation. John Wiley and Sons, Hoboken, New Jersey, USA, 2004.

7. Grandt Jr., A.F., Thakker, A.B. and Tritsch, D.E. An Experimental and Numerical Investigation of the Growth and Coalescence of Multiple Fatigue Cracks at Notches. *Fracture mechanics*, Vol. 17, ASTM STP 905, American Society for Testing and Materials, 1986, pp. 239–252.

8. Grandt Jr., A.F. and Zezula, C.E. Supplemental Data Compilation for the Influence of Initial Inhomogeneities on Notch Fatigue of 7050-T7451 Aluminum Plate. Final Report for the Aluminum Company of America (ALCOA). Project Number TC919597TC. Apr. 1994.

9. Guozhong, C., Kangda, A., and Dongdi, W. Analyses on Interactions of Two Identical Semi-Elliptical Surface Crack in the Internal Surface of a Cylindrical Pressure Vessel. *International Journal of Pressure Vessels and Piping*, 1996, Vol. 67, pp. 203–210.

10. Isida, M., Yoshida, T. and Noguchi, H. Tension of a Finite-Thickness Plate with a Pair of Semi-Elliptical Surface Cracks, *Engineering Fracture Mechanics*, 1990, Vol. 75, pp. 961-965.

11. Jiang, Z.D., Petit, J. and Bezine, G. Stress Intensity Factors of Two Parallel 3-D Surface Cracks. *Engineering Fracture Mechanics*, 1991, Vol. 40, pp. 345–354.

12. Kamaya, M., Miyokawa, E. and Kikuchi, M. Growth Prediction of Two Interacting Surface Cracks of Dissimilar Sizes. *Engineering Fracture Mechanics*, 2010, Vol. 77, pp. 3120-3131.

13. Kamaya, M. Growth Evaluation of Multiple Interacting Surface Cracks. Part I: Experiments and Simulation of Coalesced Crack. *Engineering Fracture Mechanics*, 2008, Vol. 75, pp. 1336-1349.

14. Kamaya, M. Growth Evaluation of Multiple Interacting Surface Cracks. Part II: Growth Evaluation of Parallel Cracks. *Engineering Fracture Mechanics*, 2008, Vol. 75, pp. 1350-1366.

15. Lam, K.Y. and Phua, S.P. Multiple Crack Interaction and Its Effect on Stress Intensity Factor, *Engineering Fracture Mechanics*, 1991, Vol. 40, pp. 585-592.

16. Mahmoud, M. A. Quantitative Prediction of Growth Patterns of Surface Fatigue Cracks in Tension Analysis *Engineering Fracture Mechanics*, 1988, Vol. 30, 735 - 746.

17. Moussa, W.A., Bell, R. and Tan, C.L. Investigating the Effect of Crack Shape on the Interaction Behavior of Noncoplanar Surface Cracks using Finite Element Analysis. *Journal of Pressure Vessel Technology*, 2002, Vol. 124, pp. 234-238.

18. Murakami, Y. Stress Intensity Handbook. Pergamon Press, 1996.

19. Murakami, Y. and Nemat-Nasser, S. Interacting Dissimilar Semi-Elliptical Surface Flaws under Tension and Bending. *Engineering Fracture Mechanics*, 1982, Vol. 16, pp. 373-386.

20. Needham, G. Small Crack Initiation and Formation - An Investigation into Equivalent Initial Flaw Size and Parallel Offset Surface Crack Interactions. Master's Thesis - Purdue University, West Lafayette, December 2009.

21. Newman Jr., J.C. and Raju, An empirical stress intensity factor equation for the surface crack. *Engineering Fracture Mechanics*, 1981, Vol. 15, pp. 185-192.

22. Newman Jr., J.C. and Raju, I.S. Stress Intensity Factor Equations for Cracks in Three-Dimensional Finite bodies. NASA Technical Memorandum 83200, August 1981.

23. Paris, P.C. and Erdogan, F. A Critical Analysis of Crack Propagation Laws. *ASME-Journal of Basic Engineering*, 1963, Vol. 85, No. 4, pp. 528.

24. Stonesifer, R.B., Brust, F.W. and Leis, B.N. Mixed-Mode Stress Intensity Factors for Interacting Semi-Elliptical Surface Cracks in a Plate, *Engineering Fracture Mechanics*, 1993, Vol. 45, pp. 357-380.

25. Simulia. ABAQUS. http://www.simulia.com/products/abaqus_fea.html.

26. Simulia. ABAQUS Theory and Analysis User's Manual, 2008.

27. Soboyejo, W.O. and Knott, J.F. The Propagation of Non-Coplanar Semi-Elliptical Fatigue Cracks. *Fatigue and Fracture of Engineering Materials and Structures*, 1991, Vol. 14, pp. 37–49.

28. Song, S.H. and Choi, B.H. Effect of Plastic Zone on the Fatigue Crack Propagation Behavior between Two Fatigue Cracks. *Experimental Mechanics*, 2000, Vol. 41, No. 3, pp. 225-231.

29. Sun, C.T. and Su, X.M. Effect of Crack Interaction on Ductile Fracture. FAA-NASA Symposium on the Continued Airworthiness of Aircraft Structures, 1997, Vol. 1, pp. 161-170.

30. Wang, Y. Z., Atkinson, J.D., Akid, R. and Parkins, R.N. Crack Interaction, Coalescence and Mixed Mode Fracture Mechanics. *Fatigue and Fracture of Engineering Materials and Structures*, 1996, Vol. 19, pp. 427–439.

31. Zezula, C.E. The Inuence of Initial Inhomogeneities on Notch Fatigue of 7050-T7451 Aluminum Plate. Master's Thesis - Purdue University, West Lafayette, May 1994.

APPENDICES

Appendix A Stress Intensity Factor Profiles for Symmetric Crack Shapes

Normalized mode I and mode II Stress Intensity Factor (SIF) profiles for symmetric crack shapes of c/a = 0.9 and 1.2 are presented in this Appendix. Here then normalized SIF is defined by

$$\frac{K}{\sigma\sqrt{t}}$$

where *K* is SIF, σ is the applied tensile stress, and *t* is the thickness of the plate.

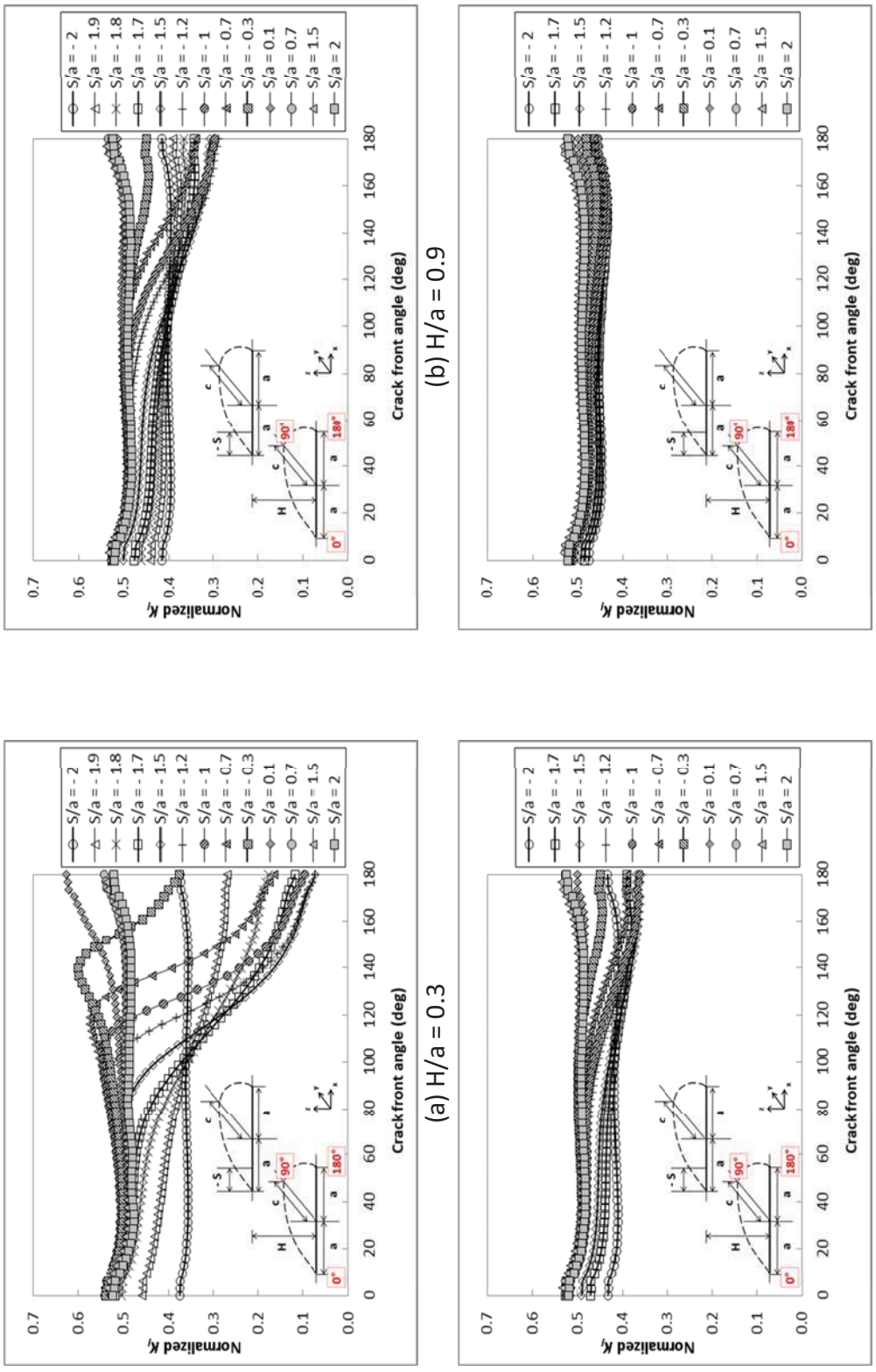

Figure A-1 Normalized mode I SIF along crack front for varying horizontal separations (S/a) at fixed vertical separations (H/a) (c/a = 0.9).

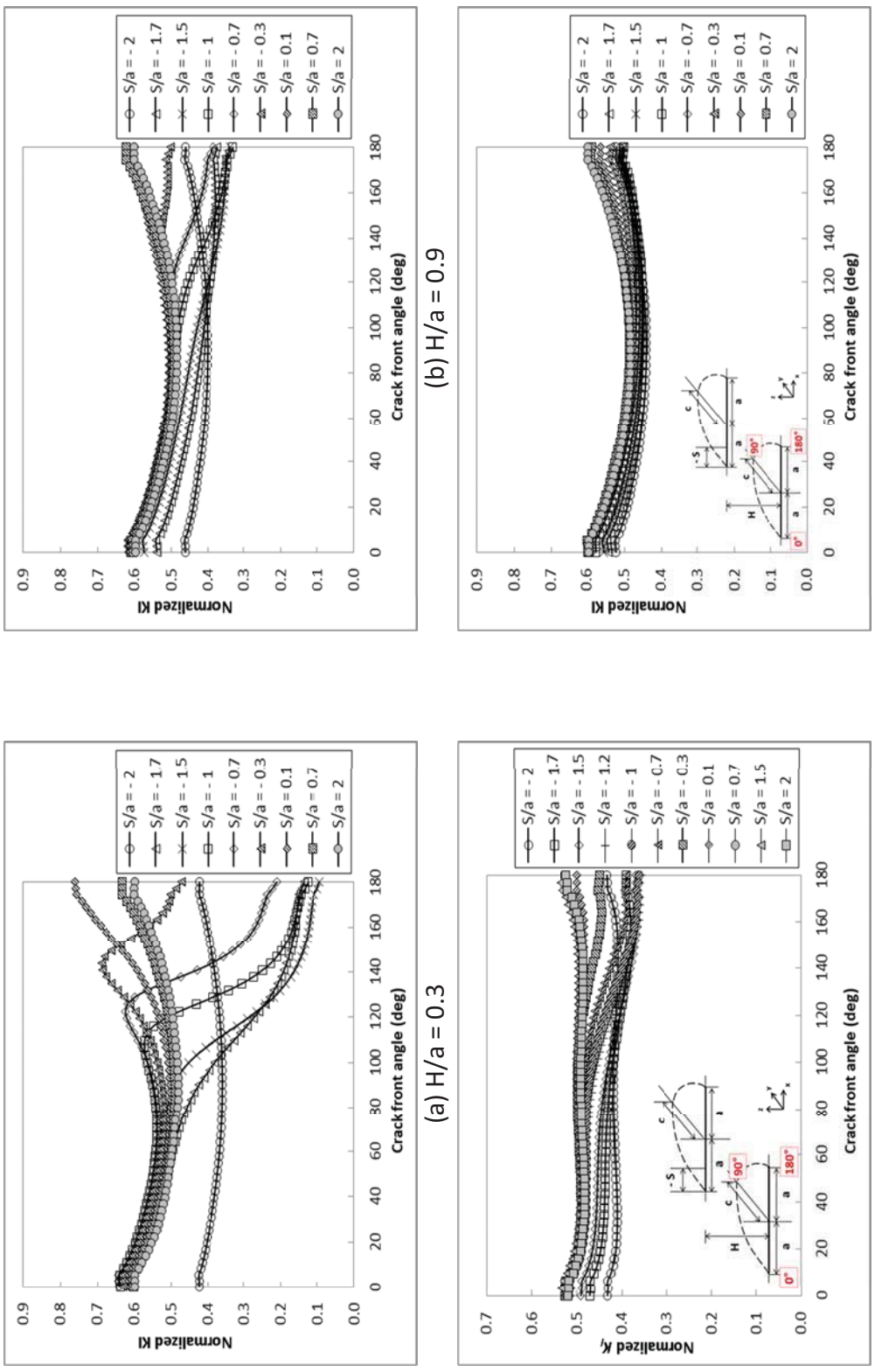

Figure A-2 Normalized mode I SIF along crack front for varying horizontal separations (S/a) at fixed vertical separations (H/a) (c/a = 1.2).

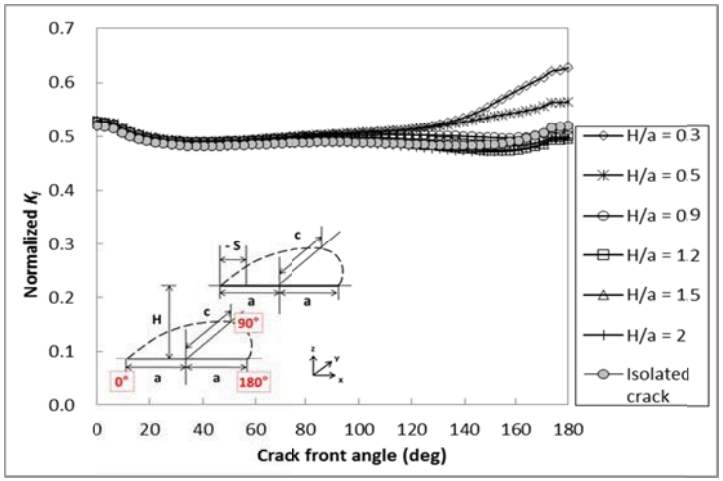

(a) S/a = 0.1

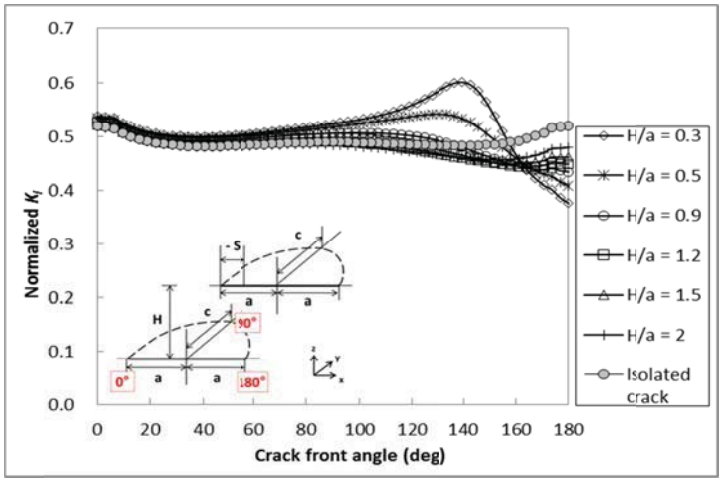

(b) S/a = - 0.3

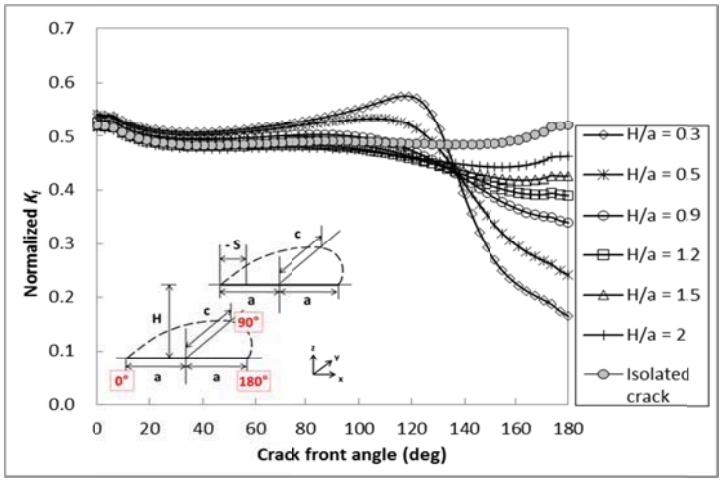

(c) S/a = -0.7

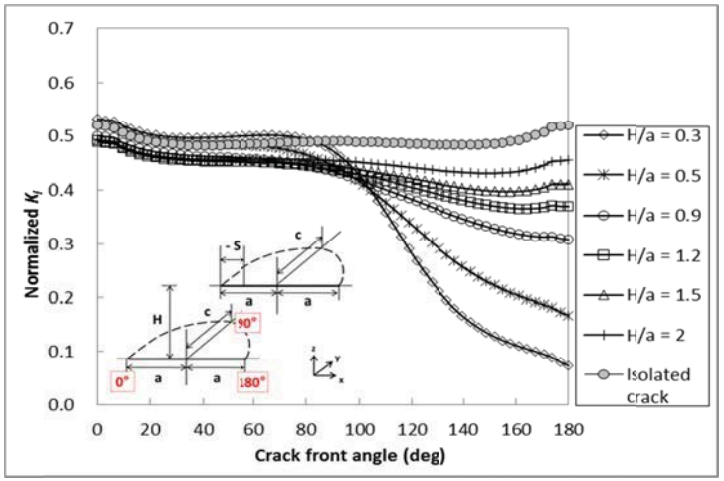

(d) S/a = -1.5

Figure A-3 Normalized mode I SIF along crack front for varying vertical separations (H/a) at fixed horizontal separations (S/a) (c/a = 0.9).

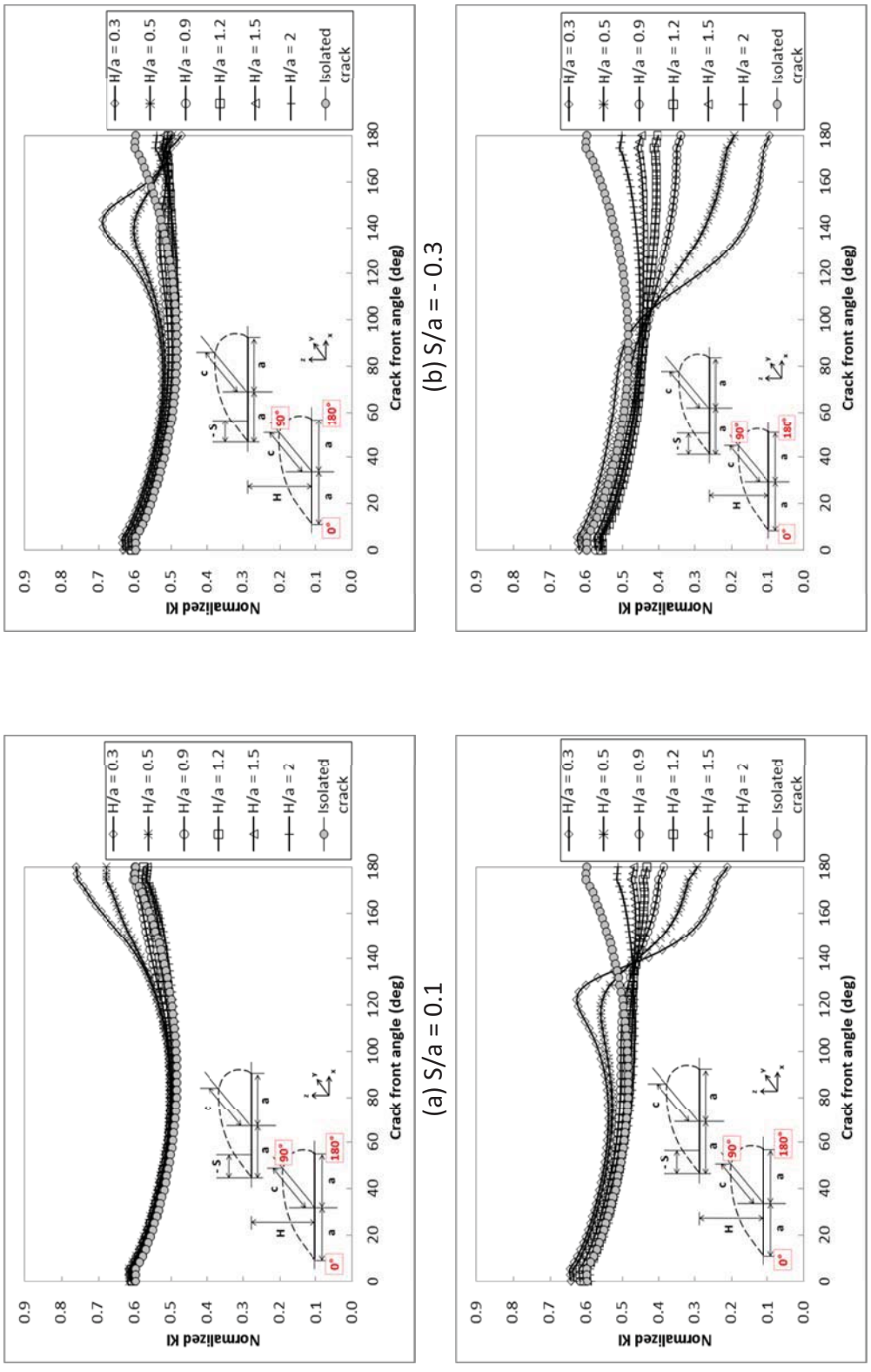

Figure A-4 Normalized mode I SIF along crack front for varying vertical separations (H/a) at fixed horizontal separations (S/a) (c/a = 1.2).

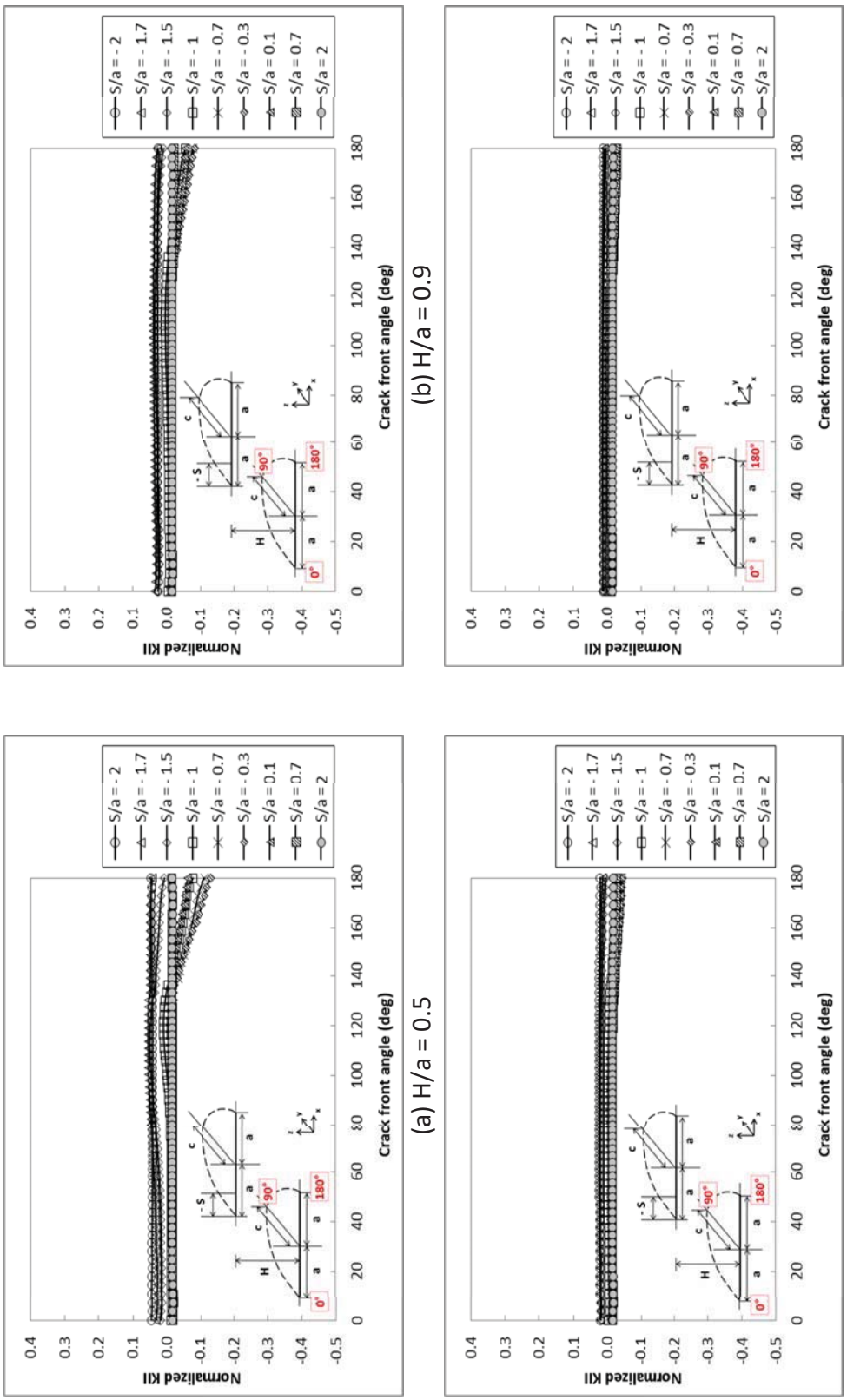

Figure A-5 Normalized mode II SIF along crack front for varying horizontal separations (S/a) at fixed vertical separations (H/a) (c/a = 0.9).

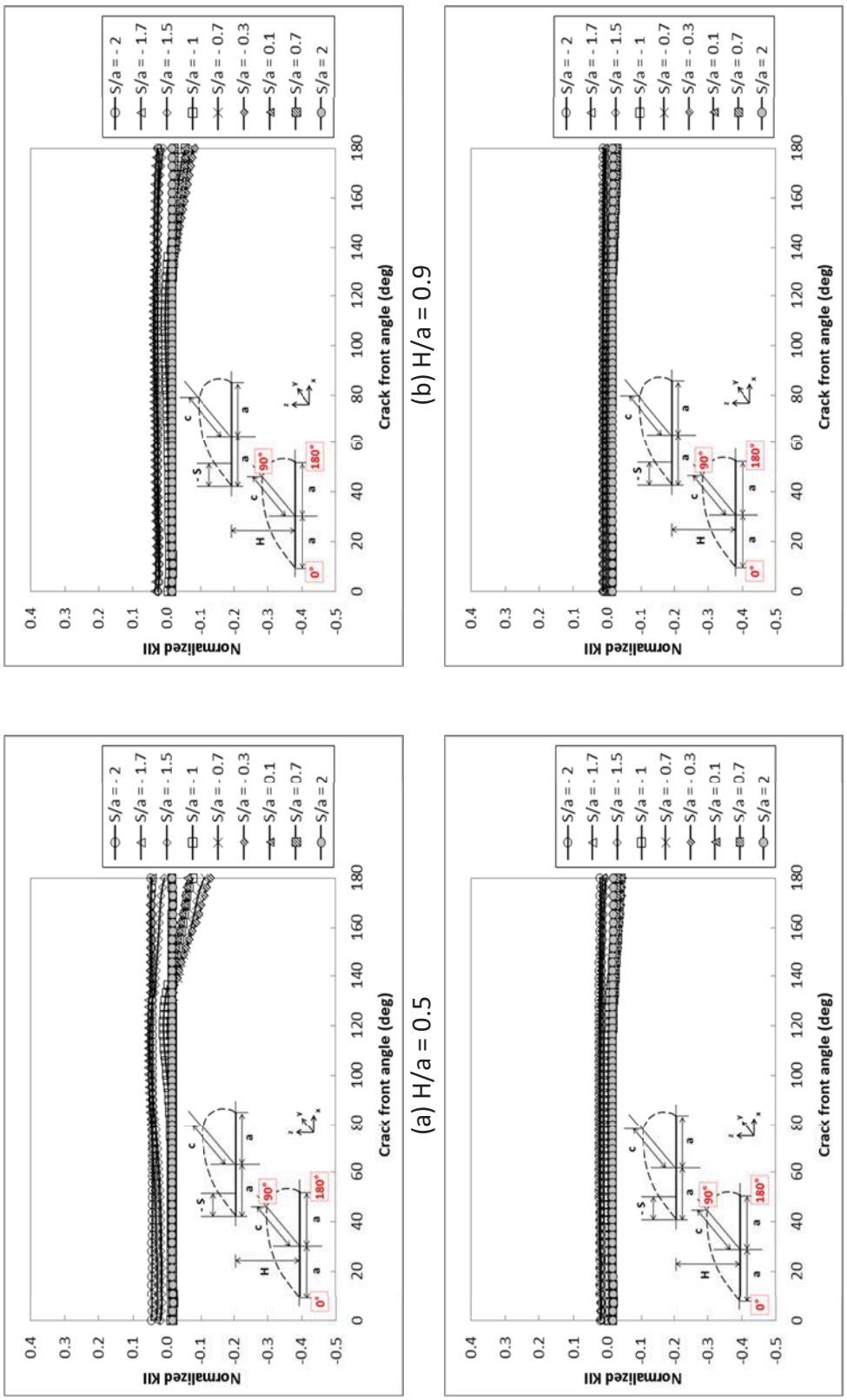

Figure A-6 Normalized mode II SIF along crack front for varying horizontal separations (S/a) at fixed vertical separations (H/a) (c/a = 1.2).

Appendix B Coefficients of the Polynomial Fits for Non-symmetric Cracks

The following tables contain the coefficients of the polynomial fits and coefficient of determination, r^2, of the regression lines for normalized K_I and K_{II} over the range of $-2 \leq \mathrm{S/a} \leq 2$ for each H/a determined for non-symmetric crack shapes. For K_{II} of Type II crack configuration, regression line over the range of $-2 \leq \mathrm{S/a} \leq 0.5$ are obtained as K_{II} converges to zero when S/a > 0.5 (Table B-4). Refer to Chapter 3.1.4 to learn how to utilize the data to reconstruct the curve fit equation.

Table B-1 Coefficients of the polynomial fits and r^2 of normalized K_I for varying horizontal distance (S/a) between cracks at fixed vertical distances (H/a). Variable *x* in the table represents the horizontal distance (S/a): **Type I**.

		H/a									
		-2 ≤ S/a ≤ 0.1					0.1 ≤ S/a ≤ 2				
		0.3	0.5	0.9	1.5	2	0.3	0.5	0.9	1.5	2
$c_2/a = 0.3$	x^6	-0.1240	-0.0409								
	x^5	-0.7712	-0.2393	0.0058							
	x^4	-1.7963	-0.5526	0.0125	0.0069						
	x^3	-1.9493	-0.6588	-0.0217	0.0228	-0.0009		0.0112	0.0114		
	x^2	-0.7876	-0.3183	-0.0273	0.0315	0.0010	0.00195	-0.0336	-0.0397	-0.0048	-0.0036
	x	0.2467	0.1127	0.0465	0.0273	0.0070	-0.0262	0.0220	0.0371	0.0131	0.0104
	C	0.5430	0.5396	0.5342	0.5342	0.5371	0.5583	0.5451	0.5353	0.5359	0.5369
	r^2	0.9999	1	1	0.9886	0.7224	0.7953	1	1	1	0.9543
$c_2/a = 0.5$	x^6	-0.1759	-0.0983								
	x^5	-1.1391	-0.5930								
	x^4	-2.7168	-1.3773	-0.0473	-0.0002						
	x^3	-2.9503	-1.5820	-0.2096	-0.0108		-0.0186	0.017	0.0209		
	x^2	-1.1476	-0.7434	-0.1991	-0.0006	0.0119	0.0770	-0.0509	-0.0729	-0.0085	-0.0036
	x	0.4217	0.2020	0.0737	0.0442	0.0287	-0.1047	0.0301	0.0707	0.0246	0.0132
	C	0.5599	0.5462	0.5306	0.5270	0.5321	0.5970	0.5517	0.5302	0.5295	0.5334
	r^2	0.9998	1	0.9309	0.9675	0.9962	1	1	1	0.9861	0.9963

Table B-1 Continued.

		H/a									
		$-2 \le S/a \le 0.1$ for $c_2/a = 0.7$ $-2 \le S/a \le 0.3$ for $c_2/a = 1$					$0.1 \le S/a \le 2$ for $a_2/a_1 = 0.7$ $0.3 \le S/a \le 2$ for $a_2/a_1 = 1$				
		0.3	0.5	0.9	1.5	2	0.3	0.5	0.9	1.5	2
$c_2/a = 0.7$	x^6	-0.1925	-0.1449								
	x^5	-1.2968	-0.8824	0.0096							
	x^4	-3.183	-2.0359	-0.0002	0.0084	-0.0011					
	x^3	-3.5200	-2.2688	-0.1421	0.0145	-0.0049	-0.0351	0.0236	0.0307	0.0036	0.0024
	x^2	-1.3916	-1.0307	-0.1499	0.0363	0.0155	0.1438	-0.0671	-0.1084	-0.0211	-0.0085
	x	0.5059	0.2691	0.1434	0.0898	0.0515	-0.1928	0.0277	0.1044	0.0377	0.0143
	C	0.5897	0.5608	0.5246	0.5223	0.5295	0.6405	0.5728	0.5279	0.5278	0.5335
	r^2	0.9998	1	1	0.9854	0.9985	1	1	1	1	1
$c_2/a = 1$	x^6	-0.0946	-0.0515								
	x^5	-0.7730	-0.3357								
	x^4	-2.1553	-0.8346	-0.0488	-0.0194	-0.0094					
	x^3	-2.6347	-1.0872	-0.2433	-0.0916	-0.0422	-0.0374	-0.0064	0.0179	0.0155	0.0034
	x^2	-1.0701	-0.5489	-0.2147	-0.0715	-0.0283	0.1751	0.0517	-0.0612	-0.0673	-0.0219
	x	0.6156	0.3855	0.2039	0.0937	0.0526	-0.2742	-0.1229	0.048	0.0919	0.0460
	C	0.6340	0.5808	0.5324	0.5152	0.5197	0.6967	0.6420	0.5579	0.5122	0.5189
	r^2	0.9998	0.9998	1	0.9986	0.9937	0.9876	0.9983	0.9982	1	0.9988

Table B-2 Coefficients of the polynomial fits and r^2 of normalized K_{II} for varying horizontal distance (S/a) between cracks at fixed vertical distances (H/a). Variable *x* in the table represents the horizontal distance (S/a): **Type I**.

		H/a									
		-2 ≤ S/a ≤ 0.1					0.1 ≤ S/a ≤ 2				
		0.3	0.5	0.9	1.5	2	0.3	0.5	0.9	1.5	2
$c_2/a = 0.3$	x^6	-0.0354									
	x^5	-0.1469	0.0223	0.0069	0.0188	0.0118	0.0229	0.0189	0.0105	0.0069	0.0098
	x^4	-0.1371	0.1083	0.0351	0.0980	0.0652	-0.1522	-0.1272	-0.0741	-0.0502	-0.0680
	x^3	0.1621	0.2094	0.0761	0.1853	0.1300	0.3888	0.3297	0.2036	0.1419	0.1815
	x^2	0.3801	0.2300	0.0957	0.1521	0.1099	-0.4724	-0.4090	-0.2710	-0.1959	-0.2313
	x	0.2530	0.1144	0.0467	0.0392	0.0275	0.2678	0.2396	0.1750	0.1323	0.1408
	C	-0.0560	-0.0461	-0.0354	-0.0298	-0.0264	-0.0540	-0.0523	-0.0446	-0.0356	-0.0343
	r^2	1	0.9999	0.9995	0.9978	0.9942	1	1	1	1	1
$c_2/a = 0.5$	x^6	-0.0346									
	x^5	-0.1018	0.0436	-0.0304	0.0202	0.0106	0.0352	0.0259	0.0062	0.0043	0.0072
	x^4	0.0789	0.2141	-0.1470	0.1006	0.0585	-0.2325	-0.1754	-0.0507	-0.0367	-0.0541
	x^3	0.5728	0.4205	-0.2077	0.1867	0.1187	0.5894	0.4598	0.1633	0.1186	0.1548
	x^2	0.7786	0.4628	-0.0274	0.1631	0.1080	-0.7082	-0.5809	-0.2577	-0.1821	-0.2095
	x	0.3632	0.2180	0.0636	0.0476	0.0293	0.3944	0.3497	0.2000	0.1374	0.1376
	C	-0.0881	-0.0758	-0.0505	-0.0399	-0.0324	-0.0763	-0.0786	-0.0621	-0.0454	-0.0400
	r^2	0.9997	1	0.9874	0.9973	0.9985	1	1	1	1	1

Table B-2 Continued.

		H/a									
		-2 ≤ S/a ≤ 0.1					0.1 ≤ S/a ≤ 2				
		0.3	0.5	0.9	1.5	2	0.3	0.5	0.9	1.5	2
$c_2/a = 0.7$	x^6	-0.0722	-0.0164								
	x^5	-0.3061	-0.0313				0.0485	0.0350			
	x^4	-0.3031	0.1149	-0.0108	-0.0041	0.006	-0.3188	-0.2368	-0.0204		
	x^3	0.3388	0.4377	0.0062	0.0085	0.0333	0.8005	0.6192	0.1181	0.0168	0.0150
	x^2	0.8649	0.6087	0.132	0.0649	0.0629	-0.9474	-0.7796	-0.2497	-0.0721	-0.0612
	x	0.4593	0.2972	0.1100	0.0415	0.0255	0.5144	0.4670	0.2310	0.1035	0.0826
	C	-0.1068	-0.1001	-0.0723	-0.0489	-0.0385	-0.0946	-0.1034	-0.0807	-0.0531	-0.0423
	r^2	0.9997	1	1	0.9939	0.9981	1	1	1	0.9968	0.988
$c_2/a = 1$	x^6	-0.2018	-0.1254	-0.0907	-0.0905	-0.0999					
	x^5	-0.9414	-0.6243	-0.5088	-0.5084	-0.5571		0.0434			
	x^4	-1.2745	-1.0434	-1.0595	-1.0483	-1.1295	-0.0106	-0.2643	0.0092	-0.0123	-0.0047
	x^3	0.0410	-0.4896	-0.9290	-0.9251	-0.9765	0.0645	0.6210	-0.0256	0.0633	0.0243
	x^2	1.2554	0.4437	-0.1272	-0.2275	-0.2620	-0.1419	-0.7079	-0.0118	-0.1107	-0.0447
	x	0.6506	0.3880	0.1641	0.0676	0.0461	0.1295	0.3921	0.0764	0.0825	0.0350
	C	-0.1205	-0.1086	-0.0788	-0.0472	-0.0296	-0.0552	-0.0987	-0.0724	-0.0511	-0.0318
	r^2	0.999	0.9997	0.999	0.9954	0.9846	0.9796	1	0.9999	0.9993	0.9963

Table B-3 Coefficients of the polynomial fits and r^2 of normalized K_I for varying horizontal distance (S/a) between cracks at fixed vertical distances (H/a). Variable *x* in the table represents the horizontal distance (S/a): **Type II**.

		H/a														
		$-2 \le S/a \le -0.7$ for $a_2/a_1 = 0.25$ $-2 \le S/a \le -1.7$ for $a_2/a_1 = 0.5$					$-0.7 \le S/a \le$ **A*** for $a_2/a_1 = 0.25$ $-1.7 \le S/a \le 0.1$ for $a_2/a_1 = 0.5$					**A***$\le S/a \le 2$ for $a_2/a_1 = 0.25$ $0.1 \le S/a \le 2$ for $a_2/a_1 = 0.5$				
		0.3	0.5	0.9	1.5	2	0.3	0.5	0.9	1.5	2	0.3	0.5	0.9	1.5	2
$a_2/a_1 = 0.25$	x^4	-0.0192	-0.0401													
	x^3	-0.1369	-0.2522	-0.0120	-0.0006	-0.0014		-0.4254	-0.0667	-0.0269	-0.0150					
	x^2	-0.3560	-0.5858	-0.0628	-0.003	-0.0037	-0.9080	-0.0344	0.0117	0.0030	0.0013	0.0113	0.0004	-0.0019	-0.0003	-0.0024
	x	-0.3997	-0.5976	-0.1092	-0.0098	-0.005	0.5874	0.1768	0.0395	0.0145	0.0082	-0.0290	0.0005	0.0051	-0.0005	0.0080
	C	0.3776	0.3142	0.4787	0.5300	0.5363	0.4916	0.5170	0.5275	0.5351	0.5384	0.5622	0.5434	0.5398	0.5440	0.5375
	r^2	1	1	0.9975	0.9629	0.9601	1	1	1	1	1	1	1	1	1	1
$a_2/a_1 = 0.5$	x^5						-1.2991	-0.5238	-0.0832							
	x^4						-5.6853	-2.3211	-0.3839							
	x^3						-8.1145	-3.3296	-0.5582	0.0092	0.005	-0.0303	0.0166	0.0125		
	x^2	0.2400	0.2728	0.2054	0.3521	0.2404	-3.5864	-1.4085	-0.1882	0.0408	0.0199	0.1168	-0.0514	-0.0476	-0.0036	-0.0008
	x	0.8856	1.0025	0.7487	1.286	0.8791	0.3079	0.2028	0.094	0.0406	0.0196	-0.1402	0.0351	0.0529	0.0116	0.0043
	C	1.3519	1.4563	1.2175	1.7027	1.3357	0.6001	0.5462	0.5252	0.5306	0.536	0.5992	0.5458	0.5273	0.5335	0.5375
	r^2	1	1	1	1	1	1	1	1	0.9966	0.9877	1	1	1	0.9771	0.9181

(**A***: **0.1** for H/a = 0.3 and **0.5** for H/a = 0.5, 0.9, 1.5, 2)

Table B-3 Continued.

		H/a														
		$-2 \le S/a \le -1.5$ for $a_2/a_1 = 0.7$ $-2 \le S/a \le 0.1$ for $a_2/a_1 = 1$ & 1.2					$-1.5 \le S/a \le 0.1$ for $a_2/a_1 = 0.7$					$0.1 \le S/a \le 2$ for $a_2/a_1 = 0.7$ $0.1 \le S/a \le 2$ for $a_2/a_1 = 1$ & 1.2				
		0.3	0.5	0.9	1.5	2	0.3	0.5	0.9	1.5	2	0.3	0.5	0.9	1.5	2
$a_2/a_1 = 0.7$	x^4						-0.0708	-0.1932	-0.0844							
	x^3	-0.5546	-0.2167	0.123	-0.0349	0.0625	-0.4134	-0.6536	-0.2638	-0.0021	0.0018	-0.0156	0.0353	0.0167	0.0047	0.0004
	x^2	-3.2227	-1.3695	0.5622	-0.1731	0.3316	-0.1172	-0.3907	-0.1493	0.0214	0.0149	0.0685	-0.104	-0.0622	-0.0205	-0.0051
	x	-6.2382	-2.8776	0.7688	-0.313	0.5723	0.5402	0.2555	0.0974	0.0415	0.0204	-0.0999	0.0667	0.0683	0.0326	0.0143
	C	-3.4816	-1.4703	0.8081	0.3207	0.8512	0.5337	0.5305	0.5233	0.5258	0.5315	0.5955	0.5458	0.525	0.5271	0.5323
	r^2	1	1	1	1	1	1	1	1	1	1	1	1	1	1	1
$a_2/a_1 = 1$	x^6	-0.1759	-0.0983													
	x^5	-1.1391	-0.593													
	x^4	-2.7168	-1.3773	-0.0473	-0.0002											
	x^3	-2.9503	-1.5820	-0.2096	-0.0108							-0.0186	0.017	0.0209		
	x^2	-1.1476	-0.7434	-0.1991	-0.0006	0.0119						0.077	-0.0509	-0.0729	-0.0085	-0.0036
	x	0.4217	0.2020	0.0737	0.0442	0.0287						-0.1047	0.0301	0.0707	0.0246	0.0132
	C	0.5599	0.5462	0.5306	0.527	0.5321						0.597	0.5517	0.5302	0.5295	0.5334
	r^2	0.9998	1	0.9309	0.9675	0.9962						1	1	1	0.9861	0.9963
$a_2/a_1 = 1.2$	x^6	-0.0580														
	x^5	-0.4388	-0.0470													
	x^4	-1.2301	-0.2564	-0.0173	0.0189											
	x^3	-1.5527	0.5276	-0.0982	0.0505	-0.0033						-0.0184	0.0196	0.0188	0.0005	
	x^2	-0.6307	-0.3493	-0.1049	0.0483	0.0012						0.0778	-0.0589	-0.0658	-0.0118	-0.0034
	x	0.4326	0.2081	0.0874	0.0547	0.0242						-0.1065	0.0354	0.063	0.0284	0.0127
	C	0.5538	0.5426	0.5321	0.5278	0.5321						0.5989	0.5563	0.534	0.5308	0.5338
	r^2	1	1	1	0.9644	0.9979						1	1	1	1	0.9752

Table B-4 Coefficients of the polynomial fits and r^2 of normalized K_{II} for varying horizontal distance (S/a) between cracks at fixed vertical distances (H/a). Variable *x* in the table represents the horizontal distance (S/a): **Type II**.

		H/a									
		$-2 \le S/a \le -0.3$ for $a_2/a_1 = 0.25$ $-2 \le S/a \le -0.7$ for $a_2/a_1 = 0.5$					$-0.3 \le S/a \le 0.5$ for $a_2/a_1 = 0.25$ $-0.7 \le S/a \le 0.5$ for $a_2/a_1 = 0.5$				
		0.3	0.5	0.9	1.5	2	0.3	0.5	0.9	1.5	2
$a_2/a_1 = 0.25$	x^5	-0.1080	-0.0572	-0.0075	-0.0004	-0.0048					
	x^4	-0.7381	-0.3956	-0.0578	-0.0125	-0.0347					
	x^3	-1.933	-1.053	-0.1758	-0.0593	-0.0978					
	x^2	-2.3902	-1.3291	-0.2597	-0.1110	-0.1339	0.1491	0.1429	0.0723	0.0411	0.0433
	x	-1.3637	-0.7765	-0.1826	-0.0923	-0.0899	0.0381	0.0186	0.0154	0.0213	0.0202
	C	-0.2932	-0.1777	-0.0646	-0.0453	-0.0417	-0.0547	-0.0463	-0.0308	-0.0234	-0.0222
	r^2	0.9995	0.9998	1	0.9996	1	1	1	1	1	1
$a_2/a_1 = 0.5$	x^5	-0.4615	-0.1360								
	x^4	-3.6312	-1.1178		-0.0165	0.004					
	x^3	-11.201	-3.6121	-0.0348	-0.0864	0.0223	-0.2476	-0.2511	-0.0263	-0.0055	0.0084
	x^2	-16.380	-5.6961	-0.1632	-0.1710	0.0409	0.1076	0.1064	0.0799	0.048	0.0438
	x	-12.196	-4.3345	-0.2434	-0.1573	0.0245	0.1477	0.1404	0.0399	0.0236	0.0188
	C	-3.3705	-1.2650	-0.1277	-0.0729	-0.0162	-0.0664	-0.0686	-0.0456	-0.0297	-0.0254
	r^2	1	1	0.9955	0.995	0.9997	1	1	1	1	1

Table B-4 Continued.

		H/a									
		-2 ≤ S/a ≤ -0.3					-0.3 ≤ S/a ≤ 0.5				
		0.3	0.5	0.9	1.5	2	0.3	0.5	0.9	1.5	2
$a_2/a_1 = 0.7$	x^4	0.1709	0.1368	0.0405							
	x^3	0.8421	0.6824	0.2107	0.0062						
	x^2	1.3237	1.0989	0.3474	0.0101	-0.0053	-0.1419	-0.0164	0.0540	0.0461	0.0482
	x	0.6294	0.5588	0.1622	-0.0207	-0.0219	0.2133	0.1360	0.0550	0.0277	0.0214
	C	-0.0528	-0.0225	-0.0393	-0.0448	-0.0362	-0.0674	-0.0663	-0.0504	-0.0339	-0.0282
	r^2	0.9948	0.9993	1	0.9963	0.9975	1	1	1	1	1
$a_2/a_1 = 1$	x^6	-0.2530									
	x^5	-1.6452	0.0523		0.0207						
	x^4	-4.2299	0.2663	0.0180	0.1035	-0.0064					
	x^3	-5.4726	0.5382	0.1195	0.1931	-0.0300					
	x^2	-3.7067	0.5849	0.2619	0.1697	-0.0486	-0.1587	-0.0404	0.0364	0.0416	0.0460
	x	-1.3020	0.2744	0.1745	0.0507	-0.0442	0.2139	0.1426	0.0677	0.0345	0.0245
	C	-0.316	-0.0671	-0.0361	-0.0395	-0.044	-0.0632	-0.0628	-0.0515	-0.0372	-0.0311
	r^2	1	1	0.9847	0.9971	0.9998	1	1	1	1	1
$a_2/a_1 = 1.2$	x^3		0.0074	0.0150	0.0067	-0.0007					
	x^2	0.0147	0.0626	0.0770	0.0279	-0.0010	-0.1629	-0.0499	0.0313	0.0446	0.0453
	x	-0.0330	0.0548	0.0720	0.0137	-0.0118	0.2080	0.1382	0.0684	0.0383	0.0263
	C	-0.1469	-0.0947	-0.0529	-0.0435	-0.0394	-0.0598	-0.0595	-0.0504	-0.0381	-0.0322
	r^2	0.9969	0.9997	0.9998	0.9946	0.9982	1	1	1	1	1

VITA

VITA

Jeeyeon Hahn
Aeronautics and Astronautics, Purdue University

Education

B.S., Aeronautics and Astronautics Engineering, 2005, Purdue University, West Lafayette, Indiana
M.S., Aeronautics and Astronautics, 2008, Purdue University, West Lafayette, Indiana
Ph.D., Engineering, 2014, Purdue University, West Lafayette, Indiana

Research Interests

Fatigue and Fracture Mechanics
Finite Element Analysis
Simulation
Data Analysis